COPPE
Instituto Alberto Luiz Coimbra de Pós-Graduação e Pesquisa de Engenharia
UFRJ

NUMERICAL ANALYSIS OF CHEMICAL-ELECTROCHEMICAL MECHANISMS IN ROTATING DISK ELECTRODE SYSTEMS

Pedro Henrique Moura Leal

Tese de Doutorado apresentada ao Programa de Pós-graduação em Engenharia Metalúrgica e de Materiais, COPPE, da Universidade Federal do Rio de Janeiro, como parte dos requisitos necessários à obtenção do título de Doutor em Engenharia Metalúrgica e de Materiais.

Orientadores: Oscar Rosa Mattos
Oswaldo Esteves Barcia

Rio de Janeiro
Junho de 2019

NUMERICAL ANALYSIS OF CHEMICAL-ELECTROCHEMICAL MECHANISMS IN ROTATING DISK ELECTRODE SYSTEMS

Pedro Henrique Moura Leal

TESE SUBMETIDA AO CORPO DOCENTE DO INSTITUTO ALBERTO LUIZ COIMBRA DE PÓS-GRADUAÇÃO E PESQUISA DE ENGENHARIA (COPPE) DA UNIVERSIDADE FEDERAL DO RIO DE JANEIRO COMO PARTE DOS REQUISITOS NECESSÁRIOS PARA A OBTENÇÃO DO GRAU DE DOUTOR EM CIÊNCIAS EM ENGENHARIA METALÚRGICA E DE MATERIAIS.

Examinada por:

Prof. Oscar Rosa Mattos, D.Sc.

Prof. Oswaldo Esteves Barcia, Dr.

Prof. José da Rocha Miranda Pontes, Dr.

Prof. Marcelo Borges Mansur, Dr.

Prof. Norberto Mangiavacchi, PhD.

Prof. Rodrigo Magalhães de Carvalho, Dr.

RIO DE JANEIRO, RJ – BRASIL
JUNHO DE 2019

Leal, Pedro Henrique Moura

Numerical analysis of chemical-electrochemical mechanisms in rotating disk electrode systems/Pedro Henrique Moura Leal. – Rio de Janeiro: UFRJ/COPPE, 2019.

XVII, 111 p.: il.; 29, 7cm.

Orientadores: Oscar Rosa Mattos

Oswaldo Esteves Barcia

Tese (doutorado) – UFRJ/COPPE/Programa de Engenharia Metalúrgica e de Materiais, 2019.

Referências bibliográficas: p. 100 – 107.

1. Diffusion impedance. 2. Electro-hydrodynamic impedance. 3. Rotating disk electrode. 4. Electrochemical simulation. I. Mattos, Oscar Rosa *et al.* II. Universidade Federal do Rio de Janeiro, COPPE, Programa de Engenharia Metalúrgica e de Materiais. III. Título.

To my parents

Acknowledgements

I'm deeply indebted to my advisor, Oscar Mattos, for all the support he has given me throughout these 6 years since I've joined the lab. Thank you for not giving up on me.

I'm also very grateful to my co-advisor, Oswaldo Barcia, for his continuous support on this journey and for letting me join the EHD study group, a decision which would lead to the work presented in this thesis.

It'd be rude not to thank the many colleagues from the lab who have made these tough years much more bearable. Thank you for all the fun during good times and for the kind words during bad times.

I must also thank all of my friends (most notably, my brothers from Ócio Criativo) who have witnessed what I've been through and who have offered good advice or, at least, a shoulder to cry on. I'd be nothing without you.

Finally, I thank my dear family, who has been through Heaven and Hell with me, always very understanding and caring. My father, my mother, my sister, my grandmothers, my aunts... You have taught me what love is - and I shall never forget it.

Resumo da Tese apresentada à COPPE/UFRJ como parte dos requisitos necessários para a obtenção do grau de Doutor em Ciências (D.Sc.)

ANÁLISE NUMÉRICA DE MECANISMOS QUÍMICO-ELETROQUÍMICOS EM SISTEMAS DE ELETRODO DE DISCO ROTATÓRIO

Pedro Henrique Moura Leal

Junho/2019

Orientadores: Oscar Rosa Mattos
Oswaldo Esteves Barcia

Programa: Engenharia Metalúrgica e de Materiais

Nesta tese, apresentamos um estudo aprofundado de mecanismos químico-eletroquímicos em sistemas de eletrodo de disco rotatório tanto em estado estacionário quanto em estado transiente. Neste intuito, discretizamos as equações exatas de convecção-difusão-reação utilizando o método das diferenças finitas em malhas lineares ou exponencialmente espaçadas, evitando a introdução de novas simplificações. Diferentes combinações de parâmetros (velocidade de rotação, número de Schmidt e constantes de reação) foram utilizados para analisar seus efeitos na densidade de corrente limite, na impedância de difusão e na impedância eletro-hidrodinâmica. Nossos resultados estacionários mostram que, mesmo em sistemas com constantes de reação elevadas, a hipótese da camada de reação sempre se mostrará falsa para velocidades de rotação suficientemente altas. Assim, um sistema de cinética rápida é simplesmente aquele para o qual a hipótese da camada de reação é válida para toda a faixa de velocidade de rotação investigada. Os resultados transientes mostram que a combinação de impedância de difusão e de impedância eletro-hidrodinâmica é capaz de identificar mecanismos químicos-eletroquímicos. Por fim, também investigamos como as variações da velocidade de rotação, da constante de equilíbrio e do número de Schmidt podem alterar as curvas de impedância obtidas, o que pode ser utilizado para ajuste de curvas experimentais.

Abstract of Thesis presented to COPPE/UFRJ as a partial fulfillment of the requirements for the degree of Doctor of Science (D.Sc.)

NUMERICAL ANALYSIS OF CHEMICAL-ELECTROCHEMICAL MECHANISMS IN ROTATING DISK ELECTRODE SYSTEMS

Pedro Henrique Moura Leal

June/2019

Advisors: Oscar Rosa Mattos
Oswaldo Esteves Barcia

Department: Metallurgical and Materials Engineering

In this thesis, we present a thorough study of chemical-electrochemical mechanisms in rotating disk electrode systems. For that purpose, we used the finite differences method to discretize the exact convection-diffusion-reaction equations in linear or exponentially spaced grids, taking care to avoid additional simplifications. Different sets of parameters (rotation speed, Schmidt number and reaction rate constants) were used to analyse their effects on the limiting current density, on the diffusion impedance and on the electro-hydrodynamic impedance. Our steady state results show that, even in systems with high reaction rate constants, the reaction layer hypothesis will fail for sufficiently high rotation speeds. Hence, a system with fast kinetics can be defined one for which the reaction layer hypothesis is valid for the whole rotation speed range investigated. The results for transient state show that combining diffusion impedance and electro-hydrodynamic impedance measurements is useful in identifying chemical-electrochemical mechanisms. Finally, we also investigated how varying the rotation speed, the equilibrium constant and the Schmidt numbers affects the impedance curves, which can be used for fitting experimental curves.

Table of Contents

List of Figures xi

List of Tables xiv

List of Symbols xv

List of Acronyms and Abbreviations xvii

1 Introduction 1

2 Theoretical background 4

2.1 Laying the bricks, paving the road 4

2.2 Heterogeneous charge transfer processes 4

2.3 Charge separation and the electrical double layer 6

2.4 Mass transport in electrolyte solutions 7

2.4.1 General equations and initial hypotheses 7

2.4.2 Migration 9

2.4.3 Diffusion 9

2.4.4 Convection 11

2.4.5 The electroneutrality hypothesis 12

2.4.6 Transport laws for ideal, dilute solutions 13

2.4.7 The role of the supporting electrolyte 13

2.4.8 Electrode surface and the solution bulk 14

2.4.9 Homogeneous reactions 15

2.4.10 What about the system? 17

2.5 Rotating disk electrodes 17

2.5.1 Fluid flow in RDE systems 18

2.5.2 Mass transfer in RDE systems 21

2.5.3 Validation and further improvements 25

2.5.4 The study of transient phenomena with RDE systems 27

2.6 Electrochemical impedance 27

2.6.1 Definition of impedance 27

2.6.2 Non-linearity of electrochemical systems . . . 28
2.6.3 Mass transport effects: Diffusion impedance . . . 30
2.7 Electro-hydrodynamic impedance . . . 39
2.7.1 Unsteady velocity profiles . . . 40
2.7.2 Unsteady concentration profile . . . 41
2.7.3 Potentiostatic control . . . 43
2.7.4 Galvanostatic control . . . 44
2.7.5 Application in the study of reaction mechanisms . . . 44
2.8 Any bricks left? . . . 45

3 Literature review **46**
3.1 Chemical-electrochemical processes . . . 46
3.1.1 Steady state current density . . . 47
3.1.2 Diffusion impedance . . . 50
3.1.3 Electro-hydrodynamical impedance . . . 52
3.2 Midway along the road . . . 52

4 Numerical methodology **54**
4.1 Relevant equations . . . 54
4.1.1 Limiting current condition . . . 55
4.1.2 Diffusion impedance . . . 56
4.1.3 Electro-hydrodynamic impedance . . . 57
4.2 Discretization procedure . . . 58
4.2.1 Linear grids . . . 59
4.2.2 Nonlinear grids . . . 63
4.3 Solution procedure . . . 65
4.3.1 Simulation parameters . . . 67
4.4 Validation procedure . . . 68
4.5 Almost there . . . 70

5 Results and discussion **71**
5.1 Steady state . . . 71
5.1.1 Fast kinetics . . . 71
5.1.2 Slow kinetics . . . 75
5.1.3 Comparison with literature data . . . 76
5.2 Transient state . . . 79
5.2.1 Effect of the rotation speed . . . 79
5.2.2 Effect of the equilibrium constant . . . 85
5.2.3 Effect of Sc_A and Sc_B . . . 88
5.2.4 Comparison with literature data . . . 93

5.3 Here, at last 95

6 Conclusions **97**

6.1 Time to move on 99

References **100**

A Mass conservation **108**

B Terminal velocity of ions in solution **110**

List of Figures

1.1 Example of cell assembly and working electrode used in RDE systems. . 2

2.1 Steps involved in a charge transfer heterogeneous process [19]. 5
2.2 Graphical representation of the electrical double layer according to the model proposed by Grahame [20]. 7
2.3 Sketch of a rotating disk electrode. Arrows represent the streamlines of the fluid. Adapted from [28]. 18
2.4 Cross section view (A) and side view (B) of the streamlines for the RDE system. Adapted from [8]. 21
2.5 Dimensionless concentration profile in an RDE system 26
2.6 Nyquist plot of a faradaic impedance given by equation 2.118.(R_{ct} = 5 ohm.cm^2, $k_h/\sqrt{D}$ = 0.8 cm.^{2}s$^{-1/2}$) 33
2.7 Nyquist plot of the global impedance of the system presented in figure 2.6.(R_{ct} = 5 ohm.cm^2, $k_h/\sqrt{D}$ = 0.8 cm.^{2}s$^{-1/2}$, R_e = 3 ohm.cm^2, C_{dl} = 100 μF/cm^2) 33
2.8 Nyquist plot of the faradaic impedance represented by equation 2.129. (R_{ct} = 3 ohm.cm^2, $R_{ct}k_h$ = 4 10^{-3} ohm.cm^2.s^{-1}, D = 9 10^{-9} m^2.s^{-1}, δ_D = 1.13 10^{-5} m) 35
2.9 Comparison between Warburg impedance and the diffusion impedance for finite δ_D. 36
2.10 Nyquist plot of the normalized diffusion impedance for a RDE system. Marks represent experimental data. Line *a* represents the diffusion impedance found by fitting the data to equation 2.129. Line *b* represents the diffusion impedance calculated by Coueignoux and Schuhmann [56]. (Adapted from [57]) 38
2.11 Bode plots of the EHD impedance for a system with facile kinetics at the limiting current condition 44

3.1 Nyquist plot of the reduced diffusion impedance as a function of reduced frequency u for different values of $K = k_A/k_B$ and χ ($Sc = 1000$): $(1)K = 0.01, \chi = 0.01$; $(2)K = 1, \chi = 1$;$(3)K = 2, \chi = 4$; $(4)K = 5, \chi = 10$; $(5)K = 10, \chi = 50$. Adapted from [16]. 51

4.1 Comparison between i_{lim} values calculated according to different procedures as a function of $\Omega^{1/2}$ 69
4.2 Nyquist plot for the diffusion impedance calculated according to our model and that of Levart and Schuhmann. ($Sc_A = Sc_B = 500$, $k_A = 5\ s^{-1}$, $k_B = 10^{-2}\ s^{-1}$) 69
4.3 Comparison of reduced amplitude and -phase as a function of reduced frequency between our model and that of Tribollet and Newman ($Sc_A = Sc_B = 1000$, $k_A = 5\,10 - 8\ s^{-1}$, $k_B = 5\,10^{-5}\ s^{-1}$) 70

5.1 i_{lim} *vs* $\Omega^{1/2}$ for systems with fast kinetics: a) $K = 1$; b) $K = 10$; c)$K = 100$; d) $K = 5\,10^4$. 71
5.2 Normalized values of C_A/C_B as a function of ξ. 72
5.3 Divergence between numerical solution and the Dogonadze equation for very high rotation speeds. 73
5.4 $(i_{lim})^{-1}$ *vs* $\Omega^{-1/2}$ graphs for different ranges of rotation speed. 74
5.5 i_{lim} *vs* $\Omega^{1/2}$ for a system with slow kinetics: a) K = 1; b) K = 10; c) K = 100. 75
5.6 i_{lim} *vs* $\Omega^{1/2}$ for systems with K = 1 and different k_A/k_B values. 77
5.7 i_{lim} *vs* $\Omega^{1/2}$ for systems with K = 1 and different k_A/k_B values. 77
5.8 C_A/C_B *vs* ξ for system expected to fail the reaction layer hypothesis according to Compton *et al.*[14]. ($D_A = 4\,10^{-9}\ m^2s^{-l}$, $D_B = 1\,10^{-9}\ m^2s^{-l}$, $\upsilon = 10^{-6}\ m^2s^{-l}$) 78
5.9 Nyquist plot of Z_D for system with slow kinetics at different rotation speeds. 80
5.10 Nyquist plot of Z_D for system whose parameters are equal to those in figure 5.9, but in the absence of homogeneous reactions. 80
5.11 Nyquist plot of Z_D for system with fast kinetics at different rotation speeds: a) General overview highlighting the convection-diffusion loop. b) Zoom at the high frequency region which displays the reaction loop. . . 81
5.12 Log-log plot of the reaction impedance characteristic frequency as a function of the reaction layer thickness ($Sc_A = 111.11$, $Sc_B = 500$, $\Omega = 1$ Hz, $k_B = 5\,10^{-1}\ s^{-1}$). 82
5.13 Nyquist plot of the overall impedance of a system with fast kinetics (Parameters are equal to those of the system presented in figure 5.11) 83
5.14 Reduced amplitude and negative phase as a function of dimensionless frequency for system with slow kinetics at different rotation speeds. . . . 83

5.15 Reduced amplitude and negative phase as a function of dimensionless frequency for system with fast kinetics at different rotation speeds. 83
5.16 Nyquist plot of Z_{EHD} for different rotation speeds. 84
5.17 Comparison of reduced amplitude and negative phase for systems with equal Schmidt numbers (of the electroactive species) in the presence and in the absence of homogeneous reactions. 85
5.18 Nyquist plots for the diffusion impedance of systems with a) fast and b) slow kinetics for different combinations of k_A and k_B. (Ω = 10 Hz; Sc_A = 111.11; Sc_B = 500) 86
5.19 Comparison of the concentration profile between a system without bulk reactions and one with a low equilibrium constant. 87
5.20 Reduced amplitude and phase as a function of dimensionless frequency for systems with slow kinetics and different equilibrium constants. 87
5.21 Reduced amplitude and phase as a function of dimensionless frequency for systems with fast kinetics and different equilibrium constants. 88
5.22 Nyquist plot of Z_{EHD} for systems with different equilibrium constants: a) slow kinetics; b) fast kinetics. 88
5.23 Nyquist plot of Z_D for systems with Sc_A values: a) fast kinetics and b) slow kinetics. 89
5.24 Nyquist plot of Z_{EHD} for systems with Sc_A values: a) slow kinetics and b) fast kinetics. 90
5.25 Nyquist plot of Z_D for systems with Sc_B values: a) fast kinetics and b) slow kinetics. 91
5.26 Nyquist plot of Z_{EHD} for systems with Sc_B values: a) fast kinetics and b) slow kinetics. 92
5.27 Transient concentration profiles of species B at ω = 0 Hz for systems with different Sc_B values: a) slow kinetics and b) fast kinetics. 92
5.28 Nyquist plot comparing Z_D values for two different potentials. (Sc_A = 111.11, Sc_B = 500, Ω = 10 Hz, k_A = 5 s^{-1}, k_B = 5 s^{-1}, k^0 = 10^{-1} m s^{-1}, b = 15 V^{-1}) 93
5.29 Reduced amplitude and negative phase as a function of $pSc^{1/3}$ for systems with σ = 100 and a = 100. 94
5.30 Reduced amplitude and negative phase as a function of $pSc^{1/3}$ for systems with σ = 100 and a = 10. 95
5.31 Reduced amplitude and negative phase as a function of $pSc^{1/3}$ for systems with σ = 100 and a = 5. 95

List of Tables

4.1 Simulation parameters used in this work and typical execution time ($Sc_A = 111.11$, $Sc_B = 500$, $k_A = 5\,10^3$ s^{-1}, $k_B = 5\,10^2$ s^{-1}, $\Omega = 5$ Hz, $E = 0.5$ V, $k_h = 1\,10^{-1}$m s^{-1} and $b_h = 15$ V^{-1}) 67

4.2 Kinetic constants used in the steady state simulations 67

4.3 Combinations of parameters used in the transient simulations 68

5.1 n_{eff} values reported by Compton *et al.* for different sets of parameters [14]. ($D_A = 4\,10^{-9}$ m^2s^{-l}, $D_B = 1\,10^{-9}$ m^2s^{-l}, $v = 10^{-6}$ m^2s^{-l}, $K = 10^2$) . 76

List of Symbols

C_{dl}	Double layer capacitance, p. 5
D_i	Diffusion coefficient of species i, p. 9
E	Interfacial Potential, p. 28
F	Faraday constant, p. 7
I	Current or total current, p. 27
K	Chemical equilibrium constant, p. 47
N_A	Avogadro's constant, p. 8
Sc	Schmidt number, p. 22
ΔX	Transient component of function X, p. 27
Ω	Angular velocity of the RDE, p. 18
Φ	Electrostatic potential in solution, p. 7
Θ	Relaxation factor used for numerical calculations, p. 66
$\bar{X}$	Steady state variable, p. 28
β_i	Coefficient used to calculate first derivatives in nonlinear grids using the Fornberg algorithm, p. 64
χ	Electric field, p. 8
δ_0	Hydrodynamic boundary layer thickness, p. 20
δ_D	Diffusion layer thickness, p. 9
δ_R	Reaction layer thickness, p. 47
δ_i	Coefficient used to calculate second derivatives in nonlinear grids using the Fornberg algorithm, p. 64

ϵ	Ratio between the oscillating, $\Delta\Omega$, and the stationary, $\bar{\Omega}$, components of the rotation speed., p. 39
J	Imaginary number $\sqrt{-1}$, p. 27
$\mathbf{J}_i$	Molar flux density of species i, p. 7
$\mathbf{i}$ or i	Current or total current density, p. 7
μ	Dynamic viscosity, p. 8
ν	Kinematic viscosity, p. 11
φ	Phase shift of a transfer function, p. 27
ρ	Fluid density, p. 10
ρ_c	Charge density, p. 7
$\tilde{X}$	Amplitude of transient component ΔX, p. 28
ε	Electric permittivity, p. 7
c_i or C_i	Molar concentration of species i, p. 7
f_D^*	Characteristic frequency of the convection-diffusion impedance, p. 84
f_R^*	Characteristic frequency of the reaction impedance, p. 81
i_{lim}	Limiting current density, p. 54
p	Dimensionless frequency, p. 40
r_i	Radius of ion i, p. 8
u_i	Electrochemical mobility of ion i, p. 8
z_i	Electric charge of species i, p. 7
q	Electrical charge, p. 5

List of Acronyms and Abbreviations

CE	Chemical-Electrochemical, p. 1
EDL	Electrical double layer, p. 4
EHD	Electro-hydrodynamic impedance, p. 38
IHP	Inner Helmholtz Plane, p. 5
OHP	Outer Helmholtz Plane, p. 5
RDE	Rotating Disk Electrode, p. 1

Chapter 1

Introduction

Since the discovery of the pre-salt layer in the Brazilian shore, much research has been devoted to overcoming the challenges imposed by the extreme conditions found therein [1, 2]. For instance, one has to deal with high concentrations of CO_2 and H_2S, which increase the corrosion rate of the pipelines used for oil extraction and transportation [3, 4]. In face of the need for a better understanding of the new operation conditions, our lab started a systematic investigation of how these substances could influence the corrosion mechanism of different alloys.

The development of proper corrosion mechanisms must rely on both experimental and theoretical work, the latter being done with the help of mathematical modelling of the processes involved (mass transport, chemical and electrochemical reaction etc). Because CO_2 and H_2S form weak acids when dissolved in water, their presence in solution acts as a H^+ buffer, thus affecting the cathodic side of the corrosion mechanism [5, 6]:

$$\begin{cases} H_2S \rightleftharpoons HS^- + H^+ \\ H^+ + e^- \longrightarrow \frac{1}{2} H_2 \end{cases} \qquad \begin{cases} CO_2 + H_2O \rightleftharpoons HCO_3{}^- + H^+ \\ H^+ + e^- \longrightarrow H_2 \end{cases} \tag{1.1}$$

For both cases, we observe that there is a chemical step *preceding* the electrochemical reaction. Indeed, in a simplified model, they could be represented as:

$$\begin{cases} A \rightleftharpoons B \\ B + e^- \longrightarrow C \end{cases} \tag{1.2}$$

Hence, we realized that a study of a general CE mechanism could shed light on the behaviour of real systems, like those taking place at the high depths of the pre-salt layer. In particular, having a mathematical model would allow us to confront experimental data. The idea to produce this thesis originated from this insight. Nevertheless, we still needed to decide which electrode configuration we would simulate. By virtue of the lab expertise, our choice was for the rotating disk electrode.

The rotating disk electrode (RDE) is one of the most important electrode configurations known to the electrochemist. It is easy to set up and manipulate (see fig. 1.1), but, more importantly, it has a firm theoretical basis which has been successfully used in interpreting experimental data [7]. Once conceived as a tool to extract steady state information (mostly, the electrode current), the RDE was soon applied to the study of transient phenomena. Again, a large body of theory was developed to provide a way for the experimentalist to extract useful parameters from data [8].

(a) Electrochemical cell used for experiments with RDE [9].

(b) Closer look at a rotating disk electrode [10].

Figure 1.1: Example of cell assembly and working electrode used in RDE systems.

Nevertheless, most of the theory is devoted to systems whose mechanisms involve a single charge transfer step without kinetic complications. The study of more complex systems - for instance, chemical-electrochemical (CE) processes, in which the electrochemical step is preceded by a chemical one - has usually followed two ways. One is the use of additional hypotheses to simplify the model equations, providing an analytical treatment that is useful, but restricted to particular situations [11, 12]. The other is the development of numerical procedures to solve the relevant equations. Currently, the latter approach is the only way to scrutinize the behaviour of CE processes with arbitrary parameters [13–16].

Although different numerical and semi-analytical methods have been employed [17, 18], there has not been a work which combines both steady state and impedance simulations, especially the diffusion impedance and the electro-hydrodynamic impedance, without resorting to further simplifications. Hence, a procedure able to tackle the *exact* governing equations is lacking.

The purpose of this thesis is to scrutinize an aspect which has been neglected by the existing literature: a thorough study of CE reactions without invoking additional hypotheses. Therefore, our aim is to explore the limitations of the other approaches as well as the

behaviour of systems which cannot be described by these more restrictive models. For this purpose, we use a numerical procedure capable of solving the exact equations governing the behaviour of CE processes in RDE systems. In particular, we focus on the study of the steady state behaviour (limiting current density) and of the mass-transfer transient processes (diffusion impedance and electro-hydrodynamic impedance).

The text is divided in six chapters: Chapter 2 introduces basic electrochemical concepts necessary to develop the model equations for the problem. Chapter 3 presents a literature review of the different procedures used to solve steady and transient state problems of CE processes in RDE systems. In chapter 4, we detail the numerical procedure employed and the methodology used to analyse the effect of different parameters. Results are presented and discussed in chapter 5. Lastly, chapter 6 contains our final conclusions and future works to be developed.

We are about to embark on a journey in search of knowledge. Although we know where we want to go, we haven't figured out which trails to take yet. But we are not worried, because we are not alone; we can count on those who came before to guide us with their knowledge until we are ready to continue on our own. Certainly, this adventure will not be an easy one, but it wouldn't be worth anything otherwise.

There's only one question to answer before we begin: is the reader ready to join us?

Chapter 2

Theoretical background

2.1 Laying the bricks, paving the road

The modelling of electrochemical processes is a very rich and diverse research field. During the course of this thesis, several different results will be presented and much of the discussion will be on a level of development in which we will be asking questions of the kind: what are the underlying hypotheses of this model? How can we interpret *this* result considering *that* result? Which mechanism is able to compile all this information without leaving any gaps? There's no doubt that these are truly essential questions which are intrinsically connected to the main goals of this thesis. However, before addressing the actual scope of this text, chemical-electrochemical reactions, it is much more important to determine *how* we are going to investigate it and *why* we chose this route. In a sense, this fundamental knowledge constitutes the road that will lead us to the matters that really interest us. This chapter is devoted to paving this road.

2.2 Heterogeneous charge transfer processes

Contrary to the so-called *homogeneous* reactions, which may happen at any point inside a single phase, electrochemical reactions always occur at an *interface*, hence the denomination *heterogeneous* commonly used to describe them. More precisely, charge transfer takes place at the interface between metal (an electronic conductor, or *electrode*) and solution (an ionic conductor, or *electrolyte*). Nevertheless, a simple charge transfer is not enough to apprehend the whole dynamics of the system. The following figure, figure 2.1, demonstrates the other steps involved in a reaction of the kind:

$$O + ne^- \underset{k_{-1}}{\overset{k_1}{\rightleftharpoons}} R \tag{2.1}$$

This example points out two important aspects:

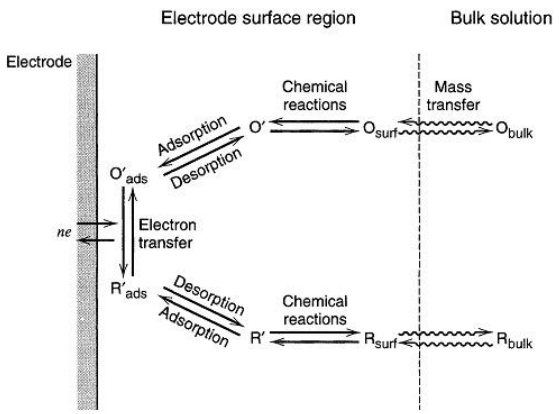

Figure 2.1: Steps involved in a charge transfer heterogeneous process [19].

- Since the charge transfer is located at the metal/solution interface, transport phenomena associated with the coming and leaving of electroactive species have to be taken into consideration. Besides, such species may adsorb on the electrode surface, *i.e.*, accumulate at the interfacial region due to electrostatic interactions, formation of covalent bonds or dipole effects [20, 21]. The sequential nature of these steps makes them as important as the electron transfer when computing transfer rates, measured in the form of electric current.

- Steady state measurements, *i.e.*, measurements made when the variable in question is no longer time-dependent, are, in principle, insufficient to describe the system properly. Why is that? Considering an *a priori* lack of knowledge of the dynamics, it's not possible to identify exactly the contribution of each step to the steady state current. Only at very specific cases, such as those specified for the proper use of the rotating disk electrode (RDE), it is possible to build a model with explicit expressions for both kinetic and mass transter rates [19]. Even so, RDE equations are unable to provide further information regarding homogeneous reactions, adsorption/desorption phenomena or even the origin of the mass transfer limitation (formation of solid film, colloidal dispersions or partially blocked surfaces [22]). Therefore, the use of techniques that allow the identification of the number of steps involved, their nature and their impact on the overall current is essential. These techniques, known as *transient techniques*, form the basis of modern electrochemical methods.

Now, a general picture of the systems we are going to model has been drafted. However, before moving on, it is important to realize that, for a charge transfer to occur, there must be an *electrical potential gradient* across the electrode/electrolyte interface. *Why* would such a potential exist and *how* could it emerge? These fundamental questions will lead us to a brief discussion about the region comprised of this very thin layer between electrode and electrolyte solution called the *electrical double layer* (EDL) [19].

2.3 Charge separation and the electrical double layer

One could argue that the development of a potential difference across the electrode/electrolyte interface is a result of the loss of symmetry that would, otherwise, exist in a homogeneous system (such as the solution bulk) [23]. In that respect, it is the very *existence* of this interface that will inevitably lead, *e.g.*, to a localized alignment of dipoles and electrons, resulting in a non-zero electric field. It is this charge separation phenomenon that gives rise to the *electrical double layer*. For matters of simplicity, we'll deal exclusively with interfaces developed between solid metallic electrodes and aqueous electrolyte solutions.

The formation of the EDL involves the segregation of positive and negative charges on the electrode/electrolyte solution interface, which may take place in the form of dipoles, polarized atoms, ions etc [20]. This segregation may occur because of preferential adsorption or the application of an external potential, for example. The build-up of charges on the solution side, q^S, leads to an equal build-up on the electrode surface, q^M, and the distance between the charged surfaces may be as small as 100 Å [19]. A careful examination allows us to notice the similarity between the EDL structure and that of a capacitor and, in fact, it is very common to characterize the former (for a given electrode/electrolyte solution pair) using a capacitance (C_{dl}). It must be said, though, that the double layer capacitance differs from the ideal capacitor because it depends, among other parameters, on the applied potential.

A more detailed description of the double layer structure, due to the work of Grahame, is presented in figure 2.2. It shows that the EDL is, in fact, divided in three regions [20, 24, 25]. The innermost, which is adjacent to the electrode surface, is composed of specifically adsorbed ions and water dipoles. The electrical center of these species is aligned and defines the so-called *inner Helmholtz plane* (IHP). Next to this layer, there is the one formed by solvated cations, or nonspecifically adsorbed anions, and their centers define the *outer Helmholtz plane* (OHP). Finally, between the OHP and the solution bulk, there is the *diffuse layer* composed of solvated species whose distribution is defined by an equilibrium between thermal motion and long range electrostatic forces. Here, we must make a distinction between the *diffuse* and the *diffusion* layers. Although it is possible for both to present a concentration gradient, there's a net charge accumulation in the diffuse layer, but not in the diffusion layer [25].

The complex structure of the EDL has been found to not only influence the results of electrochemical measurements, but the electrode kinetics itself. A classical treatment, given by Frumkin, illustrates two immediate impacts [19, 20, 25].

- If the electroactive species is not specifically adsorbed, for example, the driving force of the charge transfer will not be the potential difference between metal and the solution bulk, but roughly the potential difference between metal and the OHP.

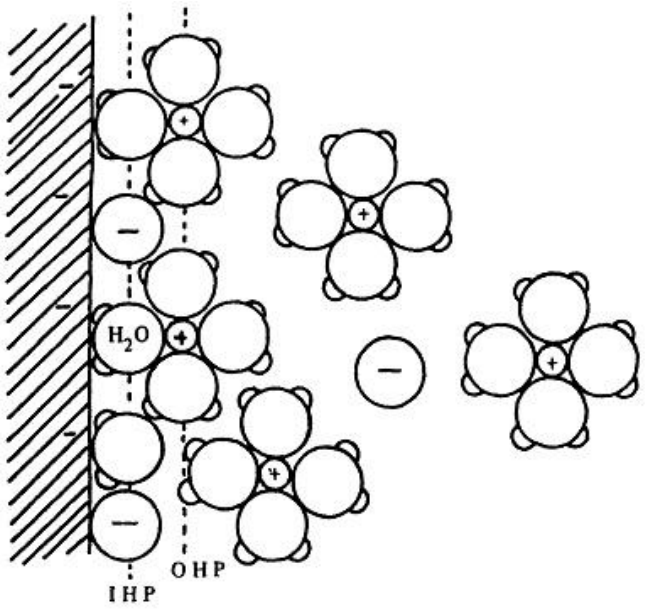

Figure 2.2: Graphical representation of the electrical double layer according to the model proposed by Grahame [20].

- Also, the concentration of these species at the OHP differs from that of the bulk solution and must be corrected.

Clearly, the existence of the EDL is not a mere theoretical artefact used to provide consistency to the electrochemical theory. Instead, it is at the heart of the charge separation phenomenon that is observed in electrode/electrolyte solution interfaces. As will be seen later, it has also an influence on the results of electrochemical impedance experiments, one of the major transient techniques used to investigate electrochemical systems.

Would a theory of charge transfer be sufficient to properly describe electrochemical systems? If we go back to figure 2.1, we'll see that any description of these systems is not complete until it takes the *mass transport* of electroactive species into account. Even in situations in which we want to focus solely on the kinetic effects, a proper knowledge of the transport phenomena is necessary to exclude their contribution to the electrode current. On the other hand, one might also be interested in designing systems in which the mass transport effects on the electrode current will provide key information on the global reaction mechanism - an approach which captures the essence of this thesis.

2.4 Mass transport in electrolyte solutions

2.4.1 General equations and initial hypotheses

The transport of ionic species in solution can be divided in three components: diffusion, convection and migration. Hence, the overall molar flux density, *i.e.*, the number

of moles crossing an unit area per unit time, of any species i will be the sum of each component contribution:

$$\mathbf{J}_i = \mathbf{J}_{i,d} + \mathbf{J}_{i,c} + \mathbf{J}_{i,m} \tag{2.2}$$

Where $\mathbf{J}_{i,d}$ stands for the diffusion flux density; $\mathbf{J}_{i,c}$, for the convective flux density and $\mathbf{J}_{i,p}$, for the migration flux density.

Since the electrical current density, $\mathbf{i}$, is the net charge per area transferred over time, the overall current density can be easily calculated from the flux densities:

$$\mathbf{i} = \sum_i z_i F \mathbf{J}_i = F \sum_i z_i \mathbf{J}_i \tag{2.3}$$

Where z_i corresponds to the electric charge of species i and F is the Faraday constant.

Also, if we apply the principle of mass conservation (a proof of this result can be found in section A of the appendix) to any species i, whose concentration is given by c_i, we find that:

$$\frac{\partial c_i}{\partial t} = -\nabla \cdot \mathbf{J}_i + R_i \tag{2.4}$$

Where R_i represents the homogeneous reactions which may take place at the solution bulk.

Finally, we can use Poisson's equation, which relates electrostatic potential, Φ, and charge density, ρ_c:

$$\nabla^2 \Phi = -\frac{\rho_c}{\varepsilon} \tag{2.5}$$

Where ε corresponds to the permittivity of the medium.

These four equations constitute the basis upon which we shall develop a model for the electrochemical systems. Moving on, we present two hypotheses that will allow us to simplify our model:

- The following developments are restricted to ideal solutions. This allows us to neglect several different interactions between ionic species and complicating factors, such as friction coefficients; thus, greatly simplifying the final equations [25, 26].

- The medium is one of homogeneous permittivity, which allows us to rewrite equation 2.5 as:

$$\nabla^2 \Phi = -\frac{F}{\varepsilon} \sum_i z_i c_i \tag{2.6}$$

We are now ready to discuss analytical expressions for each of the fluxes mentioned above. Further hypotheses will be presented as we detail the model.

2.4.2 Migration

Migration is the motion of charged particles due to the existence of an electric potential gradients in solution. Therefore, this kind of transport does not affect neutral species, such as water molecules. Even though a charged particle would tend to accelerate in the presence of an electric field, experiments show that ions in solution move at a constant speed. The reason for this is that there is a *drift force* due to the viscosity of the fluid which compensates the electromagnetic force. Thus, the average velocity of ions in solution has been estimated to be [27]:

$$\bar{\mathbf{v}}_i = \frac{z_i F \chi}{6\pi\mu r_i N_A} \tag{2.7}$$

Where χ stands for the electric field, μ for the dynamic viscosity of the solution, r_i for the radius of the ion and N_A for Avogadro's constant. A derivation of this result can be found in section B of the appendix.

Now that we know the average velocity of a charged particle in an electric field, we can use it to calculate the migration flux density. A general form of any flux density is:

$$\mathbf{J}_i = c_i \bar{\mathbf{v}}_i \tag{2.8}$$

However, instead of using the explicit equation for the velocity, it is more common to work with the *electrochemical mobility*, u_i, which represents the ratio between terminal velocity and the driving force for migration [28]. The value of u_i can be calculated as:

$$u_i = \frac{N_A v_i}{z_i F \chi} \tag{2.9}$$

Hence, equation 2.8 becomes:

$$\mathbf{J}_{i,m} = z_i F c_i u_i \chi \tag{2.10}$$

Lastly, we can substitute the electric field for the electrical potential, which is easier to manipulate. Knowing that both are related by $\chi = -\nabla\Phi$ leads to the final form of the migration flux:

$$\mathbf{J}_{i,m} = -z_i F u_i c_i \nabla\Phi \tag{2.11}$$

2.4.3 Diffusion

Diffusion expresses the movement of molecules due to a *chemical potential gradient* ($\nabla\mu$) within the solution [29].

$$\mathbf{J}_{i,d} \propto \nabla\mu_i \tag{2.12}$$

If experiments are performed under more restricted conditions, such as those of dilute and ideal solutions, one finds that the diffusion flux is *also* proportional to the concentration gradient. Therefore, we must bear in mind that *the usual view of diffusion as a*

product of concentration differences is an approximation of a more complex theory. For this simpler case, two very important equations can be used to quantitatively describe the diffusion phenomenon and its impact on the concentration profile of the species involved. The former is known as *Fick's first law*, which states that:

$$\mathbf{J}_{i,d} = -D_i \nabla c_i \tag{2.13}$$

Where D_i corresponds to the *diffusion coefficient* of species i. In this formulation, we have tacitly assumed that the diffusion coefficient of any species is constant for a given pressure and temperature.

Because the diffusion flux can only be established once a concentration difference arises, one can also expect a dependence of concentration on time. This time dependence is given by *Fick's second law*, which is no more than the conservation equation restricted to diffusion flux:

$$\frac{\partial c_i}{\partial t} = -\nabla \cdot \mathbf{J}_{i,d} \implies \frac{\partial c_i}{\partial t} = D_i \nabla^2 c_i \tag{2.14}$$

For species which are either generated or consumed at the electrode surface, a concentration build-up/depletion will take place, causing the concentration profile to differ from the *average* concentration value at the solution bulk. The length of this region, known as the *diffusion layer thickness* (δ_D), is a typical parameter used to estimate the extent of diffusion and depends on the experimental conditions [29]. Under steady state and unidirectional flow, the diffusion flux has a very simple form when the process takes place between two regions of fixed concentration:

$$\frac{\partial c_i}{\partial t} = 0 \implies \nabla \cdot \mathbf{J}_{i,d} = 0 \tag{2.15}$$

$$\mathbf{J}_{i,d} = D_i \frac{c_i^b - c_i^s}{\delta_D} \tag{2.16}$$

Where c_i^b is the concentration at the solution bulk and c_i^s is the concentration at the electrode surface.

Hence, when the electrochemical process is diffusion-controlled, the current density may be calculated as follows:

$$i = zFD_i \frac{c_i^b - c_i^s}{\delta_D} \tag{2.17}$$

The use of equation 2.17 to interpret electrochemical data is due to Nernst. He proposed that, inside the diffusion layer, there was no fluid motion and, so, a concentration gradient could be developed. For stationary processes, this also means that the concentration profile within the boundary layer must be linear [7]. Although simple, Nernst's idea of using a linear profile to estimate the diffusion layer thickness has proved use-

ful in many practical applications and is still used to this date, being sometimes labelled *Nernst's diffusion layer*.

2.4.4 Convection

Convection means the transport of dissolved species due to *fluid motion*. Consequently, it is independent of any property of the solutes (such as their charge) and is caused by a pressure or temperature gradient within the fluid [30]. The flux generated can be expressed as:

$$\mathbf{J}_{i,c} = c_i \mathbf{v} \tag{2.18}$$

Where $\mathbf{v}$ represents the average velocity field of the fluid.

Convective motion may be set in a deliberate way, for instance by mechanically stirring the solution, or it may happen due to natural processes - *e.g.*, density gradients and gravitational forces. The former is labelled *forced convection* and, the latter, *natural convection*.

To determine the velocity field, we must resort to the equations of fluid mechanics. The first one concerns the conservation of fluid mass, also known as the continuity equation [31]:

$$\frac{\partial \rho}{\partial t} = -\nabla \cdot (\rho \mathbf{v}) \tag{2.19}$$

Where ρ corresponds to the fluid density.

The second one deals with linear momentum conservation [31]:

$$\frac{\partial \mathbf{v}}{\partial t} + \mathbf{v} \cdot \nabla \mathbf{v} = -\frac{1}{\rho} \nabla p + \frac{1}{\rho} \nabla \cdot \tau + \mathbf{g} \tag{2.20}$$

Where p denotes the pressure field; τ, the viscous stress tensor and $\mathbf{g}$, the gravitational acceleration.

Because of its non-linearity, equation 2.20 present a degree of complexity which renders impossible any analytical treatment. Nonetheless, a few additional considerations can be made to help simplifying the problem. These new hypotheses will be considered valid in further treatment of fluid behaviour throughout this thesis:

- The fluid is *incompressible*, *i.e.*, it has constant density both in space and time. Consequently, equation 2.19 reduces to:

$$\nabla \cdot \mathbf{v} = 0 \tag{2.21}$$

- The fluid is *newtonian*, so its viscous stress vector is symmetric and given by:

$$\tau = \mu \left(\nabla \mathbf{v} + \nabla \mathbf{v}^{\mathrm{T}} \right) \tag{2.22}$$

This way, equation 2.20 can be rewritten as:

$$\frac{\partial \mathbf{v}}{\partial t} + \mathbf{v} \cdot \nabla \mathbf{v} = -\frac{1}{\rho}\nabla p + \upsilon \nabla^2 \mathbf{v} + \mathbf{g} \tag{2.23}$$

Where υ represents the *kinematic viscosity* of the fluid. This vector equation is referred to as the *Navier-Stokes equation* [31].

2.4.5 The electroneutrality hypothesis

A widely adopted hypothesis in electrochemical models is the *electroneutrality hypothesis*:

$$\sum_i z_i c_i = 0 \tag{2.24}$$

There is, however, a misconception about the ideas that lead to this assumption. Even though it is often portrayed as a fundamental property of these systems, the electroneutrality condition is an approximation [25, 26, 32]. We have already pointed out that the actual equation describing the distribution of net charge is given by Poisson's equation:

$$\nabla^2 \Phi = -\frac{F}{\varepsilon} \sum_i z_i c_i$$

How, then, can we get from equation 2.6 to equation 2.24? First, notice that the order of magnitude of the term $\frac{F}{\varepsilon}$ is about 10^{14} V m^{-1} s^{-1} for typical aqueous solutions. Additionally, most experiments are conducted with excess supporting electrolyte (more on this topic later) and, as a result, the electric field is nearly constant throughout most of the solution and its gradient is many orders of magnitude smaller than 10^{14} V m^{-2}. Accordingly, a very small difference between anion and cation concentrations is necessary to generate these electric field gradients. Indeed, it has been shown that even in solutions of binary electrolytes, in which migration effects are usually more pronounced, an imbalance between 10^{-11} and 10^{-7} mol L^{-1} would be sufficient to generate the calculated electric field gradients [25, 26]. Most experiments employ concentrations much higher than these and the bulk concentrations remain essentially unaltered, thus, justifying the electroneutrality hypothesis.

This rationale leads to two very important observations. First, at no point was it said that the electroneutrality hypothesis implies the Laplace equation for potential:

$$\nabla^2 \Phi = 0 \tag{2.25}$$

As a matter of fact, the correct approach when including electroneutrality is to *adopt it instead of Poisson's equation*. The negligible value of net charge density does not allow us to conclude that $\nabla^2 \Phi$ is also negligible on account of the very high value of $\frac{F}{\varepsilon}$ [25, 32].

The other observation concerns the regions where *electroneutrality does not hold*. We've mentioned in section 2.3 that the electrical double layer is a region whose main characteristic is presence of an excess of charge density. Evidently, one cannot apply the electroneutrality condition to the EDL, but that may raise the question of why, then, is it customary to develop models in which the hypothesis holds for the solution as a whole. Once again, in most cases, the thickness of the EDL will be ≤ 100 nm while the model scale will be much larger. This allows us to treat the EDL as part of the solution interface. This is further facilitated by the presence of excess supporting electrolyte. Still, in extremely dilute solutions, the EDL might extend appreciably inside the solution and one must necessarily deal with a depart from electroneutrality in the model [25, 26].

2.4.6 Transport laws for ideal, dilute solutions

Having presented our initial set of hypotheses, we can finally write an explicit equation for the flux density of a species i:

$$\mathbf{J}_i = -Fu_i z_i c_i \nabla\Phi - D_i \nabla c_i + c_i \mathbf{v} \tag{2.26}$$

And also for their mass conservation:

$$\frac{\partial c_i}{\partial t} = -\nabla \cdot \mathbf{J}_i + R_i \tag{2.27}$$

$$\frac{\partial c_i}{\partial t} = D_i \nabla^2 c_i + Fu_i z_i \nabla \cdot (c_i \nabla\Phi) - \mathbf{v} \cdot \nabla c_i + R_i \tag{2.28}$$

Finally, the current density is given by:

$$\mathbf{i} = F \sum_i z_i \mathbf{J}_i$$

$$\mathbf{i} = -F^2 \nabla\Phi \sum_i \left(z_i^2 u_i c_i\right) - F \sum_i (z_i D_i \nabla c_i) + F \sum_i \cancelto{0(\textit{Electroneutrality})}{z_i c_i} \mathbf{v}$$

$$\mathbf{i} = -F^2 \nabla\Phi \sum_i \left(z_i^2 u_i c_i\right) - F \sum_i (z_i D_i \nabla c_i) \tag{2.29}$$

There is still another condition which we can impose to further simplify the equations. In this case, though, it is not an assumption we make about the physical nature of the system, but an experimental feature: the use of *excess supporting electrolyte*.

2.4.7 The role of the supporting electrolyte

Supporting electrolyte is any electrolyte whose function is uniquely to increase the solution conductivity. Thus, when in excess, it has the effect of minimizing the migration term of the flux density by making the potential drop negligible. Under these circum-

stances, only diffusion and convection will contribute to the flux density of species:

$$\mathbf{J}_i = -D_i \nabla c_i + c_i \mathbf{v} \tag{2.30}$$

Likewise, for mass conservation:

$$\frac{\partial c_i}{\partial t} = D_i \nabla^2 c_i - \mathbf{v} \cdot \nabla c_i + R_i \tag{2.31}$$

Also, the current density will be determined exclusively by the diffusion fluxes:

$$\mathbf{i} = -F \sum_i (z_i D_i \nabla c_i) \tag{2.32}$$

From a mathematical point of view, the use of excess supporting electrolyte has a tremendous effect. Since the potential gradient is present in all flux equations, they are coupled and must be solved simultaneously. But, if we get rid of the migration term, all the equations become independent from each other. The procedure, then, becomes not only easier, but less time-consuming [25].

The amount of supporting electrolyte necessary to make migration negligible depends on the concentration of the minor, electroactive species. Oldham and Zoski have calculated that, in the case of multi-ion homovalent solutions, a 33-fold excess of supporting electrolyte is sufficient to make the migration/diffusion flux ratio equal to 1% [27]. Evidently, if the reacting species themselves are already in large concentrations, their very presence might be enough to mitigate any migration effects.

Another advantage of adding excess supporting electrolyte, already mentioned in subsection 2.4.5, is keeping the EDL length negligible when compared to the problem scale. Under these conditions, Poisson's equation can be safely replaced by the electroneutrality hypothesis.

From this point on, we'll incorporate the presence of excess supporting electrolyte in our models. By now, we have been careful to define the equations that govern the behaviour of an electrochemical system. However, we have not yet addressed what happens at the boundaries; namely the solution bulk and the electrode surface.

2.4.8 Electrode surface and the solution bulk

Boundary conditions in electrochemical systems can be of two types: we can either define a value for the concentration of a species or to its flux - and, consequently, to its current density contribution. In the case of the solution bulk, it is more common to specify boundary conditions of the first type. That happens because we can consider that the boundary (*i.e.*, the solution bulk) is far enough so as to remain undisturbed by the electrochemical reactions. It might also be the case that the species under study does not

exist in solution prior to the electrochemical reaction, so its bulk concentration is set to zero. Either way, we are assuming that the major changes in solution are contained within the problem scale.

In the subsequent discussion about boundary conditions at electrode surfaces, we'll restrict ourselves to systems in which there is a single electroactive species (no restriction on the number of non-electroactive species, though). Electrode surfaces are the regions where electrochemical reactions *do* take place, so it is much harder to guess what is the exact concentration of any species. With the use of a potentiostat, it is easier to control the potential applied or the electric current flowing through the electrochemical cell. Because the potential influences the current value, both of these are flux density conditions. A special case in which we can actually consider the surface concentration of an electroactive species to be known is that of limiting current densities, an extreme situation in which the surface concentration of the reacting species is zero. Finally, if we also have to consider the equations for non-electroactive species, we can simply set their flux at the electrode surface to zero, because they are neither produced nor consumed there.

To sum it up, we can say the boundary conditions at the solution bulk are:

$$c_i(r \to \infty) = c_i^{bulk} \tag{2.33}$$

Where r represents the position measured from the electrode surface.

At the electrode surface, we can either have (for the electroactive species):

$$z_i F D_i \left.\frac{\partial c_i(r)}{\partial r}\right|_{r=0} = i_{app} \tag{2.34}$$

Where i_{app} is the current density we want to apply.

Or:

$$c_i(0) = 0 \tag{2.35}$$

Lastly, for non-electroactive species:

$$\left.\frac{\partial c_i(r)}{\partial r}\right|_{r=0} = 0 \tag{2.36}$$

2.4.9 Homogeneous reactions

What happens if the electroactive species can also react with other substances at the solution bulk? In this case, the concentration profile will be affected not only by the flux densities, but also by a volume effect. That is well represented in equation 2.31:

$$\frac{\partial c_i}{\partial t} = D_i \nabla^2 c_i - \mathbf{v} \cdot \nabla c_i + R_i \tag{2.37}$$

The explicit form of the term R_i will depend on the reaction mechanisms involving

each species. The most commonly studied are presented below [20]:

- Chemical-electrochemical (CE): The electroactive species can also react to produce a non-electroactive species

$$\text{CE}\begin{cases}\text{A} \underset{\text{k}_\text{B}}{\overset{\text{k}_\text{A}}{\rightleftharpoons}} \text{B} \\ \text{A} + \text{ne}^- \xrightarrow{\text{k}_h} \text{C}\end{cases} \tag{2.38}$$

- Electrochemical-chemical (EC): The product of the electrochemical step reacts to produce a non-electroactive species

$$\text{EC}\begin{cases}\text{A} + \text{ne}^- \xrightarrow{\text{k}_h} \text{B} \\ \text{B} \underset{\text{k}_\text{C}}{\overset{\text{k}_\text{B}}{\rightleftharpoons}} \text{C}\end{cases} \tag{2.39}$$

- Catalytic reaction (EC'): The product of the electrochemical step acts as a catalyst to regenerate the electroactive species

$$\text{EC'}\begin{cases}\text{A} + \text{ne}^- \xrightarrow{\text{k}_h} \text{B} \\ \text{B} + \text{D} \underset{\text{k}_\text{C}}{\overset{\text{k}_\text{B}}{\rightleftharpoons}} \text{A} + \text{C}\end{cases} \tag{2.40}$$

- Electrochemical-Chemical-Electrochemical: The product of the electrochemical step reacts to produce a new species which is also electroactive.

$$\text{ECE}\begin{cases}\text{A} + \text{n}_1\text{e}^- \xrightarrow{\text{k}_h} \text{B} \\ \text{B} \underset{\text{k}_\text{C}}{\overset{\text{k}_\text{B}}{\rightleftharpoons}} \text{C} \\ \text{C} + \text{n}_2\text{e}^- \xrightarrow{\text{k}_{h2}} \text{D}\end{cases} \tag{2.41}$$

The presence of homogeneous reactions adds an extra layer of complexity to the models, because, now, the equations are coupled and, therefore, must be solved simultaneously. For instance, in the case of a CE model, the mass-conservation equations would be:

$$\begin{cases}\dfrac{\partial c_A}{\partial t} = D_A\nabla^2 c_A - \mathbf{v}\cdot\nabla c_A + (k_B c_B - k_A c_A) \\ \dfrac{\partial c_B}{\partial t} = D_B\nabla^2 c_B - \mathbf{v}\cdot\nabla c_B - (k_B c_B - k_A c_A)\end{cases} \tag{2.42}$$

Notice that, even though the species B is not electroactive, it has a clear effect on the current response because it also contributes to the concentration profile of A. Solving a set of coupled equations is very different from two independent equations and we'll see

that the kinetic constants (k_A and k_B), among other parameters, play an important role on this.

2.4.10 What about the system?

We still haven't discussed the velocity profile of the electrolyte solution, which is of great importance to determine the convective flux. In subsection 2.4.4, we presented only the equations that govern fluid flow and no mention was made to boundary conditions or to new hypotheses. That's because these are dependent on the geometries of both the electrochemical cell and of the electrode, plus the nature of the convective process - *i.e.*, if it is natural or forced.

In the case of *quiescent solutions*, we neglect the contribution of natural convection to the total flux density. However, that comes at a cost: results from prolonged experiments will deviate from theoretical predictions, because of the increasing participation of convective effects on the total flux. On the other hand, forced convection methods will provide a constant flow of electroactive species and the concentration profile can be safely regarded as constant for a much larger period of time [33].

The choice for a particular configuration is related to the quality of the data it provides (reproducibility, for instance) and the easiness to interpret the results obtained. In this thesis, we'll focus on a particular experimental arrangement which has been successfully used to study both the steady state and the transient response of electrochemical systems under mass transfer control. This is particularly useful when describing the role of chemical-electrochemical processes, which is our primary goal. This system is the rotating disk electrode (RDE).

2.5 Rotating disk electrodes

The RDE system was developed by Levich around the 1940's to study the influence of mass transter processes on electrochemical systems. Its foundations were later compiled in his seminal book *Physicochemical Hydrodynamics* [7]. It consists of a cylindrical electrode embedded in a rod of insulating material - *e.g.*, epoxy resin. This is done in a way to allow the cross-section of the electrode to be in contact with the electrolyte solution. This ensemble is connected to a motor used to rotate the RDE around the $z-$axis at different angular speeds. Preferably, the rotation axis should be as close as possible to the centroidal line of the RDE because of the axial symmetry created. A schematic representation of the system is presented in figure 2.3.

The merit of the RDE resides in the simplicity of the experimental set-up and the use of a geometry for which the velocity profile of the fluid can be expressed analytically. The imposition of forced convection also increases reproducibility, decreases the

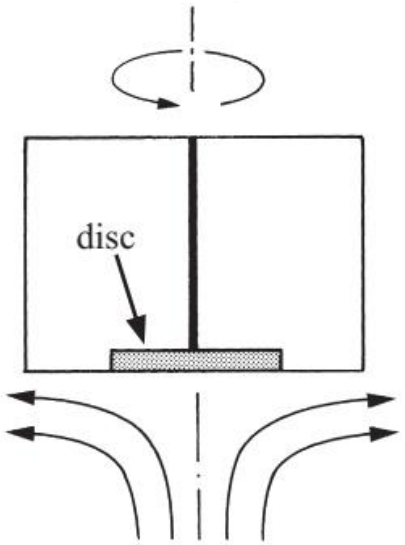

Figure 2.3: Sketch of a rotating disk electrode. Arrows represent the streamlines of the fluid. Adapted from [28].

time required to attain a steady state concentration profile and constantly replenishes electroactive species and withdraws products from the electrode surface. Another advantage is that different flow conditions can be studied with the same system by simply changing the rotation speed [8].

Before detailing the concentration profile in RDE systems; first, we must understand the conditions under which the flow is developed, *i.e.*, we must determine the velocity profile.

2.5.1 Fluid flow in RDE systems

Even though it was Levich who brought the rotating disk configuration into electrochemistry, the problem of determining the velocity profile around a rotating disk was a problem that had been intriguing the scientific community for quite some time. The first analytical solution is due to von Kárman, who posed the problem in cylindrical coordinates (r, θ, z) in the following way [34]:

- The system is composed of a rotating disk of infinite radius in a solution of infinite dimensions.
- The fluid is newtonian and flows under steady state conditions: $\frac{\partial}{\partial t} = 0$
- The coordinate system has its origin at the disk surface and the positive $z-$direction points towards the solution bulk.
- Because of the axial symmetry, there is no dependence on the azimuthal component: $\frac{\partial}{\partial \theta} = 0$

- The pressure varies only in the axial direction: $p = p(z)$

Applying these conditions, we can write the momentum equations:

$$\begin{cases} v_r \dfrac{\partial v_r}{\partial r} - \dfrac{{v_\theta}^2}{r} + v_z \dfrac{\partial v_r}{\partial z} = \nu \left[\dfrac{\partial^2 v_r}{\partial z^2} + \dfrac{\partial^2 v_r}{\partial r^2} + \dfrac{1}{r}\dfrac{\partial v_r}{\partial r} - \dfrac{v_r}{r^2} \right] \\ v_r \dfrac{\partial v_\theta}{\partial r} + \dfrac{v_r v_\theta}{r} + v_z \dfrac{\partial v_\theta}{\partial z} = \nu \left[\dfrac{\partial^2 v_\theta}{\partial z^2} + \dfrac{\partial^2 v_\theta}{\partial r^2} + \dfrac{1}{r}\dfrac{\partial v_\theta}{\partial r} - \dfrac{v_\theta}{r^2} \right] \\ v_r \dfrac{\partial v_z}{\partial r} + v_z \dfrac{\partial v_z}{\partial z} = -\dfrac{1}{\rho}\dfrac{\partial p}{\partial z} + \nu \left[\dfrac{\partial^2 v_z}{\partial z^2} + \dfrac{\partial^2 v_z}{\partial r^2} + \dfrac{1}{r}\dfrac{\partial v_z}{\partial r} \right] \end{cases} \tag{2.43}$$

Where v_r, v_θ and v_z correspond to the radial, azimuthal and axial components of the fluid velocity respectively.

For the continuity equation, we get:

$$\frac{\partial v_r}{\partial r} + \frac{v_r}{r} + \frac{\partial v_z}{\partial z} = 0 \tag{2.44}$$

To determine the boundary equations at the disk surface, von Kárman made use of the common *no-slip condition*, which asserts that the fluid in immediate contact with a surface has the same velocity as that surface [31]. For the case of a rotating disk, this means:

$$\begin{cases} v_r(r, 0) = 0 \\ v_\theta(r, 0) = \Omega r \\ v_z(r, 0) = 0 \end{cases} \tag{2.45}$$

Where Ω represents the angular velocity of the disk.

At the solution bulk, there are no radial or azimuthal velocities. However, for reasons of continuity, there must be some non-zero axial velocity. We can write that as:

$$\begin{cases} v_r(r, z \to \infty) = 0 \\ v_\theta(r, z \to \infty) = 0 \\ v_z(r, z \to \infty) = -C \end{cases} \tag{2.46}$$

Where C is a positive constant. The minus sign at v_z is due to the fact that positive vectors point towards the solution. Since at infinity the velocity field points towards the disk, it must have a negative value.

Thus, the rotating disk acts as a pump, draining solution towards its surface and then expelling it radially.

To solve this problem, von Kárman first introduced a dimensionless variable:

$$\xi = \sqrt{\frac{\nu}{\Omega}} z \tag{2.47}$$

Then, he replaced the original functions by a new set of dimensionless ones:

$$v_r(r, z) = r\Omega F(\xi) \tag{2.48}$$

$$v_\theta(r, z) = r\Omega F(\xi) \tag{2.49}$$

$$v_z(r, z) = \sqrt{\nu\Omega} H(\xi) \tag{2.50}$$

$$p(z) = \rho\nu\Omega P(\xi) \tag{2.51}$$

The new set of equations (Continuity plus Navier-Stokes) now becomes:

$$\begin{cases} 2F + H' = 0 \\ F^2 - G^2 + F'H - F'' = 0 \\ 2FG + F'H - G'' = 0 \\ HH' - P' + H'' = 0 \end{cases} \tag{2.52}$$

Where the prime indicates the derivative of the function with respect to ξ.

The new boundary conditions are:

$$\begin{cases} F(0) = 0; & F(\xi \to \infty) = 0 \\ G(0) = 1; & G(\xi \to \infty) = 0 \\ H(0) = 0; & H(\xi \to \infty) = -c \end{cases} \tag{2.53}$$

Notice that, now, one single variable is enough to describe any function. Also, the velocity field can be calculated without having to determine the pressure field and we can neglect the fourth equation in 2.52. Although von Kárman developed a formalism which continues to be used, his method for calculating the approximate solution using integration contained errors and led to wrong values. This was first pointed out by Cochran, who proposed the use of singular perturbation methods, dividing the problem in two regions: at the vicinities of the disk and very far from it [35]. Near the disk surface, the terms F, G and H were expressed as a power series:

$$\begin{cases} F(\xi) = a\xi - \dfrac{\xi^2}{2} - \dfrac{b\xi^3}{3} - \dfrac{b^2\xi^4}{12} + \dots \\ G(\xi) = 1 + b\xi + \dfrac{a\xi^3}{3} + \dfrac{(ab-1)\xi^4}{12} + \dots \\ H(\xi) = -a\xi^2 + \dfrac{\xi^3}{3} + \dfrac{b\xi^4}{6} + \dots \end{cases} \tag{2.54}$$

The relation between coefficients can be determined by substituting the truncated power series representations in the original set of equations 2.52 and comparing terms of equal power. After this, only two coefficients rest undetermined; a and b, which Cochran calculated using numerical integration and found that $a = 0.510$ and $b = -0.616$. Later works, applying more refined techniques, were able to improve the accuracy of the coefficients: $a = 0.510233$ and $b = -0.615922$ [36].

Levich used Cochran's results and went on to define a *hydrodynamic boundary layer*, a region inside which most of the velocity changes took place [7]. He defined its thickness (δ_0) to be:

$$\delta_0 = 3.6\sqrt{\frac{\nu}{\Omega}} \tag{2.55}$$

At this position, v_z has, approximately, 80% of its limiting value and v_ϑ has only 5% of its surface value. Thus, inside this boundary layer, both tangential and radial velocities have non-zero values. Outside of it, only the axial velocity has significant values. This concept will be important when we discuss the mass transport in the RDE system.

Figure 2.4 shows the streamlines obtained from the solution and confirms that the rotating disk does, indeed, act as a pump.

Figure 2.4: Cross section view (A) and side view (B) of the streamlines for the RDE system. Adapted from [8].

We have found an analytical solution for the fluid flow. The next step is to combine this information with the diffusion flux density to solve the mass transfer equation for the electroactive species.

2.5.2 Mass transfer in RDE systems

In the following discussion, we'll consider the case of a system with excess supporting electrolyte containing a single electroactive species (of concentration c and diffusion coefficient D) and without homogeneous reactions. The electrode surface is smooth and every reaction site is equivalent. Also, we're dealing with a steady state problem. Hence, the mass-conservation equation, in cylindrical coordinates, becomes:

$$D\left(\frac{\partial^2 c}{\partial r^2} + \frac{\partial^2 c}{\partial z^2} + \frac{1}{r}\frac{\partial c}{\partial r} + \frac{1}{r^2}\frac{\partial^2 c}{\partial \vartheta^2}\right) - \left(v_r\frac{\partial c}{\partial r} + \frac{v_\vartheta}{r}\frac{\partial c}{\partial \vartheta} + v_z\frac{\partial c}{\partial z}\right) = 0 \tag{2.56}$$

Because of the axial symmetry, we can, once again, consider that there's no variation in the azimuthal direction, *i.e.*, $\frac{\partial}{\partial \theta} = 0$. The equation now reads:

$$D\left(\frac{\partial^2 c}{\partial r^2} + \frac{\partial^2 c}{\partial z^2} + \frac{1}{r}\frac{\partial c}{\partial r}\right) - \left(v_r \frac{\partial c}{\partial r} + v_z \frac{\partial c}{\partial z}\right) = 0 \tag{2.57}$$

Levich, then, proposed that, even for disks with finite radius, the radial diffusion term could be neglected, since the *diffusion boundary layer* thickness was considerably smaller than the radius of the electrode surface. Smyrl and Newman used singular perturbation methods to estimate the error introduced by this simplification and found that the correction was around 0.12%, meaning that we can safely proceed to consider only the axial diffusion [37]. Once again, we rewrite the mass conservation equation:

$$D\frac{\mathrm{d}^2 c}{\mathrm{d}z^2} = v_z \frac{\mathrm{d}c}{\mathrm{d}z} \tag{2.58}$$

The concentration has become dependent only on the axial direction and equation 2.58, now an ordinary differential equation, can be solved by conventional methods. Integration of equation 2.58 gives

$$\frac{\mathrm{d}c(z)}{\mathrm{d}z} = A_1 \exp\left(\int_0^z \frac{v_z}{D}\mathrm{d}z\right) \tag{2.59}$$

Where A_1 is an integration constant. A final integration leads to:

$$c(z) = A_2 + A_1 \int_0^z \left(\exp\left(\int_0^t \frac{v_z}{D}\mathrm{d}z\right)\right)\mathrm{d}t \tag{2.60}$$

Where A_2 is another integration constant.

To determine the integration constants, we apply the boundary conditions for the concentration. Levich first studied cases of limiting current density, that is, those in which the concentration at the electrode surface approaches zero. From this, we see that:

$$c(0) = A_2 + A_1 \int_0^0 \left(\exp\left(\int_0^t \frac{v_z}{D}\mathrm{d}z\right)\right)\mathrm{d}t \tag{2.61}$$

$$A_2 = 0 \tag{2.62}$$

The other boundary condition states that the bulk concentration remains unaltered.

Ideally, the bulk is at an infinite distance from the electrode surface, so:

$$c(z \to \infty) = c^b \tag{2.63}$$

$$c^b = A_1 \int_0^\infty \left(\exp\left(\int_0^t \frac{v_z}{D}\mathrm{d}z\right)\right)\mathrm{d}t \tag{2.64}$$

$$A_1 = \frac{c^b}{\int_0^\infty \left(\exp\left(\int_0^t \frac{v_z}{D}\mathrm{d}z\right)\right)\mathrm{d}t} \tag{2.65}$$

To evaluate this integral, Levich split it in two and used the hydrodynamic boundary layer thickness to set the new integration limits :

$$\int_0^\infty \left(\exp\left(\int_0^t \frac{v_z}{D}\mathrm{d}z\right)\right)\mathrm{d}t = \underbrace{\int_0^{\delta_0} \left(\exp\left(\int_0^t \frac{v_z}{D}\mathrm{d}z\right)\right)\mathrm{d}t}_{I_1} + \underbrace{\int_{\delta_0}^\infty \left(\exp\left(\int_0^t \frac{v_z}{D}\mathrm{d}z\right)\right)\mathrm{d}t}_{I_2} \tag{2.66}$$

Levich argues that, for typical values of diffusion coefficients ($D \approx 10^{-9}$ m^{2}s^{-1}) and kinematic viscosity ($\upsilon \approx 10^{-6}$ m^{2}s^{-1}) in aqueous solutions, convective effects dominate the mass transfer throughout the whole solution, except for a small region confined near the electrode surface, the *diffusion layer*, which is much smaller than δ_0. Because of this, the velocity can be expressed as the power series used for low ξ values. Levich opted to use only the first term of the series based, again, on the thinness of the diffusion layer [7]:

$$v_z(z) \approx -\frac{a\Omega^{3/2}}{\upsilon^{1/2}} z^2 \tag{2.67}$$

$$I_1 = \int_0^{\delta_0} \exp\left(\int_0^t -\frac{a\Omega^{3/2}}{D\upsilon^{1/2}} z^2 \mathrm{d}z\right)\mathrm{d}t \approx \int_0^{\delta_0} \exp\left(-\frac{\Omega^{3/2}}{6D\upsilon^{1/2}} t^3\right)\mathrm{d}t \tag{2.68}$$

The next step involves a change of variable:

$$u = \frac{\Omega^{1/2} t}{\sqrt[3]{6} D^{1/3} \upsilon^{1/6}} \tag{2.69}$$

And the new integral becomes:

$$I_1 = \frac{1.81 D^{1/3}\upsilon^{1/6}}{\Omega^{1/2}} \int_0^{\frac{\Omega^{1/2}\delta_0}{\sqrt[3]{6}D^{1/3}\upsilon^{1/6}}} \exp\left(u^{-3}\right)\mathrm{d}u \approx \frac{1.81 D^{1/3}\upsilon^{1/6}}{\Omega^{1/2}} \int_0^{2\left(\frac{\upsilon}{D}\right)^{1/3}} \exp\left(u^{-3}\right)\mathrm{d}u \tag{2.70}$$

$$I_1 = \frac{1.81 D^{1/3}\upsilon^{1/6}}{\Omega^{1/2}} \int_0^{2\mathrm{Sc}^{1/3}} \exp\left(u^{-3}\right)\mathrm{d}u \tag{2.71}$$

Where $Sc = \frac{\upsilon}{D}$ is the Schmidt number.

Since $Sc \gg 1$ and $\exp(u^{-3})$ falls very rapidly to zero, we can rewrite the integral as:

$$I_1 = \frac{1.81 D^{1/3} \nu^{1/6}}{\Omega^{1/2}} \int_0^\infty \exp\left(u^{-3}\right) \mathrm{d}u \tag{2.72}$$

A final change of variables shows that this integral is related to the gamma function: $\Gamma(n) = \int_0^\infty e^{-t} t^{n-1} \mathrm{d}t$.

$$t = u^3 \tag{2.73}$$

$$\int_0^\infty \exp\left(u^{-3}\right) \mathrm{d}u = \frac{1}{3} \underbrace{\int_0^\infty e^{-t} t^{-2/3} \mathrm{d}t}_{\Gamma(1/3)} \tag{2.74}$$

$$I_1 = 1.61 \nu^{1/6} D^{1/3} \Omega^{-1/2} \tag{2.75}$$

To calculate I_2, we use the fact that, for distances past δ_0, the velocity field is constant:

$$v = v_z(z) = -\sqrt{\nu\Omega} c \tag{2.76}$$

Using the value of $c = 0.88446$ calculated by Rogers and Lance, we have[36]:

$$v_z(z) = -0.88446 \sqrt{\nu\Omega} \implies I_2 = \int_{\delta_0}^\infty \exp\left(\frac{-0.88446 \sqrt{\nu\Omega} t}{D}\right) \mathrm{d}t \tag{2.77}$$

$$I_2 \approx \frac{D}{0.88446 \sqrt{\nu\Omega}} \exp(-3Sc) \tag{2.78}$$

Using the same assumption about the order of magnitude of Sc, Levich considered that $I_1 \gg I_2$, thus neglecting the latter. Now, the integration constant A_1 can be evaluated:

$$A_1 = \frac{c^b}{1.61 \nu^{1/6} D^{1/3} \Omega^{-1/2}} \tag{2.79}$$

Finally, the current density can be expressed:

$$i = zFD \left.\frac{\mathrm{d}c}{\mathrm{d}z}\right|_{z=0} = \frac{zFDc^b}{\int_0^\infty \left(\exp\left(\int_0^t \frac{v_z}{D} \mathrm{d}z\right)\right) \mathrm{d}t} \tag{2.80}$$

$$i = 0.62 D^{2/3} \nu^{-1/6} c^b \Omega^{1/2} \tag{2.81}$$

These results can be extended for surface concentrations greater than zero. Assuming an arbitrary value at the electrode surface, $c(0)$, the main changes would be:

$$\begin{cases} A_2 = c(0) \\ A_1 = \dfrac{c^b - c(0)}{\int_0^\infty \left(\exp\left(\int_0^t \frac{v_z}{D} \mathrm{d}z\right)\right) \mathrm{d}t} \end{cases} \tag{2.82}$$

So that the current density would be rewritten as:

$$i = zFD\frac{c^b - c(0)}{1.61\left(\frac{D}{\nu}\right)^{1/3}\sqrt{\frac{\nu}{\Omega}}} \tag{2.83}$$

This latest form of the current density can be compared to the Nernstian formula that assumes the existence of a linear concentration gradient and the absence of fluid flow inside the diffusion layer. In doing so, we can calculate the diffusion layer thickness, δ_D:

$$zFD\frac{c^b - c(0)}{\int_0^\infty \exp\left(\int_0^t \frac{v_z}{D}\mathrm{d}z\right)\mathrm{d}t} = zFD\frac{c^b - c(0)}{\delta_D} \tag{2.84}$$

$$\delta_D = \int_0^\infty \exp\left(\int_0^t \frac{v_z}{D}\mathrm{d}z\right)\mathrm{d}t \tag{2.85}$$

$$\delta_D \approx 1.61 Sc^{-1/3}\sqrt{\frac{\nu}{\Omega}} \tag{2.86}$$

Notice that δ_D does not depend on the radius of the electrode, meaning that it is constant over its entire surface. Therefore, every reaction site on the electrode is equally accessible to the electroactive species. Also, δ_D depends on $Sc^{-1/3}$, so that it will be increasingly smaller for higher Schmidt values. Comparing the values of δ_D and δ_0, we see that:

$$\frac{\delta_D}{\delta_0} \approx \frac{0.45}{Sc^{1/3}} \tag{2.87}$$

Hence, for the Schmidt number that we've been using as reference ($\sim$ 1000), δ_D corresponds to less than 5% of δ_0. Levich, noting that the *whole* diffusion layer would be in a region very close to the electrode, used this result to justify the use of only one term of the v_z series expansion when performing the calculations [7].

We must stress that the diffusion layer thickness calculated according to equation 2.86 *does not* account for the whole region where concentration changes. As we have mentioned in subsection 2.4.3 and above, the Nerstian diffusion layer thickness assumes a linear concentration gradient, but that is not true for RDE systems, as shown in fig. 2.5:

So, what is the significance of δ_D? For one thing, it does give a good measure of the diffusion layer thickness. Also, it has a direct physical meaning (the thickness that would be observed had the gradient been linear) and it is easier to calculate than a more precise definition. For these reasons, we will adopt the Nerstian diffusion layer thickness and, from now on, refer to it as simply the diffusion layer thickness.

2.5.3 Validation and further improvements

Among the reasons for the success of the RDE is that both its predictions and assumptions were very accurate and quickly confirmed. One of the earliest confirmations came

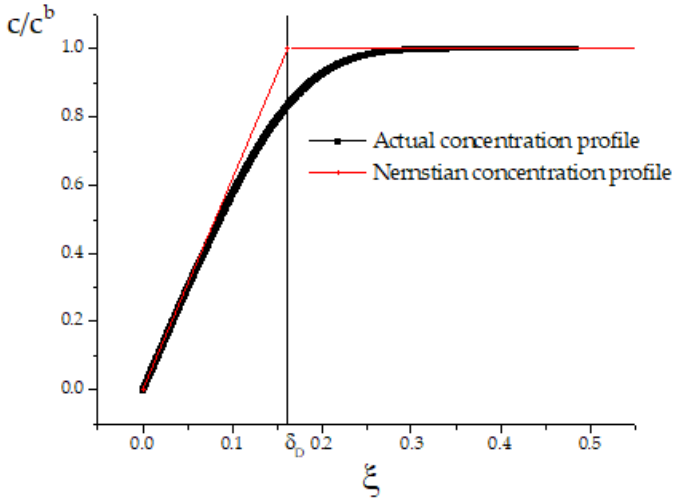

Figure 2.5: Dimensionless concentration profile in an RDE system

from a study conducted by Hogge and Kraichman, who investigated the reduction of I_3^- in an aqueous solution of $KI-KI_3$ with excess of KI. The authors found a linear relationship between the current density and $\Omega^{1/2}$ and that the diffusion coefficient for I_3^- calculated according to equation 2.81 was in good agreement with independent measurements made with non-electrochemical techniques [38].

Experiments were also conducted to assess the uniform accessibility at the limiting current condition predicted by the independence of the diffusion layer on the electrode radius and it was found to be accurate for both electrodeposition and electrodissolution processes. Beacom and Hollyer observed that copper films electrodeposited on rotating disk electrodes had uniform thickness while Kassner observed an uniform thinning of tantalum electrodes in liquid tin [39, 40]. Hence, the homogeneity of surface processes was found for both electrodeposition and electrodissolution.

Evidently, the theory also has its shortcomings and many works were devoted to making it more rigorous. For instance, Gregory and Riddiford pointed out that Levich's neglect of higher powers when integrating $\int_0^\infty \exp\left(\int_0^t \frac{v_z}{D}\mathrm{d}z\right)\mathrm{d}t$ led to considerable error when lower Schmidt numbers were used and proposed a correction found after fitting an equation dependent on Sc to numerical solutions of the integral [41]:

$$\int_0^\infty \exp\left(\int_0^t \frac{v_z}{D}\mathrm{d}z\right)\mathrm{d}t = 0.8934 + 0.316Sc^{0.36} \tag{2.88}$$

Later, Newman expanded the exponential considering three terms of the velocity power series and, after analytical integration, proposed a more precise equation [42]:

$$\int_0^\infty \exp\left(\int_0^t \frac{v_z}{D}\mathrm{d}z\right)\mathrm{d}t = \frac{0.62048Sc^{-2/3}}{1 + 0.2980Sc^{-1/3} + 0.14514Sc^{-2/3}} \tag{2.89}$$

These corrections have the effect of lowering the theoretical current density and increasing

the diffusion layer thickness.

Newman also investigated the uniformity of the current on the electrode surface and was the first to provide theoretical calculations showing that this condition was true *only in the limiting current condition*. When the surface concentration is greater than zero, there is a current distribution over the electrode surface, because of the nonuniform potential drop outside the diffusion layer. These effects are more pronounced for solutions of low conductivity and electrochemical species with large exchange current densities [43]. Further experimental investigation proved Newman's theory to be correct, but also that the nonuniformity can be minimized if excess supporting electrolyte is used to establish a constant potential in the electrolyte solution [44, 45]. Since all of our calculations assume the presence of excess supporting electrolyte, we'll consider the current to be evenly distributed on the electrode surface regardless of the total current applied.

Indeed, we can safely say that the rotating disk electrode system has been put on very a firm theoretical basis, which is why it continues to be extensively used more than 70 years after its first description.

2.5.4 The study of transient phenomena with RDE systems

Steady state measurements are seldom enough to study the reaction mechanism of electrochemical processes, which is why transient methods are important to provide additional data that can be used to develop more robust models.

Even though we have presented only steady state models for the RDE system, it can be used to study unsteady phenomena as well. Its ability to establish tightly controlled steady flow conditions makes it particularly suited for perturbation methods, which superpose small-amplitude variations to the steady control parameters (such as voltage, current or rotation speed) in order to study the system response. One of these methods is that of electrochemical impedance, which will now be discussed in more detail.

2.6 Electrochemical impedance

2.6.1 Definition of impedance

In order to have a better understanding of the electrochemical impedance technique and of the proper experimental conditions, it is essential to assimilate the concept of impedance.

Consider y(t) to be the response of a *linear time invariant system* to a perturbation x(t) and that both are related in the following way:

$$b_0\frac{d^n y(t)}{dt^n} + b_1\frac{d^{n-1} y(t)}{dt^{n-1}} + \cdots + b_n y(t) = a_0\frac{d^n x(t)}{dt^n} + a_1\frac{d^{n-1} x(t)}{dt^{n-1}} + \cdots + a_n x(t) \quad (2.90)$$

We define, then, the *transfer function* $G(s)$ of the system as the ratio between the Laplace transform of the response and the Laplace transform of the perturbation [46], *i.e.*:

$$G(s) = \frac{\mathcal{L}[y(t)]}{\mathcal{L}[x(t)]} \tag{2.91}$$

If we choose an input signal such that $x(t) = A\sin(\omega t)$, the response will be $y(t) = B\sin(\omega t + \phi)$ and the related transfer function $H(\omega)$ can be defined as [47]:

$$H(\omega) = |H(\omega)|e^{j\phi} = \frac{B}{A}e^{j\phi} \tag{2.92}$$

With $|H(\omega)|$ corresponding to the modulus of $H(\omega)$ and ϕ to the phase shift of the transfer function (j corresponds to the imaginary number). Finally, if $x(t)$ corresponds to the current ($x(t) = I(t)$) and $y(t)$, to the voltage ($y(t) = V(t)$), $H(\omega) = Z(\omega)$, which is the impedance of the system. Hence, we define the impedance as the transfer function which relates two variables (current and voltage) of a linear time invariant system in the following way:

$$Z(\omega) = \frac{\mathcal{L}[V(t)]}{\mathcal{L}[I(t)]} \tag{2.93}$$

And, if we choose to use sinusoidal perturbations,

$$Z(\omega) = \frac{\mathcal{L}[\Delta V\sin(\omega t + \phi)]}{\mathcal{L}[\Delta I\sin(\omega t)]} = \frac{\Delta V}{\Delta I}e^{j\phi} \tag{2.94}$$

Notice that the choice of the input function (the perturbation) is completely arbitrary and, in fact, it is not necessary in the definition of the impedance. Nonetheless, we often use sinusoidal signals because they're both easier to handle mathematically and to process electronically for the impedance calculation, generating a better signal-to-noise ratio [47, 48].

Now, we have just shown that defining the impedance of a system requires that it meets certain conditions. Thus, it is natural to raise the question: can electrochemical systems meet these requirements?

2.6.2 Non-linearity of electrochemical systems

Our present knowledge of electrochemical systems make it safe to say that most electrochemical systems have a (sometimes, markedly) non-linear behavior. Even the simplest models, such as the Tafel law, exhibit an exponential dependence of the current on potential:

$$\ln(i) = A + bE \tag{2.95}$$

How, then, could it be possible to apply impedance calculations to our object of study? A clever way to circumvent this problem is to linearize these complicated systems. Experimentally, this can be accomplished by applying small-amplitude sinusoidal perturbations under steady state conditions. As a result, an electrochemical impedance may be calculated [22, 47–52]. To exemplify, let's consider the following situation in which, for the sake of simplicity, the current is a function of the interfacial potential (E), of the coverage of adsorbed species (θ_i) and of the concentration of electroactive species at the electrode surface (c_k):

$$I = I\left(E, \sum_{i=1}^{n} \theta_i, \sum_{k=1}^{m} c_k(0)\right) \tag{2.96}$$

Now, let's expand the function around an equilibrium point $I = \bar{I}\left(\bar{E}, \sum_{i=1}^{n} \bar{\theta}_i, \sum_{k=1}^{m} \bar{c}_k(0)\right)$ using Taylor series. We find, then:

$$I\left(\bar{E} + \Delta E, \sum_{i=1}^{n} (\bar{\theta}_i + \Delta\theta_i), \sum_{k=1}^{m} (\bar{c}_k(0) + \Delta c_k(0))\right) = \tag{2.97}$$
$$\bar{I} + \sum_{j=1}^{\infty}\left[\frac{1}{j!}\left(\frac{\partial^j}{\partial E^j}\Delta E + \sum_{i=1}^{n}\frac{\partial^j}{\partial \theta_i^j}\Delta\theta_i + \sum_{k=1}^{m}\frac{\partial^j}{\partial c_k(0)^j}\Delta c_k(0)\right) i\left(E, \sum_{i=1}^{n}\theta_i, \sum_{k=1}^{m} c_k(0)\right)\right]\Bigg|_{\bar{E}, \sum_{i=1}^{n}\bar{\theta}_i, \sum_{k=1}^{m}\bar{c}_k(0)}$$

Should the current be a linear function, by definition we have:

$$I\left(\bar{E} + \Delta E, \sum_{i=1}^{n} (\bar{\theta}_i + \Delta\theta_i), \sum_{k=1}^{m} (\bar{c}_k(0) + \Delta c_k(0))\right) =$$
$$I\left(\bar{E}, \sum_{i=1}^{n}\bar{\theta}_i, \sum_{k=1}^{m}\bar{c}_k(0)\right) + I\left(\Delta E, \sum_{i=1}^{n}\Delta\theta_i, \sum_{k=1}^{m}\Delta c_k(0)\right) = \bar{I} + \Delta I \tag{2.98}$$

By substituting this result in equation 2.97 and assuming that the deviations from the stationary values ($\Delta E, \Delta\theta_i, \Delta c_k(0)$) are small enough to let us neglect the terms of order higher than 2, we get:

$$\bar{I} + \Delta I = \bar{I} + \left(\frac{\partial I}{\partial E}\right)\Bigg|_{\bar{E}, \sum_{i=1}^{n}\bar{\theta}_i, \sum_{k=1}^{m}\bar{c}_k(0)} \Delta E + \sum_{i=1}^{n}\left(\frac{\partial I}{\partial \theta_i}\right)\Bigg|_{\bar{E}, \sum_{i=1}^{n}\bar{\theta}_i, \sum_{k=1}^{m}\bar{c}_k(0)} \Delta\theta_i \tag{2.99}$$
$$+ \sum_{k=1}^{m}\left(\frac{\partial I}{\partial c_k(0)}\right)\Bigg|_{\bar{E}, \sum_{i=1}^{n}\bar{\theta}_i, \sum_{k=1}^{m}\bar{c}_k(0)} \Delta c_k(0)$$

Finally, remember that if the input signal is sinusoidal, so will be the response. That

is, if $\Delta E = \tilde{E}\exp(\jmath\omega t)$, then $\Delta I = \tilde{I}\exp(\jmath\omega t + \phi)$. So:

$$\frac{\Delta I}{\Delta E} = \frac{\tilde{I}}{\tilde{E}}\exp(\jmath\phi) = \frac{1}{Z_f(\jmath\omega)} \tag{2.100}$$

$$\begin{aligned}\frac{1}{Z_f(\jmath\omega)} =& \left(\frac{\partial I}{\partial E}\right)\Big|_{\bar{E},\sum_{i=1}^{n}\bar{\theta}_i,\sum_{k=1}^{m}\bar{c}_k(0)} + \sum_{i=1}^{n}\left[\left(\frac{\partial I}{\partial \theta_i}\right)\Big|_{\bar{E},\sum_{i=1}^{n}\bar{\theta}_i,\sum_{k=1}^{m}\bar{c}_k(0)}\frac{\Delta\theta_i}{\Delta E}\right] \\ &+ \sum_{k=1}^{m}\left[\left(\frac{\partial I}{\partial c_k(0)}\right)\Big|_{\bar{E},\sum_{i=1}^{n}\bar{\theta}_i,\sum_{k=1}^{m}\bar{c}_k(0)}\frac{\Delta c_k(0)}{\Delta E}\right]\end{aligned} \tag{2.101}$$

The generality of these steps makes it safe to assume that any electrochemical model, no matter how complicated, can be linearized by the use of small amplitude signals. The value of this amplitude, however, is completely dependent on the system of study and, as a consequence, no universal reference can be assumed. It is quite common to find the use of amplitudes around 10 mV, though. This may come up from experience or as a theoretical prediction [20, 49, 52]. Either way, it is always advisable to use additional data analysis to ensure that the system is close enough to linear behaviour.

2.6.3 Mass transport effects: Diffusion impedance

Many electrochemical processes are related to species in solution which need to be transported to the electrode surface in order to react. Would their impedance response be any different from the prior cases? Let's start by considering the simple case of an electroactive neutral substance A in solution:

$$\mathrm{A} + \mathrm{e}^- \xrightarrow{\mathrm{k}_h} \mathrm{B} \tag{2.102}$$

To keep things simpler, we suppose that diffusion is unidirectional, that the reaction product B is not electroactive and that there is an excess of supporting electrolyte. In this example, there are no adsorbed species. Instead, we have a substance which must be transported to the electrode and, to determine its surface concentration, we must solve the mass conservation equation. Consequently, the relevant equations are:

$$\begin{cases} I = FAk_h c_A(0) \\ \dfrac{\partial c_A}{\partial t} = D\dfrac{\partial^2 c_A}{\partial x^2} \end{cases} \tag{2.103}$$

Infinite diffusion layer and the Warburg impedance

For the boundary conditions, we consider that the concentration of A at the solution bulk remains constant and that the current is given by the diffusion flux at the electrode

surface. If we consider oxidation currents to be positive, we get:

$$\begin{cases} c_A(x \to \infty) = c_A^b \\ I = FAD \left.\dfrac{\partial c_A}{\partial x}\right|_{x=0} \end{cases} \tag{2.104}$$

The steady state equation for the current is given by:

$$\bar{I} = FAk_h \bar{c}_A(0) \tag{2.105}$$

After applying the potential perturbation, we get the transient components:

$$\begin{cases} \Delta E = \tilde{E} \exp(\jmath\omega t) \\ \Delta c_A = \tilde{c}_A \exp(\jmath\omega t) \\ \Delta I = \tilde{I} \exp(\jmath\omega t) \end{cases} \tag{2.106}$$

The oscillating current is given by:

$$\Delta I = \left.\frac{\partial \left[FAk_h c_A(0)\right]}{\partial E}\right|_{\bar{E}.\bar{c}_A(0)} \Delta E + \left.\frac{\partial \left[FAk_h c_A(0)\right]}{\partial c_A(0)}\right|_{\bar{E},\bar{c}_A(0)} \Delta c_A(0) \tag{2.107}$$

$$\Delta I = FAb_h k_h \bar{c}_A(0) \Delta E + FAk_h \Delta c_A(0) \tag{2.108}$$

As for the concentration, we have:

$$\frac{\partial \Delta c_A}{\partial t} = FAD \frac{\partial^2 \Delta c_A}{\partial x^2} \tag{2.109}$$

$$\jmath\omega \tilde{c}_A \cancel{\exp(\jmath\omega t)} = D \frac{\mathrm{d}^2 \tilde{c}_A}{\mathrm{d}x^2} \cancel{\exp(\jmath\omega t)} \tag{2.110}$$

Hence, the relevant equations are:

$$\frac{\Delta I}{FA} = b_h k_h \bar{c}_A(0) \Delta E + k_h \Delta c_A(0) \tag{2.111}$$

$$\jmath\omega \tilde{c}_A = D \frac{\mathrm{d}^2 \tilde{c}_A}{\mathrm{d}x^2} \tag{2.112}$$

$$\Delta I = FAD \left.\frac{\partial \Delta c_A}{\partial x}\right|_{x=0} \tag{2.113}$$

The general solution to equation 2.112 is given by:

$$\tilde{c}_A(x) = M_1 \exp\left(\sqrt{\frac{\jmath\omega}{D}} x\right) + M_2 \exp\left(-\sqrt{\frac{\jmath\omega}{D}} x\right) \tag{2.114}$$

In order to determine the integration constants M_1 and M_2, we must set the boundary conditions for the concentration amplitude. Note that, because the bulk concentration is constant, there will be no concentration perturbation there, that is:

$$\tilde{c}_A(x \to \infty) = 0 \tag{2.115}$$

Also, we ascribe to the perturbation at the electrode surface an arbitrary value $\Delta c_A(0)$. The resulting equation for $\tilde{c}_A$ becomes:

$$\tilde{c}_A(x) = \tilde{c}_A(0) \exp\left(-\sqrt{\frac{J\omega}{D}}x\right) \tag{2.116}$$

Substituting this result at equation 2.113, we get:

$$-\frac{\Delta c_A(0)}{\Delta I} = \frac{1}{FA\sqrt{J\omega D}} \tag{2.117}$$

The transfer function $-\dfrac{\Delta c_A(0)}{\Delta I}$ is called the *diffusion impedance*, because it relates the impact of surface concentration oscillations on the current. Since the value of $c_A(0)$ depends on the transport processes in action, its oscillation $\Delta c_A(0)$ will also be dictated by similar transport laws with appropriate boundary conditions. In this particular case, we have diffusion acting in a quiescent solution. The diffusion layer extends over the whole solution and so does the concentration amplitude, except for the superior limit of the solution bulk.

Going back to equation 2.111, we can, now, rewrite it:

$$\begin{aligned}
\underbrace{\frac{\Delta I}{\Delta E}}_{1/Z_f} &= \underbrace{FAb_h k_h \bar{c}_A(0)}_{1/R_{ct}} + FAk_h \frac{\Delta c_A(0)}{\Delta E} \\
\frac{1}{Z_f} &= \frac{1}{R_{ct}} + FAk_h \frac{\Delta c_A(0)}{\Delta I}\frac{\Delta I}{\Delta E} \\
\frac{1}{Z_f} &= \frac{1}{R_{ct}} - k_h \frac{1}{\sqrt{J\omega D}}\frac{1}{Z_f} \\
Z_f &= R_{ct} + R_{ct}\frac{k_h}{\sqrt{J\omega D}}
\end{aligned} \tag{2.118}$$

R_{ct} stands for the *charge transfer resistance*, *i.e.*, the resistance to the passage of current strictly due to kinetic limitations. The term $R_{ct}\dfrac{k_h}{\sqrt{J\omega D}}$ is known as the *Warburg impedance*, named after the scientist who was the first to study the effect of alternating current on the concentration profile of electroactive species in quiescent solutions [53]. Figure 2.6 displays how this faradaic impedance looks on a Nyquist plot.

As we can see, on a Nyquist plot, the Warburg impedance has the distinctive shape of a straight line which makes a 45° angle with the real axis. When coupled with the capacitance, the line is still discernible:

A closer look at the Warburg impedance tells us that the impedance tends towards infinity as the frequency goes towards zero. That is, on steady state, there would be no

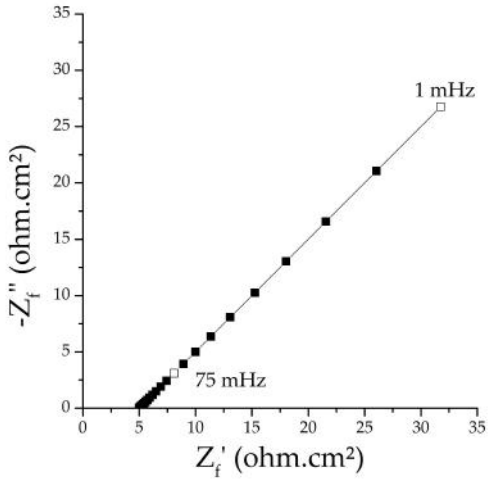

Figure 2.6: Nyquist plot of a faradaic impedance given by equation 2.118.(R_{ct} = 5 ohm.cm^2, $k_h/\sqrt{D}$ = 0.8 cm.^{2}s$^{-1/2}$)

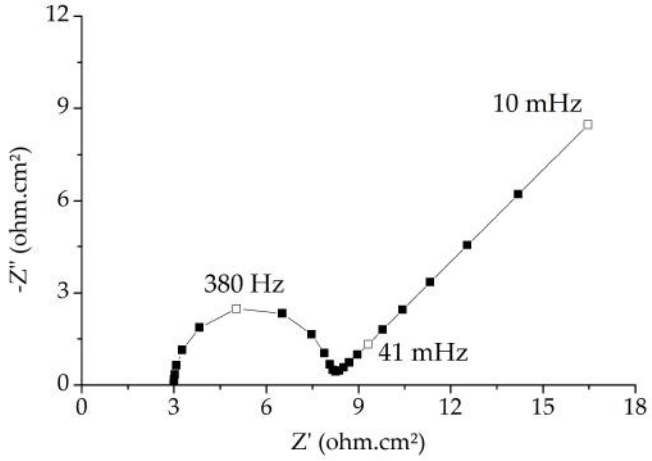

Figure 2.7: Nyquist plot of the global impedance of the system presented in figure 2.6.(R_{ct} = 5 ohm.cm^2, $k_h/\sqrt{D}$ = 0.8 cm.^{2}s$^{-1/2}$, R_e = 3 ohm.cm^2, C_{dl} = 100 μF/cm^2)

current at all. How can we interpret that? Let's go back to the mass conservation equation for the steady state and solve it:

$$D\frac{\mathrm{d}c_A^2}{\mathrm{d}x^2} = 0 \tag{2.119}$$

$$c_A(x) = A_1 x + A_2 \tag{2.120}$$

The problem arises when we try to determine the integration constants by applying the boundary condition $c(x \to \infty)$, which would lead us to physically unsound results. We conclude, then, that the conditions under which the Warburg impedance is observed *do not admit stationary solutions*. Would this be in contradiction with our prior statement that impedance measurements are performed by applying a periodical perturbation over

a steady condition? Theoretically, yes; but, in practice, this can be circumvented. The current density for this system is given by[29]:

$$i = \frac{FD_A^{1/2} c_A^b}{\pi^{1/2} t^{1/2}} \tag{2.121}$$

As expected, the current density depends on time and does not reach a non-zero steady state value. Nevertheless, the *rate* at which it decreases also follows the same pattern, which means that it takes longer for the current to change as time goes by. Thus, we can perform an experiment whose duration does not allow the current (and, thus, the concentration profile) to change considerably [49].

Finite diffusion layer: Going back to Nernst's hypothesis

We'll now consider the case of a diffusion layer of finite thickness - δ_D. This situation can be encountered, for instance, in electrodes coated with conducting membranes [54], electrodes covered with porous films or $H_{2(g)}$ diffusion in thin layers of Pd [55]. Assuming that the concentration outside this layer is constant, the new set of boundary conditions for the stationary mass conservation equation are:

$$\frac{\partial c_A}{\partial t} = D\frac{\partial^2 c_A}{\partial x^2} \rightarrow D\frac{\mathrm{d}^2 c_A}{\mathrm{d}x^2} = 0 \tag{2.122}$$

$$\begin{cases} c_A(\delta_D) = c_A^b \\ c_A(0) = \bar{c}_A(0) \end{cases} \tag{2.123}$$

Under this conditions, the concentration profile is found to be:

$$c_A(x) = \frac{c_A^b - \bar{c}_A(0)}{\delta_D} x + \bar{c}_A(0) \tag{2.124}$$

A close look shows that this situation is exactly what Nernst proposed in his hypothesis about transport in electrochemical systems.

The existence of a finite diffusion layer also changes the boundary conditions for the oscillating concentration:

$$\jmath\omega\tilde{c}_A - D\frac{\mathrm{d}^2\tilde{c}_A}{\mathrm{d}x^2} = 0 \tag{2.125}$$

$$\begin{cases} \tilde{c}_A(\delta_D) = 0 \\ \tilde{c}_A(x=0) = \tilde{c}_A(0) \end{cases} \tag{2.126}$$

Solving this differential equation, we get:

$$\tilde{c}_A(x) = \frac{\tilde{c}_A(0)}{1 - \exp\left(2\sqrt{\frac{J\omega}{D}}\delta_D\right)}\left\{\exp\left(\sqrt{\frac{J\omega}{D}}x\right) - \exp\left[\sqrt{\frac{J\omega}{D}}(2\delta_D - x)\right]\right\} \tag{2.127}$$

And the diffusion impedance is:

$$-\frac{\Delta c_A(0)}{\Delta I} = \frac{\tanh\left(\sqrt{\frac{J\omega}{D}}\delta_D\right)}{FA\sqrt{J\omega D}} \tag{2.128}$$

Where $\tanh(x)$ represents the hyperbolic tangent of x.

Finally, the faradaic impedance is given by:

$$Z_f = R_{ct} + R_{ct}k_h\frac{\tanh\left(\sqrt{\frac{J\omega}{D}}\delta_D\right)}{\sqrt{J\omega D}} \tag{2.129}$$

A Nyquist plot of this faradaic impedance is presented in figure 2.8.

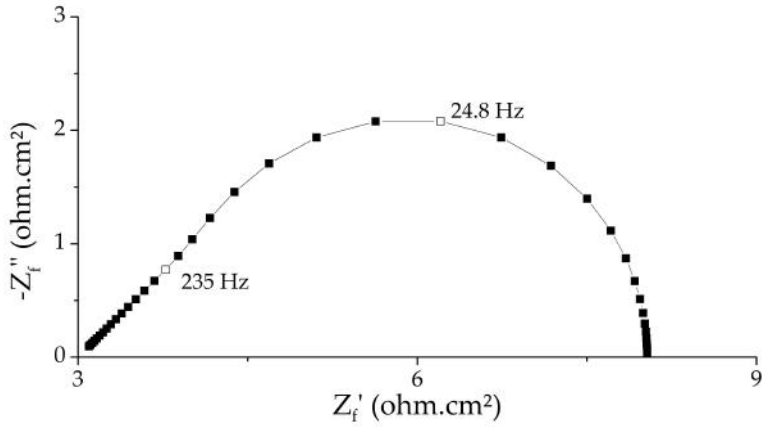

Figure 2.8: Nyquist plot of the faradaic impedance represented by equation 2.129. (R_{ct} = 3 ohm.cm^2, $R_{ct}k_h$ = 4 10^{-3} ohm.cm^2.s^{-1}, D = 9 10^{-9} m^2.s^{-1}, δ_D = 1.13 10^{-5} m)

The first thing to notice is that, for systems with finite diffusion layers, the diffusion impedance does not grow indefinitely. In fact, it tends towards a finite value as the frequency goes towards zero, much like the behaviour of loops generated by adsorbed intermediates. But, an attentive inspection of the diffusion impedance graph shows that, unlike those of the adsorbed species, it does not have an hemispherical shape. Indeed, its asymptotic limit for high frequencies is a straight line with a 45° angle with the real axis, *i.e.*, its high frequency limit is exactly the Warburg impedance:

$$\lim_{\omega\to\infty}\frac{\tanh\left(\sqrt{\frac{J\omega}{D}}\delta_D\right)}{\sqrt{J\omega D}} = \frac{1}{\sqrt{J\omega D}} \tag{2.130}$$

Figure 2.9 shows how both impedances are, at first, coincident and, then, they start diverging as $\omega \to 0$.

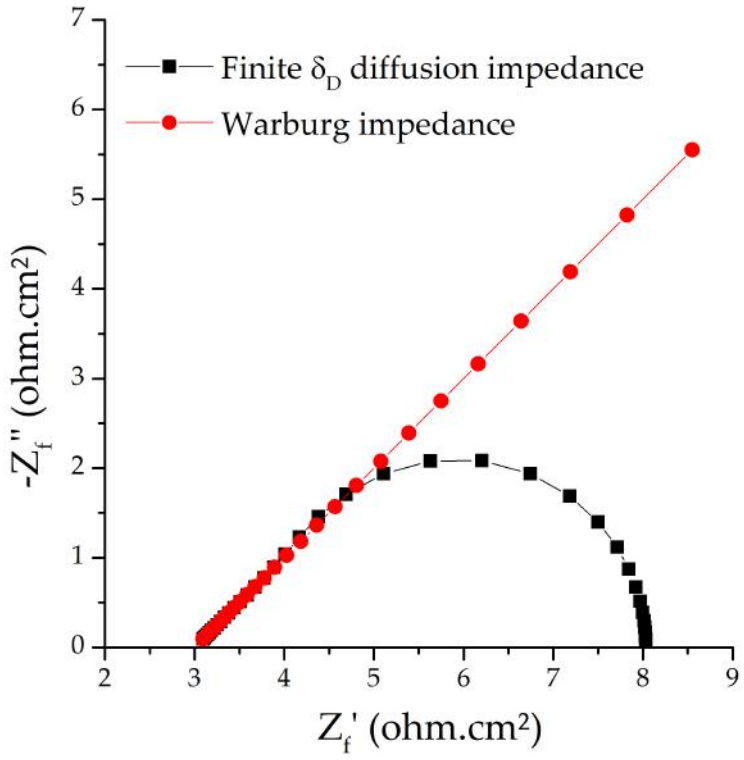

Figure 2.9: Comparison between Warburg impedance and the diffusion impedance for finite δ_D.

Can we draw some physicochemical meaning from this initial similarity between both impedances? The answer lies in the oscillating concentration profiles. At high frequencies, the concentration perturbations for both cases do not propagate much into the solution, *i.e.*, they are essentially nil by the time they reach the thickness δ_D. Hence, for the case of finite δ_D, it is *as if* the diffusion layer had infinite extent and both systems behave similarly. However, as the frequency decreases, concentration waves start reaching the diffusion layer thickness and are immediately stopped. At this point, the oscillating concentration profiles start to differ and the impedances diverge.

RDE systems and the convection-diffusion impedance

The former cases addressed systems whose sole transport mode was diffusion. However, in RDE systems, it is indispensable to include the convection contribution to the overall flux. Hence, the relevant equations for the steady state are:

$$D\frac{\mathrm{d}^2\bar{c}_A}{\mathrm{d}z^2} - v_z\frac{\mathrm{d}\bar{c}_A}{\mathrm{d}z} = 0 \tag{2.131}$$

$$\bar{I} = FAk_h\bar{c}_A(0) \tag{2.132}$$

With the following boundary conditions:

$$\begin{cases} c_A(z \to \infty) = c_A^b \\ c_A(0) = \bar{c}_A(0) \end{cases} \tag{2.133}$$

These are the same boundary conditions applied to determine the current at the original formulation by Levich. As for the transient equation for the mass transport, we have:

$$\jmath\omega\tilde{c}_A - D\frac{\mathrm{d}^2\tilde{c}_A}{\mathrm{d}z^2} + v_z\frac{\mathrm{d}\tilde{c}_A}{\mathrm{d}z} = 0 \tag{2.134}$$

And the boundary conditions are:

$$\begin{cases} \tilde{c}_A(z \to \infty) = 0 \\ \tilde{c}_A(0) = \tilde{c}_A(0) \end{cases} \tag{2.135}$$

Contrary to its steady state equivalent, equation 2.134 does not have an analytic solution. Its first numerical solution using the finite differences method was presented by Coueignoux and Schuhmann for Schmidt numbers of 10^2, 10^3 and 10^4 [56]. To validate their results, the authors made use of the fact that, as the frequency tends towards zero, the value for $\dfrac{\Delta c}{\Delta I}$ should converge to the derivative of the steady state concentration as a function of the steady state current, which can be calculated using Levich's theory. Later on, Levart and Schuhmann extended this work by incorporating an explicit dependence of the diffusion impedance on the Schmidt number. In doing so, they built graphs which could be used to determine the diffusion impedance for any Schmidt number *via* interpolation [15].

Around the same period, Deslouis *et al.* showed that the diffusion impedance calculated by Coeuignoux and Schuhmann were in better agreement with experimental data than the impedance obtained by fitting the data to equation 2.129 (see figure 2.10). They attributed this to the fact that equation 2.129 makes use of Nernst's hypothesis, disregarding the convective contribution to the mass transport [57].

Many efforts have been made to find analytical expressions for the convective-diffusion impedance. Levart and Schuhmann were the first to propose that the dimensionless diffusion impedance could be written as an asymptotic series in $Sc^{-1/3}$, that is [15]:

$$M(z, Sc, u) = M(z, \infty, u) + \frac{M_1(z, u)}{Sc^{1/3}} + \frac{M_2(z, u)}{Sc^{2/3}} + O(Sc^{-1}) \tag{2.136}$$

Where $M(z, Sc, u) = zFD\left(\dfrac{\Omega}{\nu}\right)^{1/2}\dfrac{\Delta c}{\Delta i}$ and $u = (0.51023Sc)^{-2/3}\dfrac{\omega\nu}{\Omega D}$.

However, the authors argued that an analytical solution of the relevant equations would be too troublesome and opted for determining the numerical solution for a range

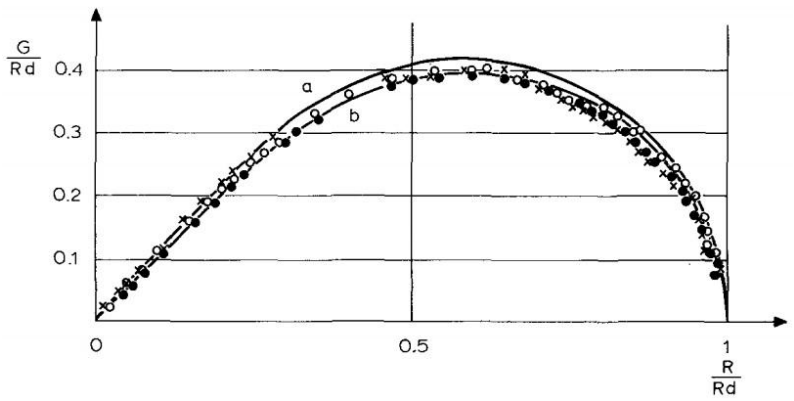

Figure 2.10: Nyquist plot of the normalized diffusion impedance for a RDE system. Marks represent experimental data. Line *a* represents the diffusion impedance found by fitting the data to equation 2.129. Line *b* represents the diffusion impedance calculated by Coueignoux and Schuhmann [56]. (Adapted from [57])

of Schmidt numbers. A few years later, they presented a new power series development whose coefficients were tabulated and could be readily used to determine the diffusion impedance for any Schmidt number [16, 58].

Newman and Homsy also worked on the problem and used singular perturbation techniques to derive an asymptotic solution valid for high frequencies and infinite Schmidt number [59]. Later on, Newman and Scherson used Laplace transforms to find a series expansions that could be used for low frequencies [60].The results were presented in the form of the derivative of the dimensionless concentration ∂' as a function of the dimensionless frequency K:

For high frequencies:

$$\begin{cases} -\dfrac{1}{\partial'_{HF}(0)} = \dfrac{a}{a^2+b^2} - J\dfrac{b}{a^2+b^2} \\ \\ a = \dfrac{\sqrt{2}}{2}\left(K^{1/2} - \dfrac{9}{32}K^{-5/2}\right);\ b = \dfrac{\sqrt{2}}{2}\left(K^{1/2} + \dfrac{9}{32}K^{-5/2}\right) - \dfrac{3}{4K} \end{cases} \tag{2.137}$$

For low frequencies:

$$\begin{cases} -\dfrac{1}{\partial'_{LF}(0)} = \dfrac{r}{s^2+r^2} - J\dfrac{s}{s^2+r^2} \\ \\ r = \dfrac{1}{\Gamma(4/3)} + K^2\displaystyle\sum_{n=0}^{\infty}\frac{B_n}{\lambda_n^2+K^2};\ s = K\sum_{n=0}^{\infty}\frac{B_n\lambda_n}{\lambda_n^2+K^2} \end{cases} \tag{2.138}$$

The terms B_n and λ_n are, respectively, the coefficients and the eigenvalues of the Sturm-Liouville system the authors used to find the solution for low frequencies.

Although these equations did approach the exact numerical solutions, they still failed to reduce their margin of error to an acceptable level. This was pointed out by Levart

and Schuhmann, who showed that, in fact, their procedure was much more accurate than Newman's for either higher or lower frequencies [61, 62]. Indeed, when Newman and Tribollet presented their seminal paper on electro-hydrodynamic impedance, they used the procedure proposed by Levart and Schuhmann to determine the diffusion impedance of an electrochemical system [63].

Also worth mentioning are the methods introduced by Deslouis *et al.*, who used Airy functions to obtain solutions for approximate versions of the diffusion-convection transient equation and reported a reasonable fit throughout the whole frequency range [64].

2.7 Electro-hydrodynamic impedance

Can we generalize the principle behind the electrochemical impedance technique? What is it really based on? In its most abstract formulation, impedance methods consist in applying a perturbation to the input signal of a system (*e.g.*, the potential of an electrochemical cell) and evaluating the behaviour of the output signal (*e.g.*, the current). *There are no restrictions to the nature of the input/output signals* as long as we can propose reliable models to interpret the results [65]. Hence, it should be no surprise that there are several different impedance techniques that have been employed to study electrochemical systems; for instance, thermoelectrochemical impedance [66–68], electro-optical transmittance [69] and electrogravimetric impedance [70, 71].

One of these techniques is the *electro-hydrodynamic impedance* (EHD), which consists in varying the rotation speed of the RDE to perturb the concentration profile and, consequently, the mass transport processes. The output signal may be either the potential or the current [49]. The idea of superposing a sinusoidal modulation to the steady rotation speed of a RDE was first proposed by Miller and Bruckenstein and it was refered to as *hydrodynamically modulated rotating disk electrode* - HMRDE [72, 73]. However, the authors were more interested in using this technique to improve analytical sensitivity than in studying mass transfer phenomena.

It was the *Groupe de Recherche "Physique de Liquides et Électrochimie"*, who had already become an international reference on the use of electrochemical impedance, who pioneered the treatment of this modulated rotation speed with an impedance formalism, initially calling it *electromechanical impedance* [74, 75]. By 1983, Tribollet and Newman would develop the theoretical basis and terminology which then became standard [49, 63].

2.7.1 Unsteady velocity profiles

We start by separating the steady state and transient components of the rotation speed:

$$\Omega = \bar{\Omega} + \Delta\Omega \exp \jmath\omega t \rightarrow \frac{\Omega}{\bar{\Omega}} = \frac{\bar{\Omega}}{\bar{\Omega}} + \underbrace{\frac{\Delta\Omega}{\bar{\Omega}}}_{\epsilon} \exp(\jmath\omega t) \tag{2.139}$$

$$\frac{\Omega}{\bar{\Omega}} = 1 + \epsilon \exp(\jmath\omega t) \tag{2.140}$$

Then, we assume that the modulation in the rotation speed is small enough to ensure that the velocity profile will behave linearly. That means we can write the new velocities as:

$$\begin{cases} v_r = \bar{v}_r + \epsilon\Delta v_r \exp(\jmath\omega t) \\ v_\partial = \bar{v}_\partial + \epsilon\Delta v_\partial \exp(\jmath\omega t) \\ v_z = \bar{v}_z + \epsilon\Delta v_z \exp(\jmath\omega t) \end{cases} \tag{2.141}$$

Now, we introduce a new set of dimensionless velocities to account for the sinusoidal components:

$$\begin{cases} v_r = r\bar{\Omega}\left[F(\xi) + \epsilon\tilde{f}(\xi,\omega)\exp(\jmath\omega t)\right] \\ v_\partial = r\bar{\Omega}\left[G(\xi) + \epsilon\tilde{g}(\xi,\omega)\exp(\jmath\omega t)\right] \\ v_z = \left(\nu\bar{\Omega}\right)^{1/2}\left[H(\xi) + \epsilon\tilde{h}(\xi,\omega)\exp(\jmath\omega t)\right] \end{cases} \tag{2.142}$$

After substitution of the velocity terms for their dimensionless counterparts in the Navier-Stokes and continuity equations, we get:

$$\begin{cases} 2\tilde{f} + \tilde{h}' = 0 \\ \jmath\tilde{f}p + 2F\tilde{f} - 2G\tilde{g} + H\tilde{f}' + F'\tilde{h} - \tilde{f}'' = 0 \\ \jmath\tilde{g}p + 2G\tilde{f} + 2F\tilde{g} + G'\tilde{h} + H\tilde{g}' - \tilde{g}'' = 0 \end{cases} \tag{2.143}$$

Where $p = \dfrac{\omega}{\Omega}$ represents a dimensionless frequency. In this development, we neglected all quadratic terms (ϵ^2) on the basis of linearity. The boundary conditions are:

$$\begin{cases} \tilde{h}(0,p) = 0;\ \tilde{f}(0,p) = 0;\ \tilde{g}(0,p) = 1 \\ \tilde{f}(\xi \rightarrow \infty, p) = 0;\ \tilde{g}(\xi \rightarrow \infty, p) = 0 \end{cases} \tag{2.144}$$

To solve this system, Newman and Tribollet first separated real and imaginary components ($\tilde{x} = \tilde{x}_1 + \jmath\tilde{x}_2$), obtaining two new systems which could be solved using a numerical

method developed by Newman [63]:

$$\begin{cases} 2\tilde{f}_1 + \tilde{h}_1' = 0 \\ 2\tilde{f}_2 + \tilde{h}_2' = 0 \\ -\tilde{f}_2 p + 2F\tilde{f}_1 - 2G\tilde{g}_1 + H\tilde{f}_1' + F'\tilde{h}_1 - \tilde{f}''_1 = 0 \\ \tilde{f}_1 p + 2F\tilde{f}_2 - 2G\tilde{g}_2 + H\tilde{f}_2' + F'\tilde{h}_2 - \tilde{f}''_2 = 0 \\ -\tilde{g}_2 p + 2G\tilde{f}_1 + 2F\tilde{g}_1 + G'\tilde{h}_1 + H\tilde{g}_1' - \tilde{g}_1'' = 0 \\ \tilde{g} p_1 + 2G\tilde{f}_2 + 2F\tilde{g}_2 + G'\tilde{h}_2 + H\tilde{g}_2' - \tilde{g}''_2 = 0 \end{cases} \tag{2.145}$$

With a new set of boundary conditions:

$$\begin{cases} \tilde{h}_1(0,p) = \tilde{h}_2(0,p) = 0;\ \tilde{f}_1(0,p) = \tilde{f}_2(0,p) = 0;\ \tilde{g}_1(0,p) = 1;\ \tilde{g}_2(0,p) = 0 \\ \tilde{f}_1(\xi \to \infty, p) = \tilde{f}_2(\xi \to \infty, p) = 0;\ \tilde{g}_1(\xi \to \infty, p) = \tilde{g}_2(\xi \to \infty, p) = 0 \end{cases} \tag{2.146}$$

In order to have an analytic expression for the transient velocities, the authors used power series to approximate these functions at distances close to the electrode surface. After substitution of the series in the Navier-Stokes and continuity equations, we get:

$$\begin{cases} f_1(\xi,p) = f_1'(0,p)\xi - \xi^2 + \left(\dfrac{1.23184 - 2g_1'(0,p) - pf_2'(0,p)}{6}\right)\xi^3 \\ f_2(\xi,p) = f_2'(0,p)\xi - \left(\dfrac{-2g_2'(0,p) - pf_1'(0,p)}{6}\right)\xi^3 \\ g_1(\xi,p) = 1 + g_1'(0,p)\xi + \left(\dfrac{1.02046 + 2f_1'(0,p) - pg_2'(0,p)}{6}\right)\xi^3 \\ g_2(\xi,p) = g_2'(0,p)\xi + \dfrac{p}{2}\xi^2 + \left(\dfrac{2f_2'(0,p) + pg_1'(0,p)}{6}\right)\xi^3 \\ h_1(\xi,p) = -f_1'(0,p)\xi^2 + \dfrac{2}{3} \\ h_2(\xi,p) = -f_2'(0,p)\xi^2 \end{cases} \tag{2.147}$$

The values for each p can, then, be calculated using numerical integration.

2.7.2 Unsteady concentration profile

To determine the effect of varying the rotation speed on the concentration profile, we have to solve the transient mass conservation equation:

$$c(z,t) = \bar{c}(z) + \Delta c \exp(\jmath\omega t) \tag{2.148}$$

$$v_z(z,t) = \left(\nu\bar{\Omega}\right)^{1/2}\left[H(\xi) + \epsilon\tilde{h}(\xi,p)\exp(\jmath\omega t)\right] \tag{2.149}$$

$$\frac{\partial c}{\partial t} = D\frac{\partial^2 c}{\partial z^2} - v_z\frac{\partial c}{\partial z} \tag{2.150}$$

Tribollet and Newman proposed the following change of variables:

$$K = \frac{\omega}{\bar{\Omega}}\left(\frac{9\nu}{a^2 D}\right)^{1/3}, B = \left(\frac{3}{a^4}\right)^{1/3}, \xi = \frac{z}{\delta}, \delta = \left(\frac{3D}{a\nu}\right)^{1/3}\left(\frac{\nu}{\bar{\Omega}}\right)^{1/2} \tag{2.151}$$

When applied to the linearized convective-diffusion equation, we get:

$$\begin{aligned}\frac{\mathrm{d}^2\Delta c}{\mathrm{d}\xi^2} + \left(3\xi^2 - \frac{B\xi^3}{Sc^{1/3}} + \ldots\right)\frac{\mathrm{d}\Delta c}{\mathrm{d}\xi} - \jmath K\Delta c = \\ -\epsilon\left(3\frac{\tilde{f}'(0,p)}{a}\xi^2 - \frac{2B}{Sc^{1/3}} + \ldots\right)\frac{\mathrm{d}\bar{c}}{\mathrm{d}\xi}\end{aligned} \tag{2.152}$$

To solve this equation, the authors used the method of separation of variables: $\Delta c(\xi) = \partial(\xi)\hat{\jmath}(\xi)$, $\partial(\xi)$ being the solution to the homogeneous equation, which is the same equation used to determine the diffusion impedance. Following the series development introduced by Levart and Schuhmann [15], they expanded $\partial(\xi)$ in powers of $Sc^{-1/3}$:

$$\partial(\xi, K, Sc) = \partial_0(\xi, K, \infty) + \partial_1(\xi, K)Sc^{-1/3} + \ldots \tag{2.153}$$

After solving the differential equations for ∂_0 and ∂_1, they tabulated the results for the dimensionless diffusion impedance:

$$-\frac{1}{\partial'(0)} = Z_0 + Z_1 Sc^{-1/3} + \ldots \tag{2.154}$$

Going back to the convective-diffusion equation, we have:

$$\frac{\mathrm{d}^2\hat{\jmath}}{\mathrm{d}\xi^2} + \left(3\xi^2 - \frac{B\xi^3}{Sc^{1/3}} + \frac{2\partial'}{\partial}\right)\frac{\mathrm{d}\hat{\jmath}}{\mathrm{d}\xi} = -\epsilon\left(3\frac{\tilde{f}'(0,p)}{a}\xi^2 - \frac{2B\xi^3}{Sc^{1/3}}\right)\frac{1}{\partial}\frac{\mathrm{d}\bar{c}}{\mathrm{d}\xi} \tag{2.155}$$

Applying boundary equations $\Delta c(\xi = 0) = \Delta c(0)$ and $\Delta c(\xi \to \infty) = 0$, the authors find that:

$$\left.\frac{\mathrm{d}\Delta c}{\mathrm{d}z}\right|_{z=0} = \frac{\Delta c(0)}{\delta}\partial'(0) + \frac{\Delta\Omega}{\bar{\Omega}}\left.\frac{\mathrm{d}\bar{c}}{\mathrm{d}z}\right|_{z=0} W \tag{2.156}$$

Where $W = \int_0^\infty \left(3\frac{\tilde{f}'(0,p)}{a}\xi^2 - \frac{2B}{Sc^{1/3}}\xi^3 + \ldots\right)\partial\mathrm{d}\xi$ is a quantity that was also tabulated by the authors in the form of a series:

$$W = \tilde{f}'(0,p)(t_1 + \jmath t_2) + \frac{1}{Sc^{1/3}}\left[\tilde{f}'(0,p)(t_3 + \jmath t_4) + t_5 + \jmath t_6 \ldots\right] \tag{2.157}$$

$$t_1 = \frac{3}{a}\int_0^\infty \xi^2 \Re\{\partial_0\} d\xi \qquad t_2 = \frac{3}{a}\int_0^\infty \xi^2 \Im\{\partial_0\} d\xi \tag{2.158}$$

$$t_3 = \frac{3}{a}\int_0^\infty \xi^2 \Re\{\partial_1\} d\xi \qquad t_4 = \frac{3}{a}\int_0^\infty \xi^2 \Im\{\partial_1\} d\xi \tag{2.159}$$

$$t_5 = -2B\int_0^\infty \xi^3 \Re\{\partial_0\} d\xi \qquad t_6 = -2B\int_0^\infty \xi^3 \Im\{\partial_0\} d\xi \tag{2.160}$$

Where $\Re\{X\}$ stands for the real part of X and $\Im\{X\}$ for its imaginary part.

To derive the relationship between the electro-hydrodynamic impedance and the electric quantities, we can use the same formalism presented for the electrochemical impedance. We'll take the case of a single electroactive species with no adsorption processes: $A + e^- \longrightarrow B$

$$\begin{aligned}
i &= i(E, c(0)) \\
\Delta i &= \left.\frac{\partial i}{\partial E}\right|_{c(0)} \Delta E + \left.\frac{\partial i}{\partial c(0)}\right|_E \Delta c(0) \\
\Delta i &= \frac{1}{R_{ct}}\Delta E + \frac{\Delta i}{FD}\frac{\delta}{\partial'(0)}\left.\frac{\partial i}{\partial c(0)}\right|_E - \frac{\Delta\Omega}{\bar{\Omega}}\frac{\bar{\imath}}{FD}\frac{\delta}{\partial'(0)} W \left.\frac{\partial i}{\partial c(0)}\right|_E \\
\Delta E &= R_{ct}\Delta i - \frac{R_{ct}}{FD}\frac{\delta}{\partial'(0)}\left.\frac{\partial i}{\partial c(0)}\right|_E \Delta i + \frac{\Delta\Omega}{\bar{\Omega}}\frac{R_{ct}\bar{\imath}}{FD}\frac{\delta}{\partial'(0)}\left.\frac{\partial i}{\partial c(0)}\right|_E W
\end{aligned} \tag{2.161}$$

2.7.3 Potentiostatic control

Further assumptions may help to simplify equation 2.161. For instance, under potentiostatic control, $\Delta E = 0$ and assuming the charge transfer step is much faster than the transport step, we get:

$$R_{ct} \ll \frac{R_{ct}}{FD}\frac{\delta}{\partial'(0)}\left.\frac{\partial i}{\partial c(0)}\right|_E \tag{2.162}$$

$$\frac{\Delta\Omega}{\bar{\Omega}}\frac{R_{ct}\bar{\imath}}{FD}\frac{\delta}{\partial'(0)}\left.\frac{\partial i}{\partial c(0)}\right|_E W - \frac{R_{ct}}{FD}\frac{\delta}{\partial'(0)}\left.\frac{\partial i}{\partial c(0)}\right|_E \Delta i = 0 \tag{2.163}$$

$$\frac{\Delta i}{\Delta\Omega} = \frac{\bar{\imath}}{\bar{\Omega}} W \tag{2.164}$$

Such condition greatly simplifies the mathematical treatment and can be achieved by conducting the experiment on the limiting current condition. There's also an additional advantage to this: it is not possible to conduct electrochemical impedance measurements at the limiting current condition, because $Z_f \to \infty$ at the current plateau. Hence, the EHD measurement can provide information about transient phenomena at regions previously unexplored.

EHD impedance data are more commonly presented using Bode diagrams. Figure 2.11 presents the reduced amplitude and the phase shift as a function of dimensionless frequency for a system described by equation 2.164.

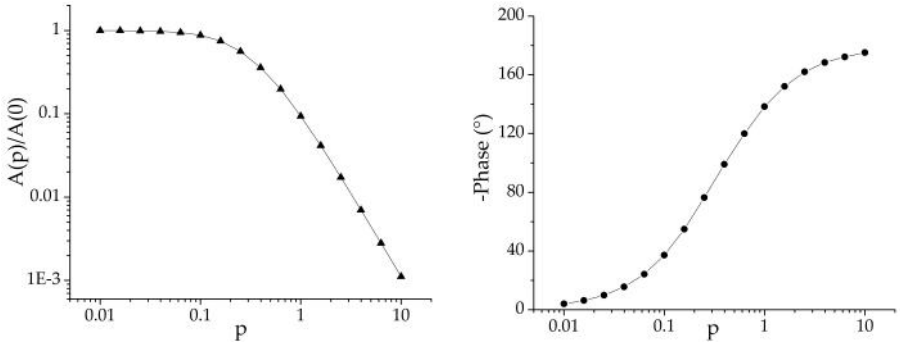

(a) Reduced amplitude as a function of dimensionless frequency

(b) −Phase as a function of dimensionless frequency

Figure 2.11: Bode plots of the EHD impedance for a system with facile kinetics at the limiting current condition

2.7.4 Galvanostatic control

Although less common, it is also possible to investigate the EHD impedance under galvanostatic control. In this case, $\Delta i = 0$ and we have:

$$\frac{\Delta E}{\Delta \Omega} = \frac{\bar{\imath}}{\bar{\Omega}} \frac{R_{ct}}{FD} \frac{\delta}{\partial'(0)} \left. \frac{\partial i}{\partial c(0)} \right|_E W \tag{2.165}$$

The term $\frac{R_{ct}}{FD} \frac{\delta}{\partial'(0)} \left. \frac{\partial i}{\partial c(0)} \right|_E$, related to the diffusion impedance, cannot be simplified without adding new hypotheses. Because of that, the EHD impedance under galvanostatic control tends to be, in general, more complex than that obtained with potentiostatic control.

2.7.5 Application in the study of reaction mechanisms

Electro-hydrodynamic impedance is suited for the study of systems which are either partially or totally controlled by mass transport phenomena [49]. It has been used, for instance, to study the behaviour of partially blocked electrodes [76], coated electrodes [77], dissolution mechanisms involving film formation, such as Cu in HCl solutions [78] and the dissolution of Fe in sulphate solutions[22, 79]. Even though it is not as widely used as the electrochemical impedance, which may be partly explained by the more laborious mathematical treatment and the lack of marketed equipment specially designed for the measurements, EHD impedance can certainly provide many valuable information about the most different systems. Its capabilities are still under exploration and many advances have been made during the last years [80]. As technology continues to advance, it may prove to be a valuable asset in the uncovering of new scientific findings.

2.8 Any bricks left?

Throughout this chapter, an attempt was made to clarify several aspects which cannot be taken for granted in the study of electrochemical systems. First, electrochemical reactions are heterogeneous and involve a charge transfer between electrode and electrolyte solution. This phenomenon creates a scenario in which several steps may participate to a bigger or lesser extent in the determination of the reaction rate (measured in the form of current). Also, the charge separation observed in the vicinities of the electrode surface leads to the formation of an electrical double layer, whose presence must be accounted for, since it influences the result of various experiments.

To understand the mechanism of electrochemical processes, we need to make use of well-controlled systems which can provide reliable data and which have firm theoretical basis. That led us to opt for the study of rotating disk electrode systems. However, steady state techniques are unable to provide enough information to describe most electrochemical processes. We have, then, decided to complement our steady state measurements with transient techniques based on the impedance concept. By disturbing an input signal, whether it be the potential or the rotation speed, we can use the output data to develop better models. Since these techniques are based on *linear time-invariant theory*, some precautions regarding the experimental parameters are necessary. The combination of electrical and non-electrical quantities provides a richer set of information that can be used to understand the mechanisms affecting the mass transfer in the electrolyte solution.

Our road is paved and we may now move forward to the next topic: the discussion about chemical-electrochemical processes and how they differ from the usual electrochemical reactions.

Chapter 3

Literature review

3.1 Chemical-electrochemical processes

Chemical-electrochemical (CE) processes are those in which a chemical (bulk) reaction precedes the electrochemical step. The simplest case would be:

$$\begin{cases} \mathrm{A} \underset{\mathrm{k_B}}{\overset{\mathrm{k_A}}{\rightleftharpoons}} \mathrm{B} \\ \mathrm{A} + \mathrm{e}^- \xrightarrow{\mathrm{k}_h} \mathrm{C} \end{cases}$$

The most familiar example of this kind of reaction is the reduction of weak acids, such as the acetic acid [20]:

$$\begin{cases} \mathrm{CH_3COOH} \underset{\mathrm{k_2}}{\overset{\mathrm{k_1}}{\rightleftharpoons}} \mathrm{CH_3COO^-} + \mathrm{H^+} \\ \mathrm{H^+} + \mathrm{e}^- \xrightarrow{\mathrm{k}_h} \frac{1}{2}\,\mathrm{H_2} \end{cases}$$

Because this multistep process includes a charge transfer, electrochemical methods are natural candidates to study these reaction mechanisms. We may be interested, *e.g.*, in determining the values of the kinetic constants involved in the chemical step [81, 82]. Or, we may want to *predict* the response of a system which is described by a CE mechanism.

As we've mentioned in subsection 2.4.9, the presence of homogeneous reactions changes the concentration profile of the electroactive species. This is evidenced by the addition of a source term to the mass conservation equations. If studied with a RDE system,

we'd have:

$$\begin{cases} \mathrm{A} \underset{\mathrm{k_B}}{\overset{\mathrm{k_A}}{\rightleftharpoons}} \mathrm{B} \\ \mathrm{A} + \mathrm{e}^- \xrightarrow{\mathrm{k}_h} \mathrm{C} \end{cases}$$

$$\begin{cases} \dfrac{\partial c_A}{\partial t} = D_A \dfrac{\partial^2 c_A}{\partial z^2} - v_z \dfrac{\partial c_A}{\partial z} + k_B c_B - k_A c_A \\ \\ \dfrac{\partial c_B}{\partial t} = D_B \dfrac{\partial^2 c_B}{\partial z^2} - v_z \dfrac{\partial c_B}{\partial z} - k_B c_B + k_A c_A \end{cases} \tag{3.1}$$

Despite the fact that species B is not electroactive, its concentration profile influences that of species A. The system is, now, comprised of a set of two partial differential equations which must be solved simultaneously.

3.1.1 Steady state current density

Koutecký and Levich were the first to provide an analytical treatment to this problem, deriving an expression for the steady state current density in the case of equal diffusion coefficients - $D_A = D_B = D$ [11]. They were soon followed by Dogonadze, which extended the results to the case of unequal diffusion coefficients [12].[1] For the limiting current condition, they arrived at the following expressions for the system displayed above:

$$i_{KL} = \frac{FD\left(c_B^b + c_A^b\right)}{\delta_D + K\sqrt{\dfrac{D}{k_A + k_B}}} \tag{3.2}$$

$$i_{DG} = \frac{FD_{eff}\left(c_B^b + c_A^b\right)}{\delta_{eff} + K\dfrac{D_A}{D_B}\sqrt{\dfrac{D_A D_B}{D_B k_A + D_A k_B}}} \tag{3.3}$$

In these equations, i_{KL} stands for the limiting current density derived by Koutecký and Levich, i_{DG} is the expression derived by Dogonadze, $K = \dfrac{k_A}{k_B}$ and represents the equilibrium constant of the chemical reaction, $D_{eff} = \dfrac{D_B k_A + D_A k_B}{k_A + k_B}$ and $\delta_{eff} = \delta_D \left(\dfrac{D_{eff}}{D_A}\right)^{1/3}$.

To get to these results, the authors had to introduce a new concept - and a new hypothesis. Assuming that the chemical step is very fast, they proposed that the chemical equilibrium would hold across the whole solution, except inside a small layer close to the electrode surface - the *reaction layer* - where the consumption of species A would break the equilibrium. The thickness of this layer, δ_R, is calculated as:

[1] Unfortunately, these articles are not easily available. For the interested reader, a derivation of these results can be found in the work by Tolmachev and Scherson [83].

For equal diffusion coefficients:

$$\delta_R = \left(\frac{D}{k_A + k_B} \right)^{1/2} \tag{3.4}$$

For unequal diffusion coefficients:

$$\delta_R = \left(\frac{D_A D_B}{D_B k_A + D_A k_B} \right)^{1/2} \tag{3.5}$$

Also implied in this formulation is the fact that the reaction layer thickness must be much smaller than the diffusion layer thickness: $\delta_R \ll \delta_D$.

These ideas were soon put to test by Vielstich and Jahn, who used the RDE system to calculate the dissociation and recombination constants of acetic acid according to the reaction layer theory. They reported good agreement between these results and those obtained from measurements conducted with different techniques [81]. Inasmuch as it can provide theoretical ground for the study of systems with fast kinetics, the reaction layer hypothesis is unable to predict the extent of its validity, *i.e.*, there's no *a priori* way of knowing if a given system meets its *criteria*. Also, the reaction layer hypothesis may turn from valid to invalid *for the same CE process*. To understand this, we have to note that the reaction layer hypothesis requires that - we'll consider the general case of unequal diffusion coefficients:

$$\underbrace{\left(\frac{D_A D_B}{D_B k_A + D_A k_B} \right)^{1/2}}_{\delta_R} \ll \underbrace{\sqrt{\frac{\nu}{\Omega}} \left(1.611 Sc_A^{-1/3} + 0.480 Sc_A^{-2/3} + 0.234 Sc_A^{-1} \right)}_{\delta_D} \tag{3.6}$$

Comparing both expressions, it is clear that, for a given solution, the value of δ_R is constant. On the other hand, the value of δ_D will not be determined until we decide which rotation speed to use. Hence, it is physically possible to have $\delta_R \ll \delta_D$ valid for a given set of rotation speeds, but, also, the opposite relation for another set of sufficiently high values of Ω, because increasing Ω decreases the value of δ_D while not having any effect on that of δ_R. We conclude that the reaction layer hypothesis will be more accurate the lower the rotation speed. More importantly, *the reaction layer hypothesis will always fail to describe systems at sufficiently high rotation speeds*. Evidently, these deviations will not be observed for systems of extremely fast kinetics, such as the decomposition of acetic acid [81, 82], or that of bisulfite, since the necessary rotating speed would be either physically unattainable or lead to turbulent behaviour before the deviation could be observed.

Aware of the limitations of the reaction layer approach, many authors have proposed semi-analytical or numerical methods that would allow the calculation of the limiting current for any rotation speed. One of the early investigators was Hale, whose interest was in

determining the transient behaviour of a RDE system according to different experimental arrangements and also in the presence of complicating bulk reactions (CE processes, for example) [84, 85]. His method consisted of a change of variables used to "collapse" the convection-diffusion equation into a new, "diffusion-like", one whose limits of integration were finite. Starting with the original problem:

$$\frac{\partial c}{\partial t} = D\frac{\partial^2 c}{\partial z^2} - v_z\frac{\partial c}{\partial z}; \qquad 0 \leq z < \infty \tag{3.7}$$

The change of variables consists in the following:

$$\begin{cases} u = \dfrac{c}{c^b} \\ x = \dfrac{1}{\delta_D}\displaystyle\int_0^z \exp\left(\int_0^z \frac{v_z}{D}\mathrm{d}z\right)\mathrm{d}z \\ \Psi = \dfrac{Dt}{{\delta_D}^2} \end{cases} \tag{3.8}$$

Thus, the final equation, according to the author, would be:

$$\frac{\partial u}{\partial \Psi} = a^2\frac{\partial^2 u}{\partial x^2}; \qquad 0 \leq x < 1 \tag{3.9}$$

Where $a = \exp\left(\int_0^z \frac{v_z}{D}\mathrm{d}z\right)$.

Years later, the Compton group would adopt the same procedure, which they called "Hale Transformation", to numerically solve the diffusion-convection equation for many processes, including the CE with unequal diffusion coefficients [13, 14]. The authors found good agreement between their calculations and the analytical equation when dealing with fast kinetics, which was already expected and served as a validation of their procedure. The authors, then, showed how their results, also expectedly, deviated from those predicted by the reaction layer hypothesis for ever slower kinetics.

However, Hale's proposal implies a step which is neither discussed in his works nor in those by the Compton group. To see this, let's take a step-by-step approach to the Hale transformation:

$$\frac{\partial c}{\partial t} = D\frac{\partial^2 c}{\partial z^2} - v_z\frac{\partial c}{\partial z} \tag{3.10}$$

Introducing $u = \dfrac{c}{c^b}$ and $\Psi = \dfrac{Dt}{{\delta_D}^2}$:

$$\frac{\partial u}{\partial \Psi}\frac{D}{{\delta_D}^2} = D\frac{\partial^2 u}{\partial z^2} - v_z\frac{\partial u}{\partial z} \tag{3.11}$$

Now, we introduce $x = \frac{1}{\delta_D}\int_0^z \exp\left(\int_0^z \frac{v_z}{D}\mathrm{d}z\right)\mathrm{d}z$:

$$\frac{\partial u}{\partial \Psi}\frac{D}{{\delta_D}^2} = \frac{D}{{\delta_D}^2}\frac{\partial^2 u}{\partial x^2}\exp\left(2\int_0^z \frac{v_z}{D}\mathrm{d}z\right) - \frac{v_z}{\delta_D}\frac{\partial u}{\partial x}\exp\left(\int_0^z \frac{v_z}{D}\mathrm{d}z\right) \tag{3.12}$$

$$\frac{\partial u}{\partial \Psi} = a^2\frac{\partial^2 u}{\partial x^2} - \frac{\delta_D v_z a}{D}\frac{\partial u}{\partial x} \tag{3.13}$$

Both Hale and the Compton group completely neglect the term $\frac{\delta_D v_z a}{D}\frac{\partial u}{\partial x}$ without ever mentioning why. This is, in fact, a simplification which excludes the contributions of the convective term. Also, we cannot be sure whether the deviations of Compton *et al.* results from the analytical expressions really represent a deviation from the reaction layer hypothesis or if they are due to this approximation. Anyway, it is certain that a rigorous approach to the behaviour of CE systems with slower kinetics is lacking.

3.1.2 Diffusion impedance

Contrary to the stationary current, no equations for the diffusion impedance of CE processes in RDE systems are available. Levart and Schuhmann, when devising a series expansion for the diffusion impedances, included the possibility of a preceding chemical step [16]:

For the CE process:

$$\begin{cases} \mathrm{A} \underset{\mathrm{k_B}}{\overset{\mathrm{k_A}}{\rightleftharpoons}} \mathrm{B} \\ \mathrm{A} \longrightarrow \mathrm{C} + \mathrm{e}^- \end{cases} \tag{3.14}$$

$$Z_e = Z_D(j\omega) + \frac{k_A}{k_B}Z_D(j\omega + k_A + k_B) \tag{3.15}$$

Where Z_e is the diffusion impedance for the CE process and Z_D the diffusion impedance without homogeneous reactions. The author's approach was to reformulate the equations using a complex frequency u whose real component would include the chemical step rate constants:

$$u = \chi + j\sigma = \frac{(1.25144)^2 \mathrm{Sc}^{1/3}}{\Omega}(k_A + k_B + j\omega) \tag{3.16}$$

In doing so, they were able to develop the series expansions that have already been mentioned in the previous sections. Nonetheless, their calculations required all diffusion coefficients to be equal. An interesting observation by the authors was that, for increasing values of k_A and k_B, two loops were observed; one related to the usual convective-diffusion impedance and the other to the homogeneous reaction, which the authors called a "reaction impedance" (*impédance de réaction*) [16]. An example of this separation of

the diffusion impedance is presented in figure 3.1.

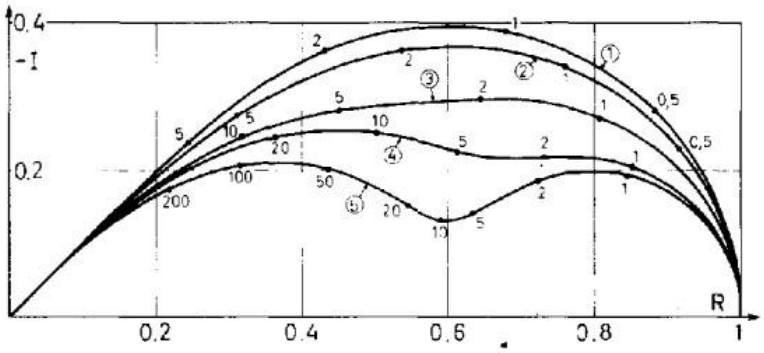

Figure 3.1: Nyquist plot of the reduced diffusion impedance as a function of reduced frequency u for different values of $K = k_A/k_B$ and χ ($Sc = 1000$): $(1)K = 0.01, \chi = 0.01$; $(2)K = 1, \chi = 1$;$(3)K = 2, \chi = 4$; $(4)K = 5, \chi = 10$; $(5)K = 10, \chi = 50$. Adapted from [16].

The existence of this reaction impedance had already been predicted by Gerischer and Vetter, but only for the case of quiescent solutions [86]. Hence, Levart and Schuhmann were, indeed, the first to present diffusion impedances which considered the effect of both convection and homogeneous reactions. More recently, Harding *et al.* developed a finite-difference scheme to account for the case of unequal diffusion coefficients and proposed a "modified Gerischer impedance" equation which could be used to fit the diffusion impedance of CE processes in RDE systems [18]. However, the calculations involve a boundary condition that seems to contradict one of their findings. For the following CE process:

$$\begin{cases} \mathrm{AB} \underset{k_b}{\overset{k_f}{\rightleftharpoons}} \mathrm{A^-} + \mathrm{B^+} \\ \mathrm{B^+} + \mathrm{e^-} \longrightarrow \mathrm{B} \end{cases} \tag{3.17}$$

The authors decided to set as boundary condition:

$$\Delta c_{B^+}(0) = 1 \tag{3.18}$$

In other words, the authors fixed the amplitude of concentration the reacting species at the electrode surface. They went on to analyse the dimensionless diffusion impedance $\frac{-1}{\delta_{D,B^+}}\left(\frac{\Delta c_{B^+}(0)}{\left.\frac{\mathrm{d}c_{B^+}}{\mathrm{d}z}\right|_{z=0}}\right)$ and concluded that it changes according to the potential applied. But, if Δc_{B^+} has no dependence on potential (neither the mass conservation of $\mathrm{B^+}$ nor the boundaries condition include this parameter) neither will its derivative. Hence, it is not possible

for $\frac{-1}{\delta_{D,B^+}}\left(\frac{\Delta c_{B^+}(0)}{\left.\frac{\mathrm{d}c_{B^+}}{\mathrm{d}z}\right|_{z=0}}\right)$ to vary with applied potential. The numerical model proposed by Harding *et al.*, although correct in its premises, does not seem to have been correctly implemented.

3.1.3 Electro-hydrodynamical impedance

To our knowledge, only the work by Vandeputte *et al.* has addressed the EHD impedance of CE processes [17]. Assuming equal diffusion coefficients, the authors have modelled the following CE process:

$$\begin{cases} \mathrm{A} \underset{\mathrm{k_B}}{\overset{\mathrm{k_A}}{\rightleftharpoons}} \mathrm{B} \\ \mathrm{A} + \mathrm{e}^- \longrightarrow \mathrm{C} \end{cases} \tag{3.19}$$

Due to the complexity of the equations, the authors used perturbations methods and, when convenient, neglected higher order terms in their calculations. Good agreement was found for their steady state current equation and the classical one by Koutecký and Levich. The authors also reported good agreement between the analytical approximations for electrochemical impedance and EHD impedance for cases of fast kinetics. Deviations between numerical solutions and analytical expressions were as high as 13% for the cases of slower kinetics at higher frequencies. Another complicating factor recognized by the authors was the neglect of the Schmidt correction for the EHD calculations. It is clear that the approximations are more suitable for systems which can be also described by the asymptotic solutions of Koutecký and Levich.

Hence, the EHD impedance for slower kinetics and also a thorough assessment of more general conditions (unequal diffusion coefficients, inclusion of the Schmidt correction) are topics still missing from the study of CE processes and would provide an important contribution to a better understanding of them.

3.2 Midway along the road

In this section, we've detailed different approaches to study the response of CE processes in RDE systems to both stationary and transient techniques. Some of them, like the works of Koutecký and Levich and Dogonadze, for steady state current, or Levart and Schuhmann for diffusion impedance, make use of simplifications which limit their scope of applicability. Following works have tried to put these ideas on more general terms, but they present inconsistencies that make us question their validity and generality. There's still space for improvement.

With that in mind, we developed a numerical procedure to study these CE processes on very general terms: no additional hypothesis have been added and accuracy is taken to a high degree. By doing so, we find ourselves in a better position to make a broad study of the effect of the physical parameters on both steady state and transient results. With the knowledge we have gathered, we find ourselves midway along our journey: now that we understand *what* we want to study, we need to explain *how* we are going to do it. This is the goal of the next chapter.

Chapter 4

Numerical methodology

4.1 Relevant equations

In this thesis, we analyse the following CE process:

$$\begin{cases} \mathrm{A} \underset{\mathrm{k_B}}{\overset{\mathrm{k_A}}{\rightleftharpoons}} \mathrm{B}; & \dfrac{k_A}{k_B} = K \\ \mathrm{A} + \mathrm{e}^- \xrightarrow{\mathrm{k}_h} \mathrm{C} \end{cases} \tag{4.1}$$

As mentioned in subsection 2.4.7, we consider the solution to have an excess of supporting electrolyte and that physicochemical parameters, such as diffusion coefficients or viscosity, do not vary with position or concentration. Also, the process occurs in a RDE system. Thus, the general mass conservation equations are:

$$\begin{cases} \dfrac{\partial c_A}{\partial t} = D_A \dfrac{\partial^2 c_A}{\partial z^2} - v_z \dfrac{\partial c_A}{\partial z} + k_B c_B - k_A c_A \\ \\ \dfrac{\partial c_B}{\partial t} = D_B \dfrac{\partial^2 c_B}{\partial z^2} - v_z \dfrac{\partial c_B}{\partial z} - k_B c_B + k_A c_A \end{cases} \tag{4.2}$$

The final format of the equations will depend on the kind of numerical experiment we are conducting: steady state limiting current, diffusion impedance or electro-hydrodynamic (EHD) impedance.

4.1.1 Limiting current condition

For the case of the limiting current density (i_{lim}), the equations simplify to:

$$\begin{cases} D_A \dfrac{\mathrm{d}^2 c_A}{\mathrm{d}z^2} - v_z \dfrac{\mathrm{d}c_A}{\mathrm{d}z} + k_B c_B - k_A c_A = 0 \\ \\ D_B \dfrac{\mathrm{d}^2 c_B}{\mathrm{d}z^2} - v_z \dfrac{\mathrm{d}c_B}{\mathrm{d}z} - k_B c_B + k_A c_A = 0 \end{cases} \tag{4.3}$$

With the following boundary conditions:

$$\begin{cases} c_A(0) = 0 \\ c_A(z \to \infty) = c_A^b \\ FD_A \left.\dfrac{\mathrm{d}c_A}{\mathrm{d}z}\right|_{z=0} = i_{lim} \end{cases} \qquad \begin{cases} \left.\dfrac{\mathrm{d}c_B}{\mathrm{d}z}\right|_{z=0} = 0 \\ c_B(z \to \infty) = c_B^b = K c_A^b \end{cases} \tag{4.4}$$

Now, we introduce the change of variables suggested by von Kárman [34]:

$$\xi = \sqrt{\frac{\nu}{\Omega}} z \tag{4.5}$$

Also, we'll replace v_z by the dimensionless velocity $H(\xi)$:

$$v_z(z) = (\nu\Omega)^{1/2} H(\xi) \tag{4.6}$$

The set of equations, then, becomes:

$$\begin{cases} \dfrac{\mathrm{d}^2 c_A}{\mathrm{d}\xi^2} - Sc_A H(\xi) \dfrac{\mathrm{d}c_A}{\mathrm{d}\xi} + \dfrac{Sc_A}{\Omega} (k_B c_B - k_A c_A) &= 0 \\ \\ \dfrac{\mathrm{d}^2 c_B}{\mathrm{d}\xi^2} - Sc_B H(\xi) \dfrac{\mathrm{d}c_B}{\mathrm{d}\xi} + \dfrac{Sc_B}{\Omega} (k_A c_A - k_B c_B) &= 0 \end{cases} \tag{4.7}$$

And the new boundary conditions are:

$$\begin{cases} c_A(0) = 0 \\ c_A(\xi \to \infty) = c_A^b \end{cases} \qquad \begin{cases} \left.\dfrac{\mathrm{d}c_B}{\mathrm{d}\xi}\right|_{\xi=0} = 0 \\ c_B(\xi \to \infty) = c_B^b = K c_A^b \end{cases} \tag{4.8}$$

The limiting current density is given by:

$$i_{lim} = FD_A \left(\frac{\Omega}{\nu}\right)^{1/2} \left.\frac{\mathrm{d}c_A}{\mathrm{d}\xi}\right|_{\xi=0} \tag{4.9}$$

4.1.2 Diffusion impedance

To deal with the diffusion impedance, we consider that a potential perturbation is applied to the RDE whilst maintaining a linear regime. As a consequence, we have modulated responses for both concentration and current density following the formalism presented in section 2.6:

$$\begin{cases} D_A \dfrac{\mathrm{d}^2\Delta c_A}{\mathrm{d}z^2} - v_z \dfrac{\mathrm{d}\Delta c_A}{\mathrm{d}z} + k_B \Delta c_B - k_A \Delta c_A = \jmath\omega \Delta c_A \\ \\ D_B \dfrac{\mathrm{d}^2\Delta c_B}{\mathrm{d}z^2} - v_z \dfrac{\mathrm{d}\Delta c_B}{\mathrm{d}z} - k_B \Delta c_B + k_A \Delta c_A = \jmath\omega \Delta c_B \end{cases} \tag{4.10}$$

To determine the boundary conditions for species A without setting arbitrary values, we made use of the fact that the current density can be calculated using either kinetic or transport equations:

$$i = Fk_A c_A(0) = FD_A \left.\frac{\mathrm{d}c_A}{\mathrm{d}z}\right|_{z=0} \tag{4.11}$$

$$\Delta\left(Fk_h c_A(0)\right) = \Delta\left(FD_A \left.\frac{\mathrm{d}c_A}{\mathrm{d}z}\right|_{z=0}\right) \tag{4.12}$$

$$k_h b_h \bar{c}_A(0)\Delta E + k_h \Delta c_A(0) = D_A \left.\frac{\mathrm{d}\Delta c_A}{\mathrm{d}z}\right|_{z=0} \tag{4.13}$$

$$\Delta c_A(0) = \frac{D_A}{k_h} \left.\frac{\mathrm{d}\Delta c_A}{\mathrm{d}z}\right|_{z=0} - b_h \bar{c}_A(0)\Delta E \tag{4.14}$$

In its present format, this boundary condition would hardly be of any use, but we'll show how we can isolate the surface concentration term after we apply the discretization procedure. Apart from this, the other boundary conditions retain the same aspect:

$$\begin{cases} \Delta c_A(0) = \dfrac{D_A}{k_h} \left.\dfrac{\mathrm{d}\Delta c_A}{\mathrm{d}z}\right|_{z=0} - b_h \bar{c}_A(0)\Delta E \\ \Delta c_A(z \to \infty) = 0 \\ FD_A \left.\dfrac{\mathrm{d}\Delta c_A}{\mathrm{d}z}\right|_{z=0} = \Delta i \end{cases} \qquad \begin{cases} \left.\dfrac{\mathrm{d}\Delta c_B}{\mathrm{d}z}\right|_{z=0} = 0 \\ \Delta c_B(z \to \infty) = 0 \end{cases} \tag{4.15}$$

Like the former case, we introduce the new variables and get a new set of equations:

$$\begin{cases} \dfrac{\mathrm{d}^2\Delta c_A}{\mathrm{d}\xi^2} - Sc_A H(\xi) \dfrac{\mathrm{d}\Delta c_A}{\mathrm{d}\xi} + \dfrac{Sc_A}{\Omega}\left[k_B \Delta c_B - (k_A + \jmath\omega)\Delta c_A\right] &= 0 \\ \\ \dfrac{\mathrm{d}^2\Delta c_B}{\mathrm{d}\xi^2} - Sc_B H(\xi) \dfrac{\mathrm{d}\Delta c_B}{\mathrm{d}\xi} + \dfrac{Sc_B}{\Omega}\left[k_A \Delta c_A - (k_B + \jmath\omega)\Delta c_B\right] &= 0 \end{cases} \tag{4.16}$$

And, also, of boundary conditions:

$$\begin{cases} \Delta c_A(0) = \dfrac{D_A}{k_h}\left(\dfrac{\Omega}{\nu}\right)^{1/2} \left.\dfrac{\mathrm{d}\Delta c_A}{\mathrm{d}\xi}\right|_{\xi=0} - b_h \bar{c}_A(0)\Delta E \\ \Delta c_A(\xi \to \infty) = 0 \\ FD_A\left(\dfrac{\Omega}{\nu}\right)^{1/2} \left.\dfrac{\mathrm{d}\Delta c_A}{\mathrm{d}\xi}\right|_{\xi=0} = \Delta i \end{cases} \qquad \begin{cases} \left.\dfrac{\mathrm{d}\Delta c_B}{\mathrm{d}\xi}\right|_{\xi=0} = 0 \\ \Delta c_B(\xi \to \infty) = 0 \end{cases} \tag{4.17}$$

In this thesis, we'll calculate the diffusion impedance as:

$$Z_D = -FD_A \frac{\Delta c_A(0)}{\Delta i} = -\frac{\Delta c_A(0)}{\left(\dfrac{\Omega}{\nu}\right)^{1/2} \left.\dfrac{\mathrm{d}\Delta c_A}{\mathrm{d}\xi}\right|_{\xi=0}} \tag{4.18}$$

4.1.3 Electro-hydrodynamic impedance

The EHD impedance is a generalization of the diffusion impedance in which the perturbation is applied in the rotation speed. In this situation, the equations are:

$$\begin{cases} D_A \dfrac{\mathrm{d}^2\Delta c_A}{\mathrm{d}z^2} - v_z \dfrac{\mathrm{d}\Delta c_A}{\mathrm{d}z} - \Delta v_z \dfrac{\mathrm{d}\bar{c}_A}{\mathrm{d}z} + k_B \Delta c_B - k_A \Delta c_A = \jmath\omega \Delta c_A \\ D_B \dfrac{\mathrm{d}^2\Delta c_B}{\mathrm{d}z^2} - v_z \dfrac{\mathrm{d}\Delta c_B}{\mathrm{d}z} - \Delta v_z \dfrac{\mathrm{d}\bar{c}_B}{\mathrm{d}z} + k_A \Delta c_A - k_B \Delta c_B = \jmath\omega \Delta c_B \end{cases} \tag{4.19}$$

As for the boundary conditions, they're almost the same as those of the diffusion impedance, the difference being that we are under potentiostatic control, hence, there is no potential oscillation ($\Delta E = 0$).

$$\begin{cases} \Delta c_A(0) = \dfrac{D_A}{k_h} \left.\dfrac{\mathrm{d}\Delta c_A}{\mathrm{d}z}\right|_{z=0} \\ \Delta c_A(z \to \infty) = 0 \\ FD_A \left.\dfrac{\mathrm{d}\Delta c_A}{\mathrm{d}z}\right|_{z=0} = \Delta i \end{cases} \qquad \begin{cases} \left.\dfrac{\mathrm{d}\Delta c_B}{\mathrm{d}z}\right|_{z=0} = 0 \\ \Delta c_B(z \to \infty) = 0 \end{cases} \tag{4.20}$$

Proceeding to the change of variables, we can also replace the modulated axial velocity by a dimensionless velocity:

$$\Delta v_z(z, \omega) = \epsilon \tilde{h}(z, \omega) \tag{4.21}$$

The resulting equations are:

$$\begin{cases} \dfrac{d^2\Delta c_A}{d\xi^2} - Sc_A H(\xi)\dfrac{d\Delta c_A}{d\xi} + \dfrac{Sc_A}{\bar{\Omega}}\left[k_B\Delta c_B - (k_A + \jmath\omega)\Delta c_A\right] &= -Sc_A\epsilon\tilde{h}(\xi,\omega)\dfrac{d\bar{c}_A}{d\xi} \\ \dfrac{d^2\Delta c_B}{d\xi^2} - Sc_B H(\xi)\dfrac{d\Delta c_B}{d\xi} + \dfrac{Sc_B}{\bar{\Omega}}\left[k_A\Delta c_A - (k_B + \jmath\omega)\Delta c_B\right] &= -Sc_B\epsilon\tilde{h}(\xi,\omega)\dfrac{d\bar{c}_B}{d\xi} \end{cases} \tag{4.22}$$

And the boundary conditions:

$$\begin{cases} \Delta c_A(0) = \dfrac{D_A}{k_h}\left(\dfrac{\bar{\Omega}}{\nu}\right)^{1/2}\left.\dfrac{d\Delta c_A}{d\xi}\right|_{\xi=0} \\ \Delta c_A(\xi\to\infty) = 0 \\ FD_A\left(\dfrac{\bar{\Omega}}{\nu}\right)^{1/2}\left.\dfrac{d\Delta c_A}{d\xi}\right|_{\xi=0} = \Delta i \end{cases} \qquad \begin{cases} \left.\dfrac{d\Delta c_B}{d\xi}\right|_{\xi=0} = 0 \\ \Delta c_B(\xi\to\infty) = 0 \end{cases} \tag{4.23}$$

In this thesis, we'll deal exclusively with the potentiostatic EHD impedance, calculated as:

$$Z_{EHD} = \frac{\Delta i}{\Delta\Omega} = \frac{FD_A\left(\dfrac{\bar{\Omega}}{\nu}\right)^{1/2}\left.\dfrac{d\Delta c_A}{d\xi}\right|_{\xi=0}}{\epsilon\bar{\Omega}} \tag{4.24}$$

The value of ϵ is set to 0.1, which is in agreement with experimental practice and has been found to keep the system within linear behaviour. However, because the equations already assume linearity holds, any value for ϵ would provide the same results.

4.2 Discretization procedure

We used the finite difference method to discretize all governing equations and their boundary conditions. This numerical method consists in discretizing the functions domain and substituting the derivatives for combinations of numerical values of the functions [87]. This can be accomplished, for instance, by using Taylor expansions. Suppose we have a discretized domain with regular spacing Δx between nodes. Then, a Taylor expansion around any node can be expressed as:

$$f(x_0+\Delta x) = f(x_0) + \left.\frac{df(x)}{dx}\right|_{x_0}\Delta x + \frac{1}{2!}\left.\frac{d^2f(x)}{dx^2}\right|_{x_0}\Delta x^2 + \cdots + \frac{1}{n!}\left.\frac{d^nf(x)}{dx^n}\right|_{x_0}\Delta x^n \ldots \tag{4.25}$$

If we neglect terms of order higher than 2, we can rewrite this equation as:

$$\left.\frac{df(x)}{dx}\right|_{x_0} = \frac{f(x_0+\Delta x) - f(x_0)}{\Delta x} + O(\Delta x) \tag{4.26}$$

The term $O(\Delta x)$ is the *approximation order* and indicates that the error introduced by truncating the expansion after the first derivative is of order Δx. Now, the derivative at point x_0 can be written in a discretized fashion:

$$\left.\frac{\mathrm{d}f(x)}{\mathrm{d}x}\right|_{x_0} \approx \frac{f(x_0+\Delta x)-f(x_0)}{\Delta x} \tag{4.27}$$

It is clear that the derivative will be more accurate as we make $\Delta x \to 0$. However, a grid that is too small will require much more nodes to cover the entire function domain. Consequently, a compromise must be made between the derivative approximation and the number of nodes used. Because of that, using approximations of higher orders becomes preferable: the accuracy of a scheme of order $O(\Delta x^4)$ will increase much faster than that of a scheme of order $O(\Delta x)$, saving much computational time and memory. Therefore, it is always advantageous to work with approximations of the higher possible order that do not add too much complexity to the numerical calculations.

4.2.1 Linear grids

When all nodes are equally spaced, we have a linear grid regularly spaced. In our discretization, we divided our domain in N nodes, such that $i = 0$ represents the boundary condition at the electrode/electrolyte interface and $i = N + 1$ represents the boundary condition at the solution bulk. Inside the grid (for nodes $i = 1$ up to $i = N$), derivatives were approximated using central differences of second order.

Limiting current condition

The linearized equations for the limiting current condition are:

For $1 \leq i \leq N$:

$$\left(\frac{2+\Delta\xi Sc_A H^i}{2\Delta\xi^2}\right)c_A^{i-1} - \left(\frac{2\Omega + Sc_A k_A \Delta\xi^2}{\Omega\Delta\xi^2}\right)c_A^i \tag{4.28}$$

$$+\left(\frac{2-\Delta\xi Sc_A H^i}{2\Delta\xi^2}\right)c_A^{i+1} = \frac{-Sc_A k_B c_B^i}{\Omega} \tag{4.29}$$

$$\left(\frac{2+\Delta\xi Sc_B H^i}{2\Delta\xi^2}\right)c_B^{i-1} - \left(\frac{2\Omega + Sc_B k_B \Delta\xi^2}{\Omega\Delta\xi^2}\right)c_B^i \tag{4.30}$$

$$+\left(\frac{2-\Delta\xi Sc_B H^i}{2\Delta\xi^2}\right)c_B^{i+1} = \frac{-Sc_B k_A c_A^i}{\Omega} \tag{4.31}$$

As for the boundary conditions, we have:

$$\begin{cases} c_A^0 = 0 \\ c_A^{N+1} = c_A^b \end{cases} \qquad \begin{cases} c_B^0 = \dfrac{4c_B^1 - c_B^2}{3} \\ c_B^{N+1} = K_{eq} c_A^{N+1} \end{cases} \tag{4.32}$$

Notice that the boundary condition for species B at the electrode surface is a simple rearrangement of the non-discretized equation. Using forward differences of second order, we have [88]:

$$\left.\frac{dc_B}{d\xi}\right|_{\xi=0} = \frac{-3c_B^0 + 4c_B^1 - c_B^2}{2\Delta\xi} = 0 \tag{4.33}$$

$$c_B^0 = \frac{4c_B^1 - c_B^2}{3} \tag{4.34}$$

Thus, the discretized equation for the limiting current density is:

$$i_{lim} = FD_A\left(\frac{\Omega}{\nu}\right)^{1/2}\left(\frac{2c_A^1 - 0.5c_A^2 - 1.5c_A^0}{\Delta\xi}\right) \tag{4.35}$$

Diffusion impedance

To discretize the equations of diffusion impedance and EHD impedance, we found it better to separate the real part from the imaginary part. Hence, a set of two equations became a set of four equations:

For $1 \leq i \leq N$:

For the real part of $\Delta c_A = \Delta c_{A,R}$

$$\left(\frac{2 + \Delta\xi Sc_A H^i}{2\Delta\xi^2}\right)\Delta c_{A,R}^{i-1} - \left(\frac{2\Omega + Sc_A k_A \Delta\xi^2}{\Omega\Delta\xi^2}\right)\Delta c_{A,R}^{i} + \left(\frac{2 - \Delta\xi Sc_A H^i}{2\Delta\xi^2}\right)\Delta c_{A,R}^{i+1} = -\frac{Sc_A}{\Omega}\left(k_B\Delta c_{B,R}^i + Sc_A\omega\Delta c_{A,I}^i\right) \tag{4.36}$$

For the imaginary part of $\Delta c_A = \Delta c_{A,I}$

$$\left(\frac{2 + \Delta\xi Sc_A H^i}{2\Delta\xi^2}\right)\Delta c_{A,I}^{i-1} - \left(\frac{2\Omega + Sc_A k_A \Delta\xi^2}{\Omega\Delta\xi^2}\right)\Delta c_{A,I}^{i} + \left(\frac{2 - \Delta\xi Sc_A H^i}{2\Delta\xi^2}\right)\Delta c_{A,I}^{i+1} = -\frac{Sc_A}{\Omega}\left(k_B\Delta c_{B,I}^i - Sc_A\omega\Delta c_{A,R}^i\right) \tag{4.37}$$

For the real part of $\Delta c_B = \Delta c_{B,R}$

$$\left(\frac{2 + \Delta\xi Sc_B H^i}{2\Delta\xi^2}\right)\Delta c_{B,R}^{i-1} - \left(\frac{2\Omega + Sc_B k_B \Delta\xi^2}{\Omega\Delta\xi^2}\right)\Delta c_{B,R}^{i} + \left(\frac{2 - \Delta\xi Sc_B H^i}{2\Delta\xi^2}\right)\Delta c_{B,R}^{i+1} = -\frac{Sc_B}{\Omega}\left(k_A\Delta c_{A,R}^i + Sc_B\omega\Delta c_{B,I}^i\right) \tag{4.38}$$

For the imaginary part of $\Delta c_B = \Delta c_{B,I}$

$$\left(\frac{2 + \Delta\xi Sc_B H^i}{2\Delta\xi^2}\right)\Delta c_{B,I}^{i-1} - \left(\frac{2\Omega + Sc_B k_B \Delta\xi^2}{\Omega\Delta\xi^2}\right)\Delta c_{B,I}^{i} + \left(\frac{2 - \Delta\xi Sc_B H^i}{2\Delta\xi^2}\right)\Delta c_{B,I}^{i+1} = -\frac{Sc_B}{\Omega}\left(k_A\Delta c_{A,I}^i - Sc_B\omega\Delta c_{B,R}^i\right) \tag{4.39}$$

The boundary conditions for the new equations are:

$$\begin{cases} \Delta c_{A,R}^{0} = \dfrac{D_A\sqrt{\frac{\Omega}{\nu}}}{\Delta\xi}\left(\dfrac{2\Delta c_{A,R}^{1} - 0.5\Delta c_{A,R}^{2} - b_h k_h \bar{c}_A(0)\Delta E}{k_h + \dfrac{3}{2\Delta\xi}D_A\sqrt{\dfrac{\Omega}{\nu}}}\right) \\ \Delta c_{A,R}^{N+1} = 0 \end{cases} \qquad \begin{cases} \Delta c_{A,I}^{0} = \dfrac{4c_{A,I}^{1} - c_{A,I}^{2}}{3} \\ \Delta c_{A,I}^{N+1} = 0 \end{cases} \tag{4.40}$$

$$\begin{cases} \Delta c_{B,R}^{0} = \dfrac{4c_{B,R}^{1} - c_{B,R}^{2}}{3} \\ \Delta c_{B,R}^{N+1} = 0 \end{cases} \qquad \begin{cases} \Delta c_{B,I}^{0} = \dfrac{4c_{B,I}^{1} - c_{B,I}^{2}}{3} \\ \Delta c_{B,I}^{N+1} = 0 \end{cases} \tag{4.41}$$

To understand the boundary condition for $\Delta c_{A,R}^{0}$, we go back to the equation mentioned in subsection 4.1.2:

$$\Delta c_A(0) = \frac{D_A}{k_h}\left.\frac{\mathrm{d}\Delta c_A}{\mathrm{d}z}\right|_{z=0} - b_h\bar{c}_A(0)\Delta E \tag{4.42}$$

After discretization, this equation becomes:

$$\Delta c_{A,R}^{0} = \frac{D_A}{k_h}\sqrt{\frac{\Omega}{\nu}}\frac{\left(4\Delta c_{A,R}^{1} - 3\Delta c_{A,R}^{0} - \Delta c_{A,R}^{2}\right)}{2\Delta\xi} - b_h c_A^{0}\Delta E \tag{4.43}$$

Rearranging this equation gives us the form presented in the boundary condition. Note that, in order to calculate the value of $\Delta c_{A,R}^{0}$, we need to know the steady state concentration of A at the surface. Hence, the diffusion impedance calculation requires a previous determination of the stationary concentration profile.

The discretized equation for the Z_D is given by:

$$Z_D = -FD_A\frac{\Delta c_A(0)}{\Delta i} \tag{4.44}$$

$$Z_D = -\frac{\sqrt{\nu}\Delta c_{A,R}^{0}\Delta\xi}{\sqrt{\Omega}\left[2\Delta c_{A,R}^{1} - 0.5\Delta c_{A,R}^{2} - 1.5\Delta c_{A,R}^{0} + J\left(2\Delta c_{A,I}^{1} - 0.5\Delta c_{A,I}^{2} - 1.5\Delta c_{A,I}^{0}\right)\right]} \tag{4.45}$$

Electro-hydrodynamic impedance

The discretized equations for the case of electro-hydrodynamic impedance are similar to those of the diffusion impedance:

For $1 \leq i \leq N$:

For the real part of $\Delta c_A = \Delta c_{A,R}$

$$\left(\frac{2+\Delta\xi Sc_A H^i}{2\Delta\xi^2}\right)\Delta c_{A,R}^{i-1} - \left(\frac{2\bar{\Omega}+Sc_A k_A \Delta\xi^2}{\bar{\Omega}\Delta\xi^2}\right)\Delta c_{A,R}^{i} + \left(\frac{2-\Delta\xi Sc_A H^i}{2\Delta\xi^2}\right)\Delta c_{A,R}^{i+1} =$$
$$= -Sc_A\left(\frac{k_B}{\bar{\Omega}}\Delta c_{B,R}^{i} + Sc_A\frac{\omega}{\bar{\Omega}}\Delta c_{A,I}^{i} - \epsilon\tilde{h}_R\frac{\mathrm{d}\bar{c}_A}{\mathrm{d}\xi}\right) \tag{4.46}$$

For the imaginary part of $\Delta c_A = \Delta c_{A,I}$

$$\left(\frac{2+\Delta\xi Sc_A H^i}{2\Delta\xi^2}\right)\Delta c_{A,I}^{i-1} - \left(\frac{2\bar{\Omega}+Sc_A k_A \Delta\xi^2}{\bar{\Omega}\Delta\xi^2}\right)\Delta c_{A,I}^{i} + \left(\frac{2-\Delta\xi Sc_A H^i}{2\Delta\xi^2}\right)\Delta c_{A,I}^{i+1} =$$
$$= -Sc_A\left(-\frac{k_B}{\bar{\Omega}}\Delta c_{B,I}^{i} - Sc_A\frac{\omega}{\bar{\Omega}}\Delta c_{A,R}^{i} - \epsilon\tilde{h}_I\frac{\mathrm{d}\bar{c}_A}{\mathrm{d}\xi}\right) \tag{4.47}$$

For the real part of $\Delta c_B = \Delta c_{B,R}$

$$\left(\frac{2+\Delta\xi Sc_B H^i}{2\Delta\xi^2}\right)\Delta c_{B,R}^{i-1} - \left(\frac{2\bar{\Omega}+Sc_B k_B \Delta\xi^2}{\bar{\Omega}\Delta\xi^2}\right)\Delta c_{B,R}^{i} + \left(\frac{2-\Delta\xi Sc_B H^i}{2\Delta\xi^2}\right)\Delta c_{B,R}^{i+1} =$$
$$= -Sc_B\left(\frac{k_A}{\bar{\Omega}}\Delta c_{A,R}^{i} + Sc_B\frac{\omega}{\bar{\Omega}}\Delta c_{B,I}^{i} - \epsilon\tilde{h}_R\frac{\mathrm{d}\bar{c}_B}{\mathrm{d}\xi}\right) \tag{4.48}$$

For the imaginary part of $\Delta c_B = \Delta c_{B,I}$

$$\left(\frac{2+\Delta\xi Sc_B H^i}{2\Delta\xi^2}\right)\Delta c_{B,I}^{i-1} - \left(\frac{2\bar{\Omega}+Sc_B k_B \Delta\xi^2}{\bar{\Omega}\Delta\xi^2}\right)\Delta c_{B,I}^{i} + \left(\frac{2-\Delta\xi Sc_B H^i}{2\Delta\xi^2}\right)\Delta c_{B,I}^{i+1} =$$
$$= -Sc_B\left(-\frac{k_A}{\bar{\Omega}}\Delta c_{A,I}^{i} - Sc_B\frac{\omega}{\bar{\Omega}}\Delta c_{B,R}^{i} - \epsilon\tilde{h}_I\frac{\mathrm{d}\bar{c}_B}{\mathrm{d}\xi}\right) \tag{4.49}$$

The terms $\tilde{h}_R$ and $\tilde{h}_I$ identify the real and the imaginary components of the modulated dimensionless velocity $\tilde{h}$.

The boundary conditions for this case are:

$$\begin{cases} \Delta c_{A,R}^{0} = \dfrac{D_A\sqrt{\frac{\bar{\Omega}}{\nu}}}{\Delta\xi}\left(\dfrac{2\Delta c_{A,R}^{1} - 0.5\Delta c_{A,R}^{2}}{k_h + \dfrac{3}{2\Delta\xi}D_A\sqrt{\dfrac{\bar{\Omega}}{\nu}}}\right) \\ \Delta c_{A,R}^{N+1} = 0 \end{cases} \qquad \begin{cases} \Delta c_{A,I}^{0} = \dfrac{4c_{A,I}^{1} - c_{A,I}^{2}}{3} \\ \Delta c_{A,I}^{N+1} = 0 \end{cases} \tag{4.50}$$

$$\begin{cases} \Delta c_{B,R}^{0} = \dfrac{4c_{B,R}^{1} - c_{B,R}^{2}}{3} \\ \Delta c_{B,R}^{N+1} = 0 \end{cases} \qquad \begin{cases} \Delta c_{B,I}^{0} = \dfrac{4c_{B,I}^{1} - c_{B,I}^{2}}{3} \\ \Delta c_{B,I}^{N+1} = 0 \end{cases} \tag{4.51}$$

Finally, the discretized equation for Z_{EHD} is:

$$Z_{EHD} = \frac{\Delta i}{\Delta\Omega} \tag{4.52}$$

$$Z_{EHD} = \frac{FD_A}{\Delta\xi\Delta\Omega}\left(\frac{\bar{\Omega}}{\nu}\right)^{1/2}\left[2\Delta c_{A,R}^{1} - 0.5\Delta c_{A,R}^{2} - 1.5\Delta c_{A,R}^{0} + J\left(2\Delta c_{A,I}^{1} - 0.5\Delta c_{A,I}^{2} - 1.5\Delta c_{A,I}^{0}\right)\right] \tag{4.53}$$

4.2.2 Nonlinear grids

Studying CE processes with a linear grid may be troublesome when the chemical step becomes too fast. As the values of the kinetic constants increase, the reaction layer gets thinner and most of the concentration gradient is confined within a few nodes from the electrode surface. On the other hand, most boundary conditions require the grid to extend up to the solution bulk. If we had to use a linear grid, the value of $\Delta\xi$ would have to be very small in order to account for the concentration changes near the electrode. However, because of the need to get to the solution bulk, it would also be necessary to have a huge amount of nodes. It is clear that it would become impractical to use linear grids to study ever-faster processes.

One way of circumventing this problem is using nonlinear grids. For instance, using an exponential grid allows the distance between nodes to increase along the domain:

$$\Delta\xi_i = \Delta\xi_1 \gamma^{i-1} \tag{4.54}$$

Where $\Delta\xi_1$ stands for the first spacing between nodes and γ is the stretching parameter [89].

With a suitable choice of γ, it is possible to have sufficient nodes close to the electrode surface and, then, having the grid extend at a faster pace to reach the solution bulk. This approach is successfully used to work with systems whose changes occur mainly in a very small region of the whole domain. Because the values of $\Delta\xi$ vary along the grid, the discretized equations are different from those of linear grids, which assume a constant value. Hence, the coefficients used to calculate the derivatives have to be previously computed for each choice of parameters. For example, the second derivative calculated with three terms would be written as:

$$\frac{\mathrm{d}^2X}{\mathrm{d}y^2} = \delta_{i-1}X^{i-1} + \delta_i X^i + \delta_{i+1}X^{i+1} \tag{4.55}$$

The computation of the coefficients is performed according to the algorithm developed by Fornberg, which applies for grids of any kind and also allows the choice of the order of the approximation[88]. Britz and Strutwolf wrote a routine in Fortran90 implementing the algorithm, which was adapted for our purposes [89].

Limiting current condition

The equations for the steady state in an exponential grid are:

For $1 \leq i \leq N$:

$$(\delta_{i-1} - H^i \beta_{i-1} Sc_A)\, c_A^{i-1} - \left(\delta_i - H^i \beta_i Sc_A - \frac{Sc_A k_A}{\Omega}\right) c_A^i \tag{4.56}$$

$$+ (\delta_{i+1} - H^i \beta_{i+1} Sc_A)\, c_A^{i+1} = \frac{-Sc_A k_B c_B^i}{\Omega} \tag{4.57}$$

$$(\delta_{i-1} - H^i \beta_{i-1} Sc_B)\, c_B^{i-1} - \left(\delta_i - H^i \beta_i Sc_B - \frac{Sc_B k_B}{\Omega}\right) c_B^i \tag{4.58}$$

$$+ (\delta_{i+1} - H^i \beta_{i+1} Sc_B)\, c_B^{i+1} = \frac{-Sc_B k_A c_A^i}{\Omega} \tag{4.59}$$

Where β_i represents the coefficients used to calculate the first derivative and δ_i, the coefficients used to calculate the second derivative.

Diffusion impedance

In the case of diffusion impedance, we have:

For $1 \leq i \leq N$:

For the real part of $\Delta c_A = \Delta c_{A,R}$

$$(\delta_{i-1} - H^i \beta_{i-1} Sc_A)\, \Delta c_{A,R}^{i-1} - \left(\delta_i - H^i \beta_i Sc_A - \frac{Sc_A k_A}{\Omega}\right) \Delta c_{A,R}^i \tag{4.60}$$

$$+ (\delta_{i+1} - H^i \beta_{i+1} Sc_A)\, \Delta c_{A,R}^{i+1} = -Sc_A \left(\frac{k_B c_{B,R}^i}{\Omega} + \frac{\omega \Delta c_{A,I}}{\Omega}\right) \tag{4.61}$$

For imaginary real part of $\Delta c_A = \Delta c_{A,I}$

$$(\delta_{i-1} - H^i \beta_{i-1} Sc_A)\, \Delta c_{A,I}^{i-1} - \left(\delta_i - H^i \beta_i Sc_A - \frac{Sc_A k_A}{\Omega}\right) \Delta c_{A,I}^i \tag{4.62}$$

$$+ (\delta_{i+1} - H^i \beta_{i+1} Sc_A)\, \Delta c_{A,I}^{i+1} = -Sc_A \left(\frac{k_B c_{B,R}^i}{\Omega} - \frac{\omega \Delta c_{A,R}}{\Omega}\right) \tag{4.63}$$

For the real part of $\Delta c_B = \Delta c_{B,R}$

$$(\delta_{i-1} - H^i \beta_{i-1} Sc_B)\, \Delta c_{B,R}^{i-1} - \left(\delta_i - H^i \beta_i Sc_B - \frac{Sc_B k_B}{\Omega}\right) \Delta c_{B,R}^i \tag{4.64}$$

$$+ (\delta_{i+1} - H^i \beta_{i+1} Sc_B)\, \Delta c_{B,R}^{i+1} = -Sc_B \left(\frac{k_A c_{A,R}^i}{\Omega} + \frac{\omega \Delta c_{B,I}}{\Omega}\right) \tag{4.65}$$

For imaginary real part of $\Delta c_B = \Delta c_{B,I}$

$$(\delta_{i-1} - H^i \beta_{i-1} Sc_B)\, \Delta c_{B,I}^{i-1} - \left(\delta_i - H^i \beta_i Sc_B - \frac{Sc_B k_B}{\Omega}\right) \Delta c_{B,I}^i \tag{4.66}$$

$$+ (\delta_{i+1} - H^i \beta_{i+1} Sc_B)\, \Delta c_{B,I}^{i+1} = -Sc_B \left(\frac{k_A c_{A,R}^i}{\Omega} - \frac{\omega \Delta c_{B,R}}{\Omega}\right) \tag{4.67}$$

Electro-hydrodynamic impedance

Finally, for the EHD impedance, we have:

For $1 \leq i \leq N$:

For the real part of $\Delta c_A = \Delta c_{A,R}$

$$(\delta_{i-1} - H^i \beta_{i-1} Sc_A)\, \Delta c_{A,R}^{i-1} - \left(\delta_i - H^i \beta_i Sc_A - \frac{Sc_A k_A}{\bar{\Omega}}\right) \Delta c_{A,R}^{i} \tag{4.68}$$

$$+ (\delta_{i+1} - H^i \beta_{i+1} Sc_A)\, \Delta c_{A,R}^{i+1} = -Sc_A \left(\frac{k_B c_{B,R}^{i}}{\bar{\Omega}} + \frac{\omega \Delta c_{A,I}}{\bar{\Omega}} - \epsilon \tilde{h}_R \frac{\mathrm{d}\bar{c}_A}{\mathrm{d}\xi}\right) \tag{4.69}$$

For imaginary real part of $\Delta c_A = \Delta c_{A,I}$

$$(\delta_{i-1} - H^i \beta_{i-1} Sc_A)\, \Delta c_{A,I}^{i-1} - \left(\delta_i - H^i \beta_i Sc_A - \frac{Sc_A k_A}{\bar{\Omega}}\right) \Delta c_{A,I}^{i} \tag{4.70}$$

$$+ (\delta_{i+1} - H^i \beta_{i+1} Sc_A)\, \Delta c_{A,I}^{i+1} = -Sc_A \left(\frac{k_B c_{B,R}^{i}}{\bar{\Omega}} - \frac{\omega \Delta c_{A,R}}{\bar{\Omega}} - \epsilon \tilde{h}_I \frac{\mathrm{d}\bar{c}_A}{\mathrm{d}\xi}\right) \tag{4.71}$$

For the real part of $\Delta c_B = \Delta c_{B,R}$

$$(\delta_{i-1} - H^i \beta_{i-1} Sc_B)\, \Delta c_{B,R}^{i-1} - \left(\delta_i - H^i \beta_i Sc_B - \frac{Sc_B k_B}{\bar{\Omega}}\right) \Delta c_{B,R}^{i} \tag{4.72}$$

$$+ (\delta_{i+1} - H^i \beta_{i+1} Sc_B)\, \Delta c_{B,R}^{i+1} = -Sc_B \left(\frac{k_A c_{A,R}^{i}}{\bar{\Omega}} + \frac{\omega \Delta c_{B,I}}{\bar{\Omega}} - \epsilon \tilde{h}_R \frac{\mathrm{d}\bar{c}_B}{\mathrm{d}\xi}\right) \tag{4.73}$$

For imaginary real part of $\Delta c_B = \Delta c_{B,I}$

$$(\delta_{i-1} - H^i \beta_{i-1} Sc_B)\, \Delta c_{B,I}^{i-1} - \left(\delta_i - H^i \beta_i Sc_B - \frac{Sc_B k_B}{\bar{\Omega}}\right) \Delta c_{B,I}^{i} \tag{4.74}$$

$$+ (\delta_{i+1} - H^i \beta_{i+1} Sc_B)\, \Delta c_{B,I}^{i+1} = -Sc_B \left(\frac{k_A c_{A,R}^{i}}{\bar{\Omega}} - \frac{\omega \Delta c_{B,R}}{\bar{\Omega}} - \epsilon \tilde{h}_R \frac{\mathrm{d}\bar{c}_B}{\mathrm{d}\xi}\right) \tag{4.75}$$

The boundary conditions for all measurements are identical to those used for linear grids. This is acceptable, even in the case of derivatives, because the first values of $\Delta\xi_i$ are very close to each other and assuming them to be constant and equal to $\Delta\xi_1$ was found to be an accurate approximation. Hence, we could also use the same discretized equations of i_{lim}, Z_D and Z_{EHD} to determine their values in simulations with exponential grids.

4.3 Solution procedure

After discretization, the set of differential equations becomes a set of N algebraic equations. We purposedly decided to use three-point approximations to generate a tridiagonal matrix, which is solved using the Thomas algorithm [87, 89]. An initial guess is necessary for both concentration profiles, but it does not require any accuracy. The equations are solved iteratively until they meet the stopping criterion, which requires that the maximum difference between successive iterations for all nodes be smaller than 10^{-16}.

To determine the domain size necessary to meet the conditions at the solution bulk, we have to let the solution naturally converge to the boundary conditions. A trial-and-error procedure showed that a domain size equals to three times the largest diffusion layer thickness was sufficiently far from the electrode surface to be considered "infinitely away".

For linear grids, the grid spacing is set to $\max\left\{\frac{3\delta_{D,A}}{N}; \frac{3\delta_{D,B}}{N}\right\}$. In the case of nonlinear grids, we designed two scenarios:

- If $\left(3\frac{\delta_{D,A/B}}{N} < \frac{\delta_R}{\zeta}\right)$, ζ being an adjustable parameter, typically, between 20 and 10^3, we set $\Delta\xi_1 = \frac{3\delta_{D,A/B}}{N}$, because this condition is sufficient to provide enough accuracy near the electrode surface.

- Otherwise, we set $\Delta\xi_1 = \frac{\delta_R}{\zeta}$ to make sure that enough nodes are present in the region of major concentration changes. The value of the stretching parameter, γ, is chosen *via* trial-and-error to create a grid of size close to $3\delta_{D,A/B}$.

The dimensionless axial velocity is calculated with power series expansion valid for ξ-values close to the electrode surface. Our calculations use the first three terms to assure a higher accuracy:

$$H(\xi) = -0.51023\xi^2 + \frac{\xi^3}{3} - \frac{0.615922}{6}\xi^3 \tag{4.76}$$

This series fits the actual axial velocity profile with enough precision up to $\xi \approx 1$. Since our choice of parameters led to maximum grid size $\xi_{\max} \leq 1$, the errors due to the truncation of series after the third term are negligible. As for $\tilde{h}$, we used values tabulated by Barcia for different dimensionless frequencies $p = \frac{\omega}{\Omega}$ [22].

Even though the system of equations is linear, the coupling imposed by the boundary conditions in the calculations of the diffusion and the EHD impedances made it necessary to introduce a relaxation factor, Θ:

$$X^i = \Theta X^i + (1 - \Theta)X^{i-1} \tag{4.77}$$

This factor is used to avoid abrupt adjustments of the concentrations after each iteration, which can cause instabilities and divergence of the procedure. The optimal value for Θ depends on the frequency, so our strategy was to set $\Theta = 1$ at the beginning of each step. If divergence is detected, Θ is multiplied by 0.9 and a new solution is attempted. This prevents the persistence of very small Θ values for subsequent frequencies, which often leads to an unnecessary increase of computational time.

All routines were written in Fortran90 and compiled with Microsoft Visual Studio Ultimate 2012. The computer used in most simulations has an Intel$^{\text{R}}$Core$^{\text{TM}}$i5-3337U processor and 4GB of RAM memory operating @ 1.6 GHz. To give an idea of the orders of magnitude involved, table 4.1 presents numerical parameters, with respective execution time, used in simulations for this thesis and which provided good results.

Table 4.1: Simulation parameters used in this work and typical execution time (Sc_A = 111.11, Sc_B = 500, $k_A = 5\,10^3$ s^{-1}, $k_B = 5\,10^2$ s^{-1}, $\Omega = 5$ Hz, $E = 0.5$ V, $k_h = 1\,10^{-1}$m s^{-1} and $b_h = 15$ V^{-1})

Parameters	Z_D	Z_{EHD}
Number of nodes - N	1000	1000
Desired grid size (ξ)	1.004680	1.004680
Actual grid size (ξ)	1.006359	1.006359
First step - $\Delta\xi_1$	$2.491364\,10^{-6}$	$2.491364\,10^{-6}$
Stretching parameter - γ	1.00813	1.00813
Number of frequencies	50	19
Execution time (s)	216	877

4.3.1 Simulation parameters

Our investigation can be divided into two categories: *steady state* and *transient state* simulations. For each case, different parameters were varied to assess their effects on i_{lim}, Z_D and Z_{EHD}.

Steady state measurements

We used fixed values for the kinematic viscosity ($\upsilon = 10^{-6}$ m^{2}s^{-1}) and for the diffusion coefficients of both species ($D_A = 9\,10^{-9}$ m^{2}s^{-1} and $D_B = 2\,10^{-9}$ m^{2}s^{-1}). They were chosen among those typically reported in the literature for aqueous solutions [5, 82]. The rotation speed varied between 0.1 and 50 Hz and the different combinations of k_A/k_B values used are presented in table 4.2. Our main interest here is in evaluating the effect of the homogeneous reactions on the limiting current density.

Table 4.2: Kinetic constants used in the steady state simulations

k_A (s^{-1})	k_B (s^{-1})	K
Slow kinetics		
5	5	1
5	$5\,10^{-1}$	10
5	$5\,10^{-2}$	100
Fast kinetics		
$5\,10^2$	$5\,10^2$	1
$5\,10^3$	$5\,10^2$	10
$5\,10^4$	$5\,10^{-2}$	100
$1.5\,10^5$	3	$5\,10^4$

Transient measurements

The complexity of the impedance data requires a broader study of the impact of different parameters. Hence, we decided to vary not only the kinetic constants and the rotation

speed, but also the diffusion coefficients of both A and B, *i.e.*, their Schmidt numbers. The combinations of values are presented in table 4.3.

Table 4.3: Combinations of parameters used in the transient simulations

Ω (Hz)	Sc_A	Sc_B	k_A/k_B (s^{-1})	
Effect of the rotation speed				
			Slow	Fast
1 5 10 50	111.11	500	5 / 0.5	$5\,10^3$ / $5\,10^2$
Effect of Sc_A				
			Slow	Fast
10	111.11 250 500	500	5 / 0.5	$5\,10^3$ / $5\,10^2$
Effect of Sc_B				
			Slow	Fast
10	500	111.11 333.33 500	5 / 0.5	$5\,10^3$ / $5\,10^2$
Effect of k_A/k_B				
			Slow	Fast
10	111.11	500	5 / 0.5 5 / 5 50 / 5	5 / 100 100 / 100 500 / 100

4.4 Validation procedure

To validate our numerical procedure, we compared our results to well-established models in the literature. Because these models are not as general as ours, so they should be seen as *limiting cases* we expect to see if the physical parameters comply to particular considerations. Nonetheless, not being able to fit them would already point out a failure in our calculations, so this inspection is an important step.

For the steady state, we calculated i_{lim} for a system with very sluggish homogeneous reactions, whose response tends to that of a system without bulk reactions. These values were compared with those obtained by a numerical procedure which does not account for chemical reactions and also with analytical values obtained from the Levich equation [7]. Results are presented in figure 4.1, showing excellent agreement. We see that, in fact, the results from the procedure which includes the homogeneous reactions approaches those obtained from the numerical one without bulk reactions and the analytical values from the Levich equation.

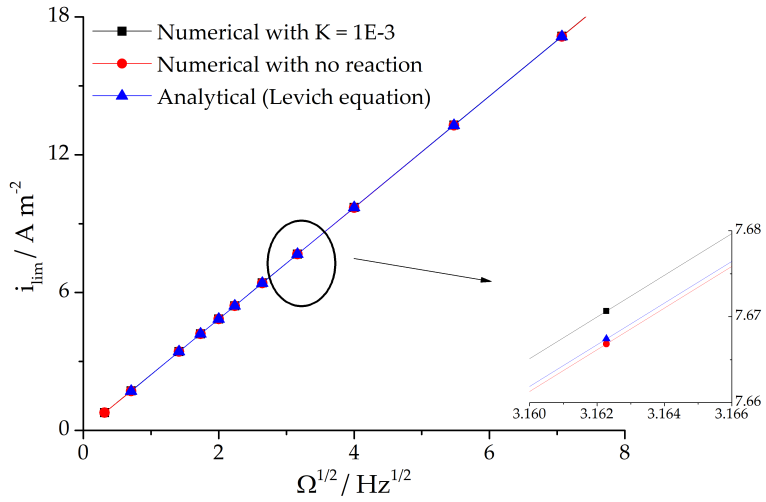

Figure 4.1: Comparison between i_{lim} values calculated according to different procedures as a function of $\Omega^{1/2}$

In the case of diffusion impedance, we compared our results with those by Levart and Schuhmann [16]. The simplification required for this case was the use of equal diffusion coefficients for species A and B. Once again, complete superposition between data was observed (see figure 4.2).

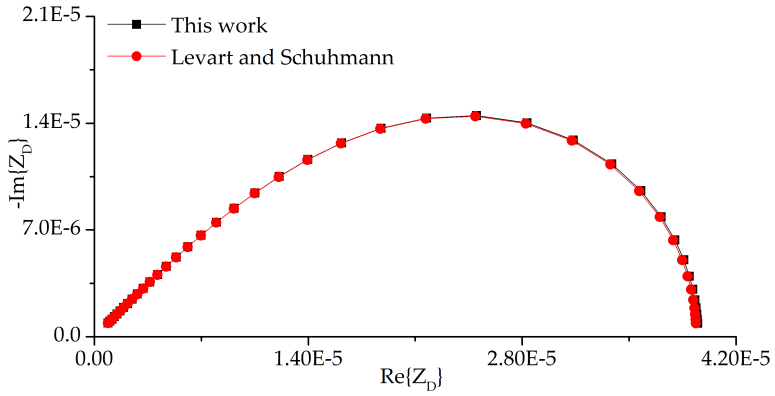

Figure 4.2: Nyquist plot for the diffusion impedance calculated according to our model and that of Levart and Schuhmann. ($Sc_A = Sc_B = 500$, $k_A = 5$ s^{-1}, $k_B = 10^{-2}$ s^{-1})

Finally, the EHD impedance was validated by comparison with results by Tribollet and Newman, whose model does not include bulk reactions [63]. Accordingly, very small chemical rate constants were used to emulate a system with no homogeneous reactions. Like the previous cases, results presented in figure 4.3 show very good agreement.

Now that our procedures have been tested against existing models and proved accurate, we proceed to our investigation of what these same models cannot show us. Remember: they are only approximations of our model, which means that there is much to explore beyond their results.

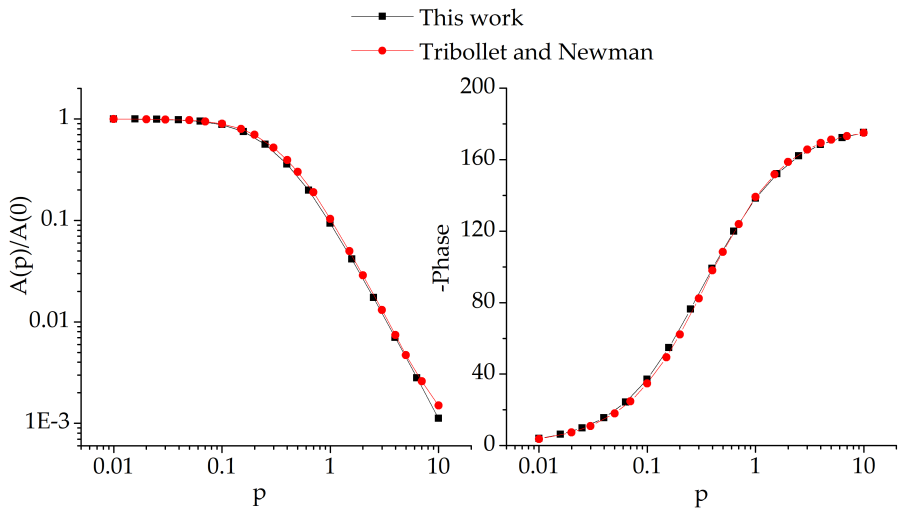

Figure 4.3: Comparison of reduced amplitude and -phase as a function of reduced frequency between our model and that of Tribollet and Newman ($Sc_A = Sc_B = 1000$, $k_A = 5\,10 - 8$ s^{-1}, $k_B = 5\,10^{-5}$ s^{-1})

4.5 Almost there

When we started our journey, we were led primarily by our intuition: we knew where we wanted to get, but we didn't know exactly which paths to take. As we gathered information and our knowledge accrued, we saw *what had been done* and *what could be done*. At that point, we were finally able to take our conceptual map and *trace our own route towards our destination*, which is presented in this chapter.

Because of the coupling effect due to the homogeneous reactions, an analytical solution for that set of differential equations that govern CE processes has only been obtained through approximations. Instead of trying to achieve a general solution, we decided to use numerical procedures to tackle the equations, a short-cut which also has its challenges. That's why we had to improve our simulations by incorporating exponential grids that allow us to work with a wider range of values for the physical parameters of interest. This is how we decided to build our road.

By no means, we claim that it is the only possible road to take. But it is *our* road; built after rigorous analysis of different options and careful discussion about their costs and outcomes. We invite the reader to catch his/her breath and stay alongside us: after all, we're almost there.

Chapter 5

Results and discussion

5.1 Steady state

5.1.1 Fast kinetics

Figure 5.1 shows the limiting current density as a function of $\Omega^{1/2}$ for different combinations of reaction rate constants. An excellent agreement is found between our calculations and the Dogonadze equation, which attests that reaction rate constants of 10^2 s^{-1} already are high enough to assure the validity of the reaction layer hypothesis.

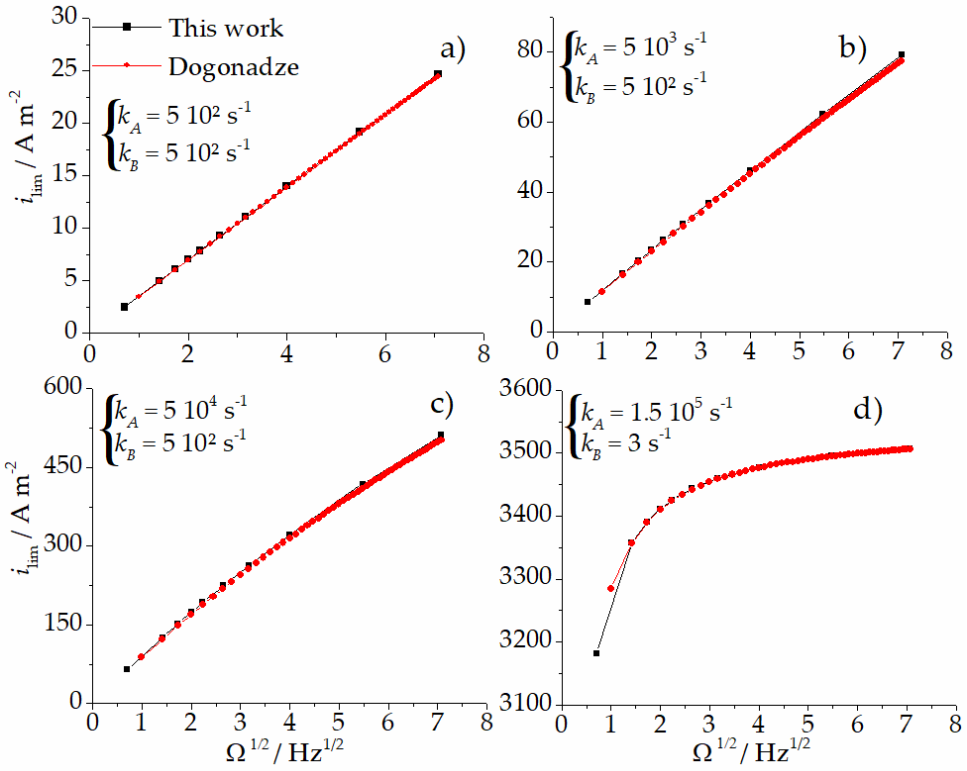

Figure 5.1: i_{lim} *vs* $\Omega^{1/2}$ for systems with fast kinetics: a) $K = 1$; b) $K = 10$; c)$K = 100$; d) $K = 5\ 10^4$.

This can also be confirmed by looking at the inverse of the equilibrium quotient, C_A/C_B, as a function of the axial distance. According to the reaction layer hypothesis, chemical equilibrium should be attained at the vicinities of the electrode surface - a distance much smaller than the diffusion layer thickness. Figure 5.2 illustrates this point. For all cases, chemical equilibrium (*i.e.*, the $C_A/C_B = C_A^b/C_B^b$) is attained at distances at least one order of magnitude smaller than δ_D.

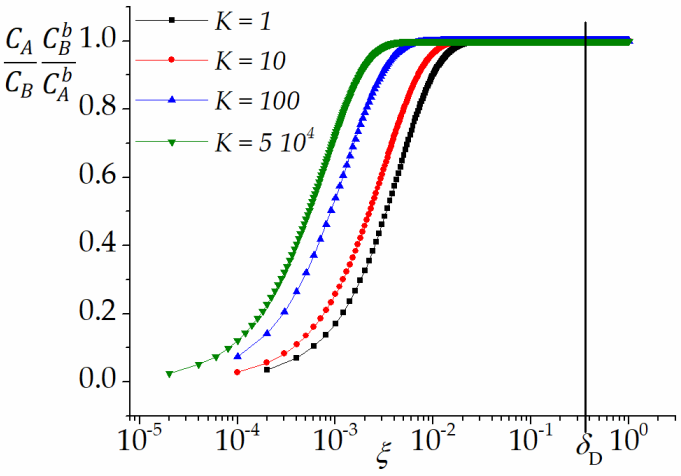

Figure 5.2: Normalized values of C_A/C_B as a function of ξ.

It should also be noticed that, even for very high reaction rate constants, there will always be deviations between approximate and exact solutions. If the rotation speed is sufficiently high, the condition $\delta_D \gg \delta_R$ will no longer be valid. Figure 5.3 shows the divergence between our calculations and the Dogonadze equation when $\Omega \to \infty$. To see this more clearly, we can analyse what happens to the Dogonadze equation when we take the limit $\Omega \to \infty$:

$$\lim_{\Omega\to\infty} i_{DG} = \lim_{\Omega\to\infty} \frac{FD_{eff}\left(c_B^b + c_A^b\right)}{\delta_{eff} + K\frac{D_A}{D_B}\sqrt{\frac{D_A D_B}{D_B k_A + D_A k_B}}} \tag{5.1}$$

$$\lim_{\Omega\to\infty} i_{DG} = \frac{FD_{eff}\left(c_B^b + c_A^b\right)}{K\frac{D_A}{D_B}\sqrt{\frac{D_A D_B}{D_B k_A + D_A k_B}}} \tag{5.2}$$

It is clear that the limiting current approaches a constant value, since it assumes that δ_R will *always* be smaller than δ_D and, hence, that the concentration gradient will be controlled by the homogeneous reactions instead of the convective-diffusive transport.

However, if we take the same limit of the original equations, we get different results:

$$\begin{cases} \lim\limits_{\Omega\to\infty}\left(\dfrac{\mathrm{d}^2c_A}{\mathrm{d}\xi^2} - Sc_A H(\xi)\dfrac{\mathrm{d}c_A}{\mathrm{d}\xi} + \dfrac{Sc_A}{\Omega}(k_B c_B - k_A c_A)\right)^{0} = \dfrac{\mathrm{d}^2c_A}{\mathrm{d}\xi^2} - Sc_A H(\xi)\dfrac{\mathrm{d}c_A}{\mathrm{d}\xi} \\ \lim\limits_{\Omega\to\infty}\left(\dfrac{\mathrm{d}^2c_B}{\mathrm{d}\xi^2} - Sc_B H(\xi)\dfrac{\mathrm{d}c_B}{\mathrm{d}\xi} + \dfrac{Sc_B}{\Omega}(k_A c_A - k_B c_B)\right)^{0} = \dfrac{\mathrm{d}^2c_B}{\mathrm{d}\xi^2} - Sc_B H(\xi)\dfrac{\mathrm{d}c_B}{\mathrm{d}\xi} \end{cases} \tag{5.3}$$

Hence:

$$\begin{cases} \dfrac{\mathrm{d}^2c_A}{\mathrm{d}\xi^2} - Sc_A H(\xi)\dfrac{\mathrm{d}c_A}{\mathrm{d}\xi} = 0 \\ \dfrac{\mathrm{d}^2c_B}{\mathrm{d}\xi^2} - Sc_B H(\xi)\dfrac{\mathrm{d}c_B}{\mathrm{d}\xi} = 0 \end{cases} \tag{5.4}$$

Notice that the limit for infinite rotation speed is equal to that of the absence of bulk reactions. This means that, for very high Ω, the limiting current will be described by the Levich equation, which increases with $\Omega^{1/2}$. Therefore, it never reaches a constant value. This transition takes place when the diffusion layer thickness becomes smaller than the reaction layer thickness and convection-diffusion transport regains control of the concentration gradient. This is not observed in the reaction layer hypothesis, since it presupposes that δ_R will always be much smaller than δ_D. Evidently, the rotation speeds required to spot the divergence in our example cannot be achieved experimentally, so the approximation $\delta_D \gg \delta_R$ is very accurate for the systems presented. This may, indeed, be used as a practical definition of a system with fast kinetics: one for which, given a set of experimental data, the reaction layer hypothesis is valid.

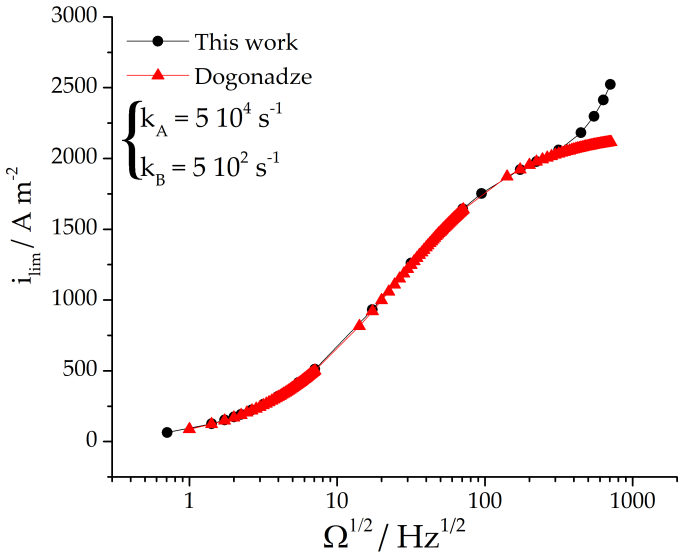

Figure 5.3: Divergence between numerical solution and the Dogonadze equation for very high rotation speeds.

Finally, contrary to the Levich equation, the Dogonadze equation is not described

by a linear function of $\Omega^{1/2}$. However, depending on the rotation speed range and the parameters used, we may observe what *seems to be* a linear function. For instance, if we try to fit the data in graphs 5.1 a) and b) with a straight line crossing the origin, we find $R^2 > 0.99$ for both cases. This indicates that the linearity of the i_{lim} *vs* $\Omega^{1/2}$ graph is not sufficient to conclude that the electrochemical system under study does not involve chemical reactions and further evidence must be collected to support such claim.

An immediate consequence of this non-linearity is in the analysis of $(i_{lim})^{-1}$ *vs* $\Omega^{-1/2}$ graphs. Let's look, for example, at figure 5.4. The graph presents a straight line, which is accordance with the classical Levich theory, and its extrapolation towards $\Omega^{-1/2} = 0$ intercepts the ordinate axis at $\approx 4.6\ 10^{-4}$ A^{-1} m^2. This observation could be attributed, *e.g.*, to a parallel reaction, because one would expect the intersection at the limiting current to be very close to zero. But if we expand the rotation speed range, as shown in figure 5.4b, we find a sharp change in slope and what we see is that the curve does tend towards the origin. Therefore, the initial extrapolation has no clear physical meaning. This is another reminder that we must always confirm the validity of our hypotheses (in this case, that the system has no bulk reactions) before using them to interpret parameters obtained by manipulation of experimental data.

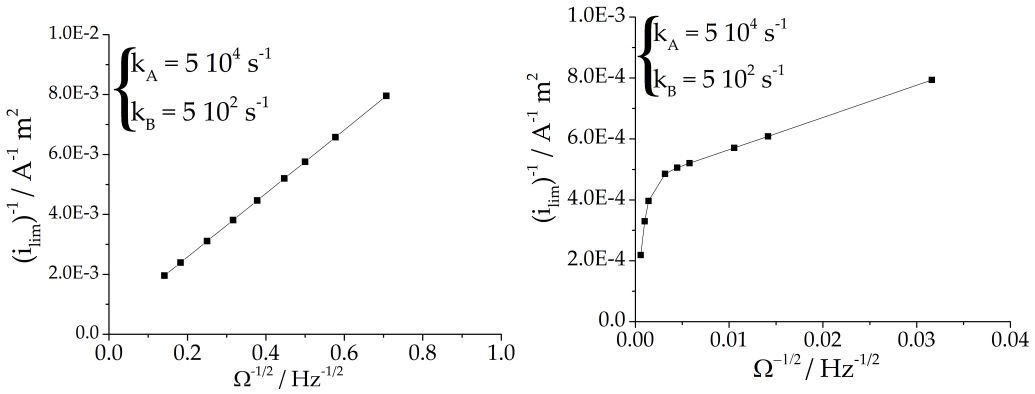

(a) Smaller $\Omega^{-1/2}$ range suggesting linear behaviour.

(b) Broader $\Omega^{-1/2}$ range displaying the non-linearity of the curve.

Figure 5.4: $(i_{lim})^{-1}$ *vs* $\Omega^{-1/2}$ graphs for different ranges of rotation speed.

We conclude this subsection by noting that the reaction layer hypothesis provides a very suitable approach to deal with systems with fast kinetics, since its predictions agree satisfactorily with the exact solutions. However, we must bear in mind that *it is an approximation* and, thus, it is limited to a domain which assures the validity of its premises. We must also be aware that a linear behaviour of the i_{lim} *vs* $\Omega^{1/2}$ graph does not necessarily imply a simple charge transfer system.

5.1.2 Slow kinetics

The plots for systems with slow kinetics, presented in figure 5.5, show large deviations between the exact and approximate solutions within an experimentally accessible rotation speed range. As we have pointed out, the separation between *fast* and *slow* kinetics is determined by the possibility of fitting the Dogonadze limiting current to the data. Also, we see that, even for the reaction rate constants used, an overlap for smaller rotation speeds occurs. This is no coincidence: because δ_D becomes larger for smaller Ω values, there will always be a sufficiently small rotation speed past which the reaction layer hypothesis becomes valid. However, that may not always be observable in practice due to both experimental and theoretical reasons. In the former case, very small rotation speeds may not be achievable with the experimental apparatus. As for the latter, the main equations used to derive these results assume that the hydrodynamic layer thickness is much smaller than the electrode radius and, since $\delta_0 = f(\Omega^{-1/2})$, a minimum rotation speed is required to make sure the system will behave accordingly [8].

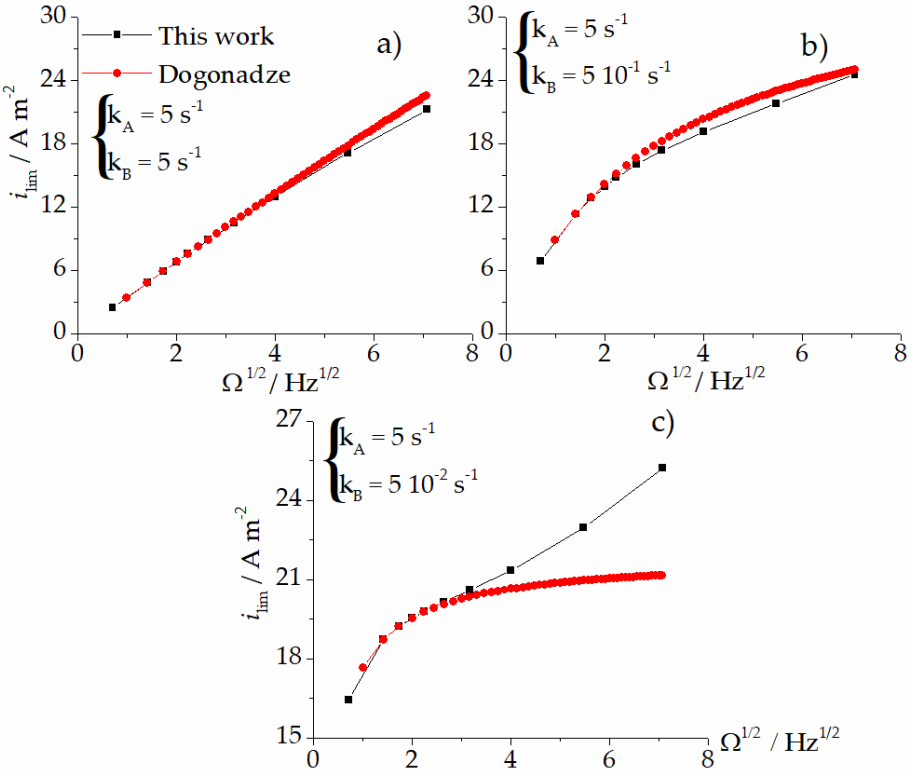

Figure 5.5: i_{lim} *vs* $\Omega^{1/2}$ for a system with slow kinetics: a) K = 1; b) K = 10; c) K = 100.

It is clear that the equilibrium constant itself has no prediction power over the limiting current behaviour of any system. Comparing figures 5.1 and 5.5, we conclude that the absolute values of the reaction rate constants are much more determining than K. For instance, in the case of $K = 1$, figure 5.6 shows that the system with slow kinetics diverges from the Dogonadze equation at much smaller Ω values than that with fast kinetics.

5.1.3 Comparison with literature data

We also compared our calculations with values reported in the literature. Compton *et al.* proposed a numerical procedure which, according to the authors, could be applied to any combination of reaction rate constants and diffusion coefficients [14]. In this article, the authors report that the limiting current density (using our terminology) is given by:

$$i_{lim} = 1.554 n_{eff} D_A^{2/3} F (C_A^b + C_B^b) \upsilon^{-1/6} \Omega^{1/2} \tag{5.5}$$

Where n_{eff} is termed the 'effective number of electrons transferred' [14]. Table 5.1 presents n_{eff} calculated by the authors for different combinations of parameters.

Using the results reported by the authors, we calculated the corresponding limiting current densities and plotted on a i_{lim} *vs* $\Omega^{1/2}$ graph together with our calculations and those of Dogonadze (see figure 5.7). Our calculations are in very good agreement with the reaction layer hypothesis, while those of Compton *et al.* suggest the opposite, which they explain by stating that, for the parameters used, the reaction layer hypothesis was no longer valid. Nonetheless, the authors never actually showed any additional evidence to support their claims: since their procedure was able to give correct calculations for fast kinetics, they assumed that any divergence for slower kinetics was a result of the invalidity of the reaction layer hypothesis under these new circumstances.

Table 5.1: n_{eff} values reported by Compton *et al.* for different sets of parameters [14]. ($D_A = 4\,10^{-9}$ m^{2}s^{-l}, $D_B = 1\,10^{-9}$ m^{2}s^{-l}, $\upsilon = 10^{-6}$ m^{2}s^{-l}, $K = 10^2$)

k_A (s^{-1})	Ω (Hz)	n_{eff}
10	5	0.2085
8	4	0.2075
6	3	0.2087
2	1	0.2077
1	0.5	0.2074
0.5	0.25	0.2088

To check whether or not the reaction layer hypothesis holds, we analysed the system which presented the greatest disparity between our results and those of Compton *et al.* - $k_B = 1000$ and $\Omega = 5$ Hz. Figure 5.8 shows the C_A/C_B profile along the axial distance. There is no doubt that equilibrium is attained at distances much smaller than δ_D. Indeed, the δ_R/δ_D ratio is about $1.63\,10^{-2}$, *i.e.*, the reaction layer thickness represents less than 2% of the diffusion layer thickness. Under these conditions, it is highly unlikely that a correct calculation would depart from the Dogonadze limiting current by more than 100%.

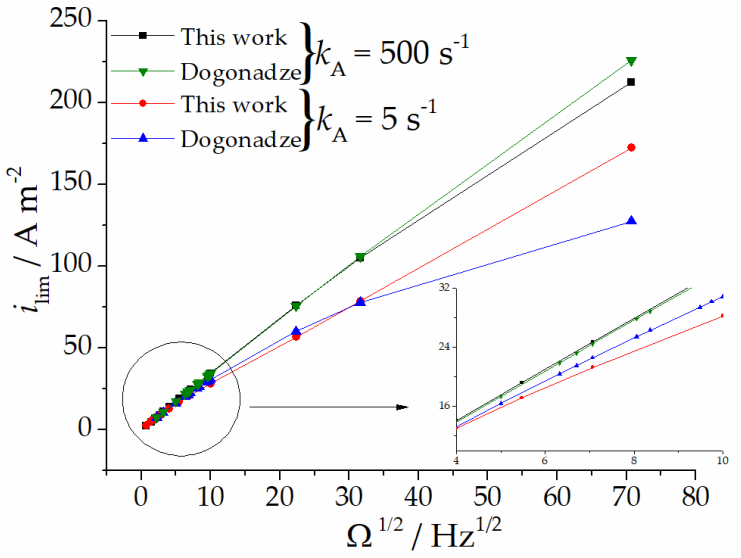

Figure 5.6: i_{lim} *vs* $\Omega^{1/2}$ for systems with K = 1 and different k_A/k_B values.

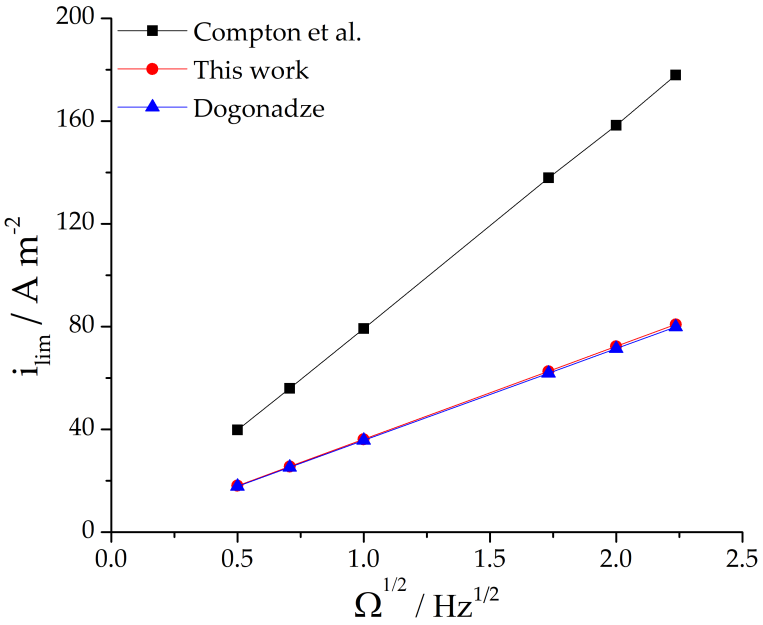

Figure 5.7: i_{lim} *vs* $\Omega^{1/2}$ for systems with K = 1 and different k_A/k_B values.

A possible reason for the lack of accuracy of the Compton procedure is in the change of variables which they use to simplify their equations and which we have already pointed out as being flawed (see the final remarks in 3.1.1). To make things more convenient, we will briefly review their procedure. It is based on the work by Hale [84, 85], who starts with the original convection-diffusion equation:

$$\frac{\partial C}{\partial t} = D\frac{\partial^2 C}{\partial z^2} - v_z\frac{\partial C}{\partial z} \tag{5.6}$$

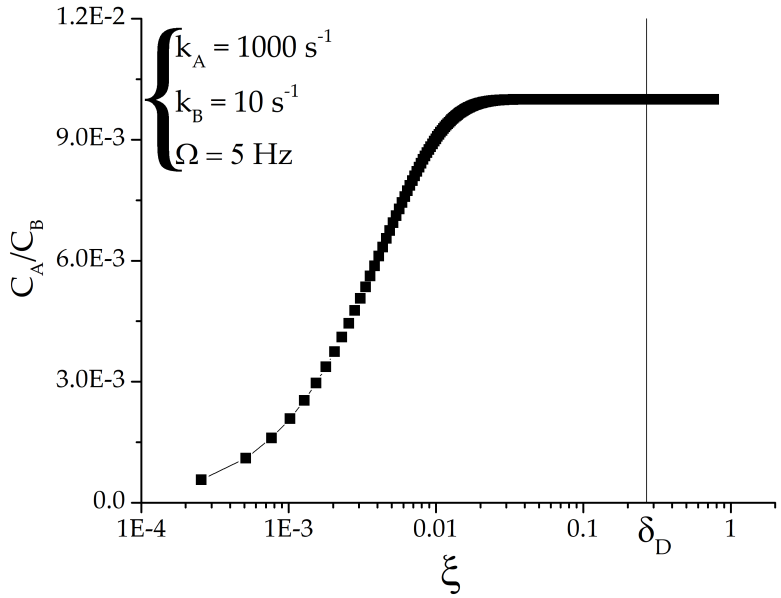

Figure 5.8: C_A/C_B *vs* ξ for system expected to fail the reaction layer hypothesis according to Compton *et al.*[14]. ($D_A = 4\ 10^{-9}$ m^{2}s^{-l}, $D_B = 1\ 10^{-9}$ m^{2}s^{-l}, $\upsilon = 10^{-6}$ m^{2}s^{-l})

Then, he performs a change to dimensionless variables:

$$\begin{cases} u = C/C^b \\ y = \frac{1}{\delta_D}\int_0^z \exp\left[\int_0^z \frac{\upsilon_z}{D}\mathrm{d}z\right]\mathrm{d}z \\ \partial = Dt/\delta_D^2 \end{cases} \tag{5.7}$$

Given that $\delta_D = \int_0^\infty \exp\left[\int_0^z \frac{\upsilon_z}{D}\mathrm{d}z\right]\mathrm{d}z$, Hale concludes that the new convection-diffusion equation is:

$$\frac{\partial u}{\partial \partial} = a^2\frac{\partial^2 u}{\partial y^2} \tag{5.8}$$

Where $a^2 = \exp\left(2\left[\int_0^z \frac{\upsilon_z}{D}\mathrm{d}z\right]\right)$. But that is not correct at all. To see this, let's perform the change of variables step-by-step:

$$\frac{\partial u}{\partial \partial}\frac{\mathrm{d}\partial}{\mathrm{d}t} = D\frac{\partial^2 u}{\partial z^2}\left(\frac{\mathrm{d}y}{\mathrm{d}z}\right)^2 - \upsilon_z\frac{\partial C}{\partial z}\frac{\mathrm{d}y}{\mathrm{d}z} \tag{5.9}$$

$$\frac{\partial u}{\partial \partial}\frac{D}{\delta_D^2} = D\frac{\partial^2 u}{\partial z^2}\left(\frac{\exp\left(2\left[\int_0^z \frac{\upsilon_z}{D}\mathrm{d}z\right]\right)}{\delta_D^2}\right) - \upsilon_z\frac{\partial u}{\partial z}\left(\frac{\exp\left(\left[\int_0^z \frac{\upsilon_z}{D}\mathrm{d}z\right]\right)}{\delta_D}\right) \tag{5.10}$$

$$\frac{\partial u}{\partial \partial} = a^2\frac{\partial^2 u}{\partial y^2} \underbrace{- \frac{\upsilon_z \delta_D a}{D}\frac{\partial u}{\partial z}}_{\text{Absent from the original papers}} \tag{5.11}$$

In his papers, Hale does not explain why he decided to neglect the term $\frac{\upsilon_z \delta_D a}{D}\frac{\partial u}{\partial z}$ and,

in fact, there is no reasonable argument to do this at all. Hence, his procedure is, at best, an approximation of the set of equations which must be used to determine the concentration profiles. Since Compton *et al.* employ the *same* transformation in their work, this is one of the reasons for the divergences between our results and theirs: contrary to their claims, their calculations do not solve the exact system of equations, only an approximate one. On the other hand, ours does not invoke any additional assumptions and is able to work with any combination of parameters.

5.2 Transient state

5.2.1 Effect of the rotation speed

Changes in the rotation speed improve the convective transport of species, but they have no direct effect on phenomena linked to bulk reactions. This is what we see in figure 5.9: the convection-diffusion loop, with lower characteristic frequency, gets smaller with increasing rotation speed and its own characteristic frequency increases too. On the other hand, the reaction impedance loop, with higher characteristic frequency, remains relatively unaltered (both in phase and in modulus) up to $\Omega = 10$ Hz. As the frequency spectra of both loops start to overlap, convective-diffusive effects have greater impact on the concentration gradient and, consequently, on the overall impedance. This is why, at some point, the loops merge and start decreasing as a whole for increasing Ω values.

Further analysis shows that, although the separation between reaction and convection-diffusion loops does correlate with the δ_R/δ_D ratio, it is a much less sensitive tool to judge the validity of the reaction layer hypothesis than, *e.g.*, the analysis of concentration profiles or of the limiting current densities. For $\Omega = 1$ Hz, we have clear separation between loops and $\delta_R/\delta_D \approx 9.84\%$, with very good agreement between i_{lim} and i_{DG} - deviations around 1%. However, although the loops for $\Omega = 5$ Hz also are visibly distinct, $\delta_R/\delta_D \approx 22\%$ and the divergence between i_{lim} and i_{DG} becomes more discernible (see figure 5.5). For $\Omega = 10$ Hz, when we get to see a slight change at the reaction loop, $\delta_R/\delta_D \approx 31\%$ and the reaction layer hypothesis clearly is no longer applicable. This is also confirmed by the larger disparity between our calculations and those of Dogonadze (which apply the reaction layer hypothesis) at the i_{lim} *vs* $\Omega^{1/2}$ graph. Finally, for $\Omega = 50$ Hz, $\delta_R/\delta_D \approx 70\%$, *i.e.*, they have the same order of magnitude and comparable impact on the concentration profile. Also, the characteristic frequency of the diffusion-convection loop is now of order $10^0 Hz$. This explains the merging between loops and progressive control of the convection-diffusion term over the diffusion impedance.

Besides the fact that the characteristic frequency of the lower frequency loop depends on the rotation speed, another evidence that this loop corresponds to the convection-diffusion term is given by figure 5.10. It displays the Nyquist plot for systems whose pa-

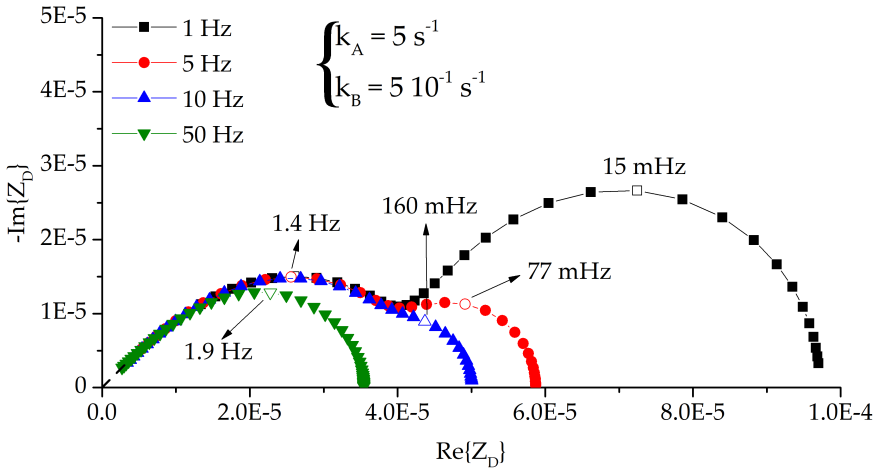

Figure 5.9: Nyquist plot of Z_D for system with slow kinetics at different rotation speeds.

rameters are equal to those presented in figure 5.9, except for the reaction rate constants, which are negligible in latter case. Hence, what we see is a pure convection-diffusion impedance. Comparing both results, we observe that the lower frequency loops in figure 5.9 are at the same frequency range as the convection-diffusion loops in figure 5.10. Also, it is clear that both loops have the same dependency on the rotation speed value. Therefore, we feel safe to conclude that the low frequency loops are, indeed, linked to convective-diffusive effects.

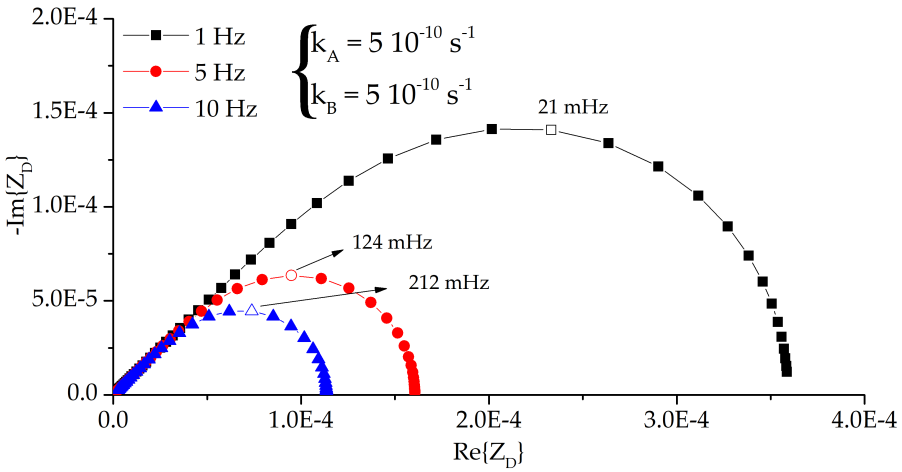

Figure 5.10: Nyquist plot of Z_D for system whose parameters are equal to those in figure 5.9, but in the absence of homogeneous reactions.

Nyquist plots for Z_D when the kinetics are fast are similar in shape to those for slow kinetics (see figure 5.11). But, in this case, the characteristic frequency of the reaction loop is much higher ($\approx$ 1.5 kHz) than that of the convection-diffusion one and the rotation speed range employed is not enough to cause them to overlap. Comparing the different kinetic regimes, we also observe that the characteristic frequencies of reaction and convection-diffusion impedances are independent of each other. For equal rotation

speeds, the convection-diffusion impedance has the same characteristic frequency regardless of the chemical rate constants. As for the reaction impedance, its characteristic frequency seems to depend on the absolute value of the reaction rate constants (and, hence, on δ_R), but not on Ω.

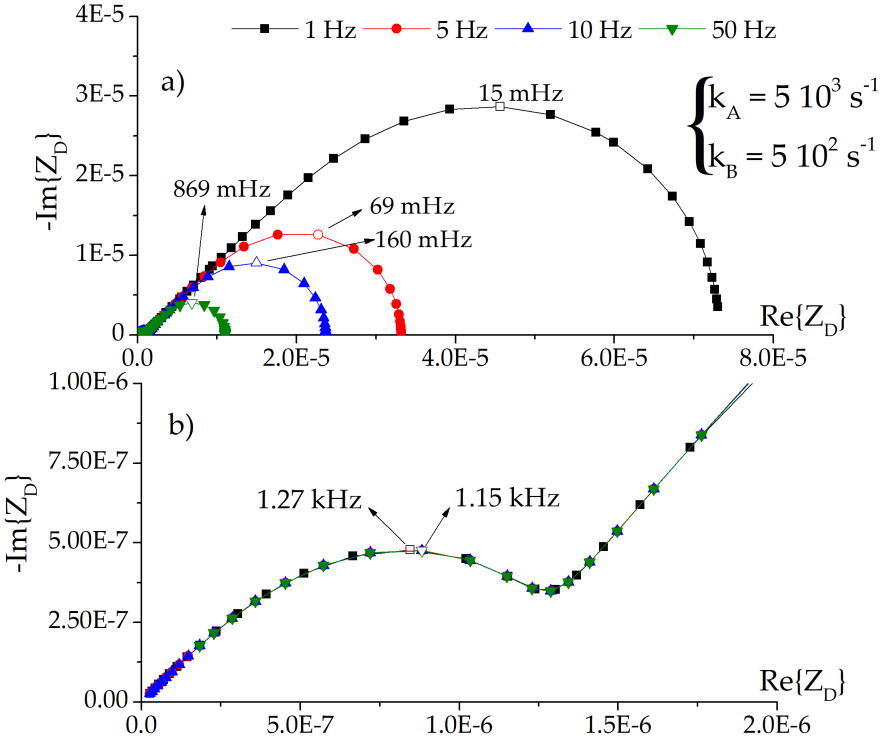

Figure 5.11: Nyquist plot of Z_D for system with fast kinetics at different rotation speeds: a) General overview highlighting the convection-diffusion loop. b) Zoom at the high frequency region which displays the reaction loop.

Systems with fast kinetics provide a better case for inferring the applicability of the reaction layer hypothesis based on the separation of the diffusion impedance loops. In this scenario, there is no overlap whatsoever between both loops , even for the higher rotation speed employed. Also, the δ_R/δ_D ratio varies from 0.31% to 2.2%, a range in which the reaction layer hypothesis can be safely applied. Because the characteristic frequencies of the convection-diffusion and the reaction impedance depend on the thickness of the corresponding layers, a complete separation between loops can be used as a evidence that $\delta_R \ll \delta_D$ and, thus, that we can apply the reaction layer hypothesis. As these frequencies get closer and the loops start interacting, we get to the point in which applying the reaction layer hypothesis is no longer possible. Nonetheless, it is important to emphasize that, based on our results for slow kinetics, there is no need for a complete overlap between both impedances for the invalidity of the hypothesis.

Based on our suspicion of the link between the characteristic frequency of the reaction impedance f_R^* and the reaction layer thickness, we decided to plot one against the other and check for a functional dependency. The log-log plot presented in figure 5.12 was obtained

by measuring f_R^* for systems whose value of k_A increased by factors of 2 (starting with $k_A = 5\ s^{-1}$) while holding every other parameter constant. The fitting procedure clearly shows that $f_R^* = F(\delta_R^{-2})$, confirming that increasing f_R^* can be correctly interpreted as causing δ_R to decrease.

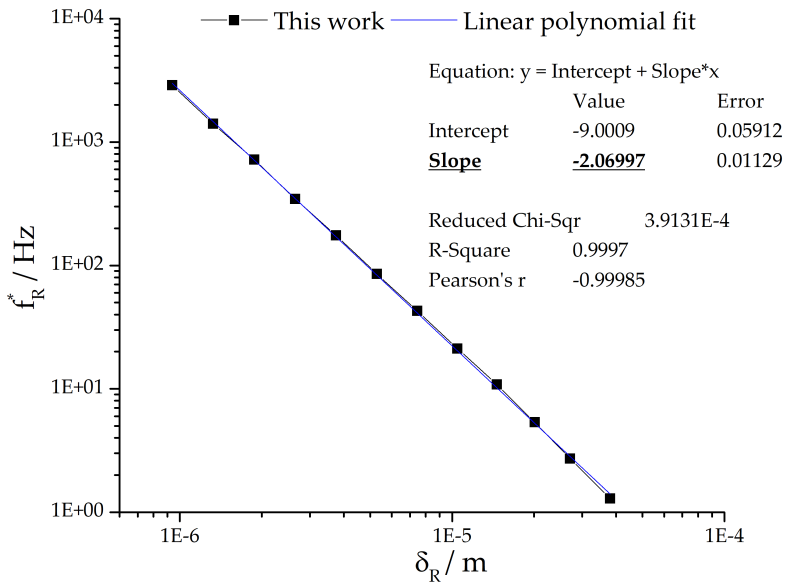

Figure 5.12: Log-log plot of the reaction impedance characteristic frequency as a function of the reaction layer thickness ($Sc_A = 111.11$, $Sc_B = 500$, $\Omega = 1$ Hz, $k_B = 5\ 10^{-1}\ s^{-1}$).

We can also observe that, for fast kinetics, the reaction loop would most likely not be experimentally observable, because its frequency spectrum is in the same range as that of the double-layer relaxation. Thus, the overall impedance would not display both loops and additional information would be required to identify the presence of homogeneous reactions. Figure 5.13 illustrates this point by showing the Nyquist plot of the overall impedance of the same system presented in figure 5.11. Notice that the reaction impedance loop, with characteristic frequency *circa* 1.3 kHz, is no longer discernible, because it overlaps with the loop generated from the coupling between the double layer capacitance and charge transfer resistance. Hence, even though we know, theoretically, that a reaction loop is to be observed for CE mechanisms, we might not be able to identify it in experimental data. In other words, by having to rely on the electrochemical impedance alone, we risk not having access to critical information regarding the complete reaction mechanism. Thus, it is important to have ancillary measurements which can help us identify these reaction steps.

This complementary information can be provided by EHD impedance measurements. Figures 5.14 and 5.15 show that the graphs for reduced amplitude and negative phase for different rotation speeds do not overlap, which contrasts with the behaviour of systems with no bulk reaction, for which overlap is expected to occur.

Although these modified Bode plots reveal important changes in the Z_{EHD} patterns,

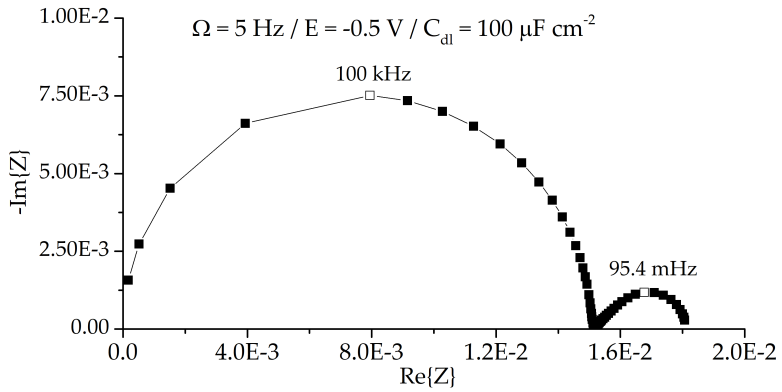

Figure 5.13: Nyquist plot of the overall impedance of a system with fast kinetics (Parameters are equal to those of the system presented in figure 5.11)

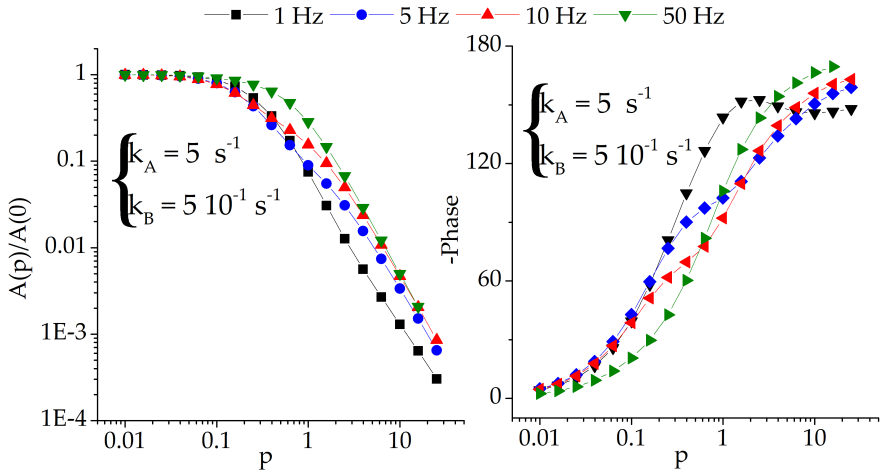

Figure 5.14: Reduced amplitude and negative phase as a function of dimensionless frequency for system with slow kinetics at different rotation speeds.

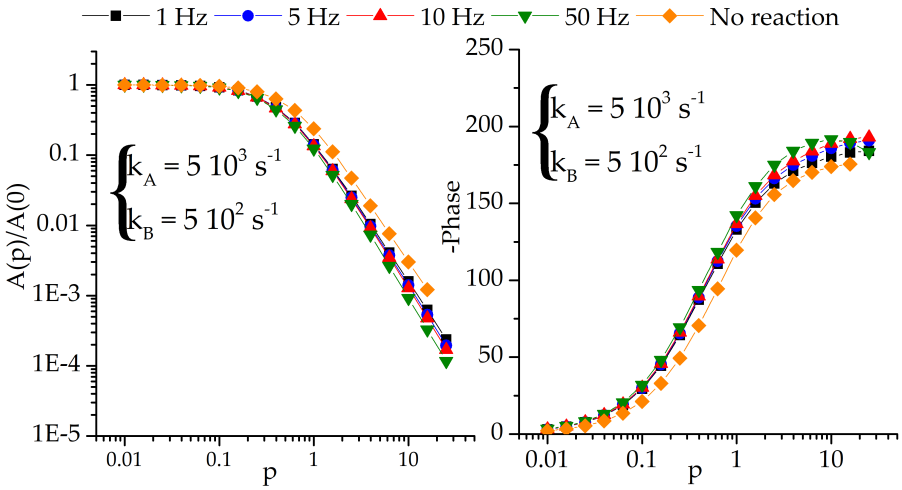

Figure 5.15: Reduced amplitude and negative phase as a function of dimensionless frequency for system with fast kinetics at different rotation speeds.

there are better ways to investigate the degree of overlap between convection-diffusion and reaction impedance loops. Because of that, we decided to also investigate the Nyquist plots for both kinetic regimes, which are presented in figure 5.16. In both cases, the prevailing loop has a characteristic frequency which depends on the rotation speed, being readily identifiable with convection-diffusion phenomena. However, even for fast kinetics, the loop for the reaction impedance is not clearly discernible even if the effects the reaction has on the impedance are quite evident. Hence, the main correlation we find is between the convection-diffusion characteristic frequency, f_D^*, and Ω, which can be restated as: $f_D^* = \mathrm{F}(\delta_D^{-2})$, since $\delta_D \propto \Omega^{-1/2}$.

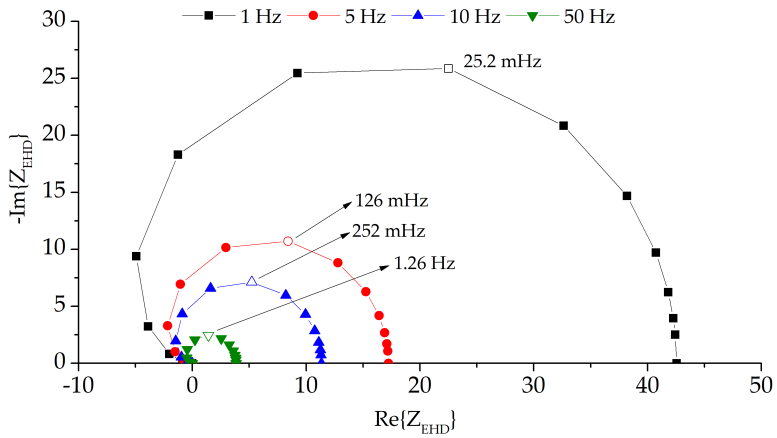

(a) Nyquist plot of Z_{EHD} for system with fast kinetics.

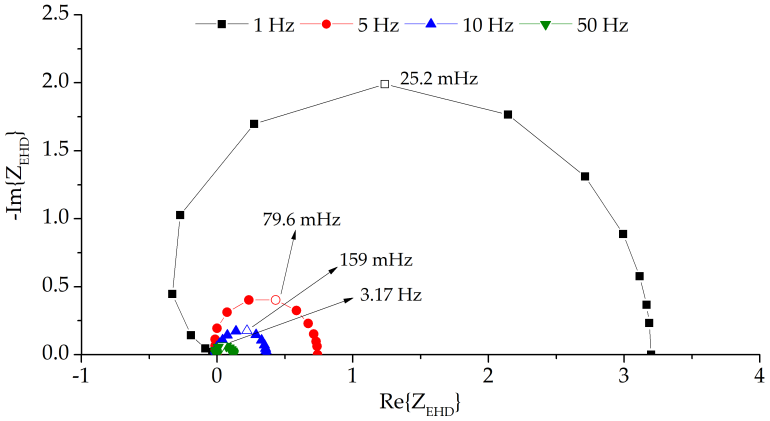

(b) Nyquist plot of Z_{EHD} for system with slow kinetics.

Figure 5.16: Nyquist plot of Z_{EHD} for different rotation speeds.

We see, then, that combining both electrochemical and electro-hydrodynamic impedance measurements is useful in identifying the presence of additional phenomena in the system - and the total exclusion of the mechanism corresponding to that of a simple electron transfer without complications. We have also observed that, for increasing reaction rate constants, the mismatch between curves for different rotation speeds becomes less pronounced. Since this is one way of identifying more complex mechanisms, it would be interesting to have supplementary methods for distinguishing them. An al-

ternative procedure is the analysis of the negative phase for higher p values. Figure 5.17 shows $A(p)/A(0)$ *vs* p for two systems with equal Schmidt numbers, but with one difference: in one of them, there are no homogeneous reactions. The shape of both reduced amplitude plots is very similar and, at a first glance, does not provide evidence of a more complex mechanism. Nonetheless, the superior limit of the negative phase is remarkably different from the 180° value expected for simpler systems. This observation allows us to conclude that the reaction mechanism must be more complex than that of a single electron transfer.

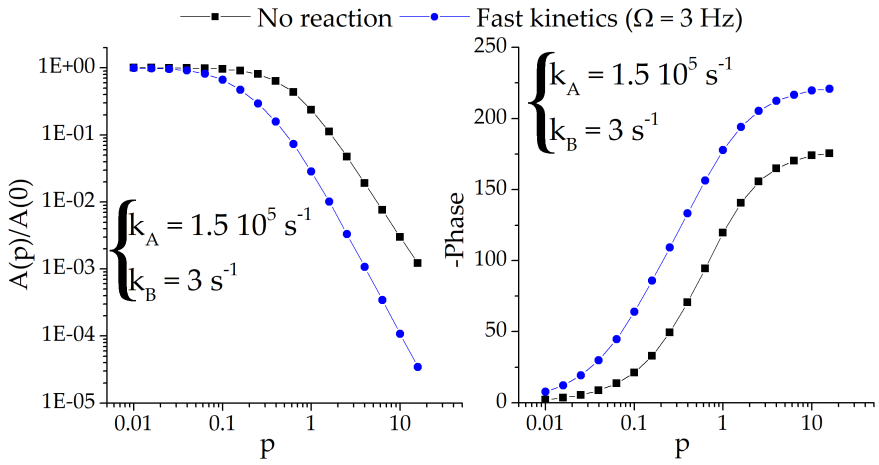

Figure 5.17: Comparison of reduced amplitude and negative phase for systems with equal Schmidt numbers (of the electroactive species) in the presence and in the absence of homogeneous reactions.

Overall, we see that the rotation speed has a straightforward effect on both Z_D and Z_{EHD}, because it has an explicit impact on the concentration gradient. Increasing Ω reduces the magnitude of both impedances and increases their associated characteristic frequencies, which leads to an overlapping of reaction and convection-diffusion in the diffusion impedance. This, and the fact that we can only measure the overall impedance, points out to the importance of combining different techniques in order to assess the reaction mechanism of an electrochemical process. In this case, we have shown that EHD impedance can assist us in this task.

5.2.2 Effect of the equilibrium constant

To measure the effect of reaction rate constants, we kept k_B constant and varied k_A, *i.e.*, we varied the equilibrium constant. As mentioned before, the equilibrium constant has no direct connection to the shape of the impedance curves, so we still had to discern between systems with slow kinetics and systems with fast kinetics.

As shown in figure 5.18, systems with lower K values have higher Z_D magnitudes, but smaller contributions from the reaction impedance. This means that the homogeneous

reactions play a smaller role in determining the concentration profile of the electroactive species in systems with lower equilibrium constants.

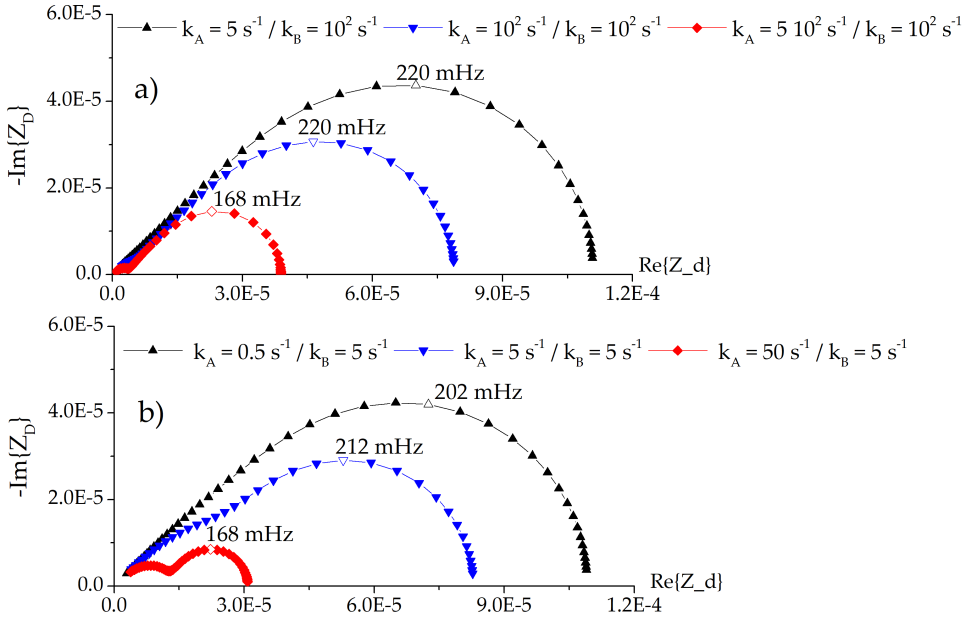

Figure 5.18: Nyquist plots for the diffusion impedance of systems with a) fast and b) slow kinetics for different combinations of k_A and k_B. (Ω = 10 Hz; Sc_A = 111.11; Sc_B = 500)

Why would that be? First, we must notice that, since K is low, then C_B^b/C_A^b is also low. Because we keep C_A^b fixed at 1 mol m^{-3}, $C_B^b = K_{eq}$. Also, remember that C_B^b is the *higher* concentration value of B in solution, because at any other point it will be consumed to replenish the A species consumed at the electrode. Therefore, C_B will have small values *throughout* the solution and its impact on the concentration profile of the electroactive species will be much smaller than that of convective-diffusive effects, which explains why the overall diffusion impedance resembles the convection-diffusion impedance. To confirm this, we compared the concentration profile of the electroactive species in the absence of homogeneous reactions and in a system with $K = 5\ 10^{-2}$. The graph, presented in figure 5.19, shows that the presence of homogeneous reactions has no visible effect on the concentration profile, *i.e.*, the system behaves *as if* there were no bulk reactions at all.

Higher equilibrium constants have the opposite effect: they lead to smaller magnitudes and a more pronounced effect of the reaction impedance. Here, $C_B \gg C_A$ and the electroinactive species acts as an efficient buffer of the electroactive species. As a consequence, the concentration profile of A is primarily determined by the kinetics of the homogeneous reactions, which explains the development of the reaction loop. Besides that, the electroactive concentration profile becomes much steeper near the electrode surface due to the replenishments by species B. As a result, changes in $C_A(0)$ induce higher concentration gradients and, thus, smaller Z_D.

EHD results for different equilibrium constants (see figures 5.20 and 5.21) present

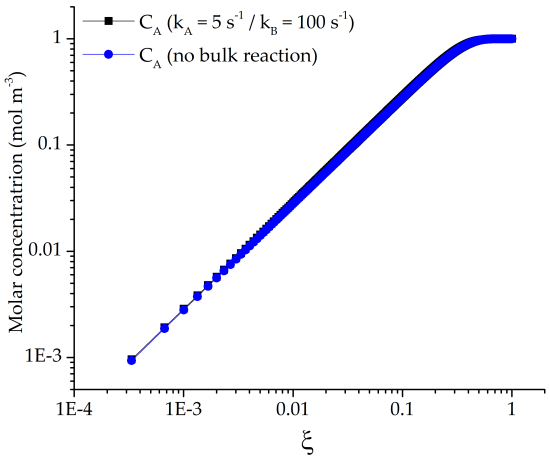

Figure 5.19: Comparison of the concentration profile between a system without bulk reactions and one with a low equilibrium constant.

the same trends outlined for the diffusion impedance: Lower values of K lead to reduced amplitude and phase values closer to those of a system without homogeneous reactions. As it increases, we notice that the reduced amplitude graphs bend downward, while the phase goes upward - at least, up to a tipping point, in the case of slow kinetics.

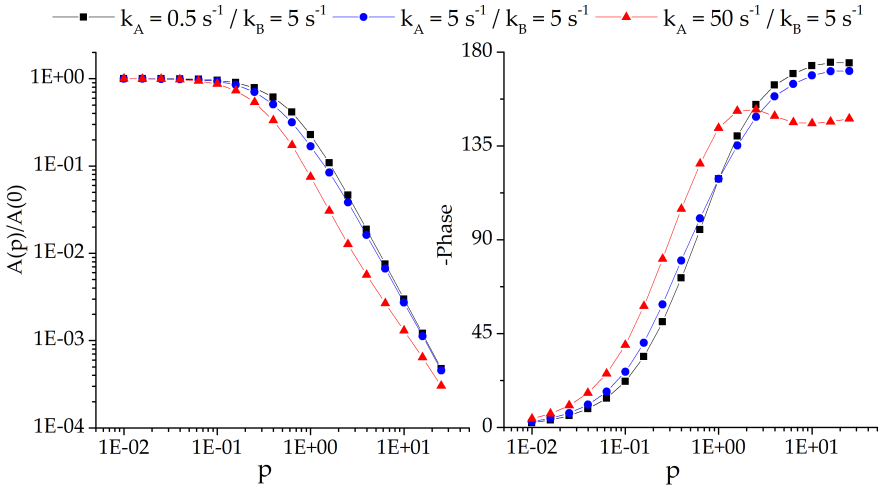

Figure 5.20: Reduced amplitude and phase as a function of dimensionless frequency for systems with slow kinetics and different equilibrium constants.

To have a better understanding of the equilibrium constant effects, we also investigated the Nyquist plot of EHD data (see figure 5.22). For both slow and fast kinetics, the increase of the equilibrium constant causes an increase of the EHD impedance magnitude and of the characteristic frequency without having much influence on the shape of the plot. We have already seen that increasing K_{eq} produces steeper C_A slopes near the electrode surface, *i.e.*, higher currents (both stationary and transient). Since $Z_{EHD} = \Delta i/\Delta\Omega$, this will also cause the Z_{EHD} to increase.

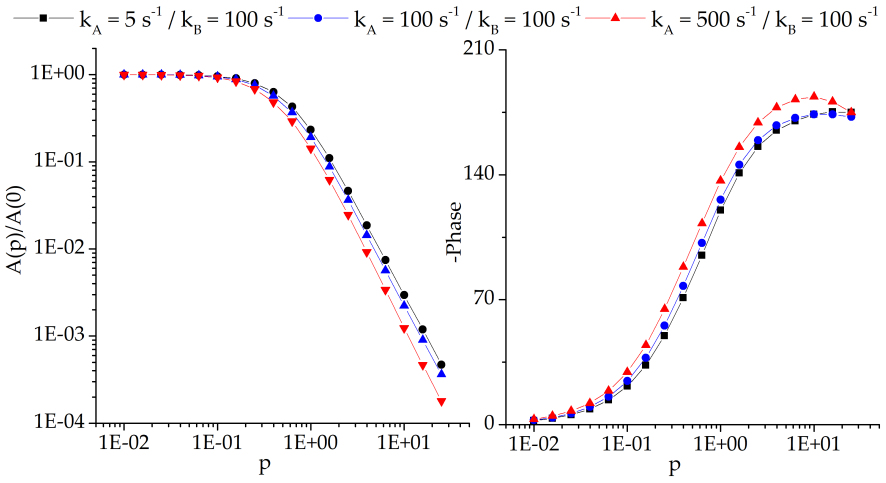

Figure 5.21: Reduced amplitude and phase as a function of dimensionless frequency for systems with fast kinetics and different equilibrium constants.

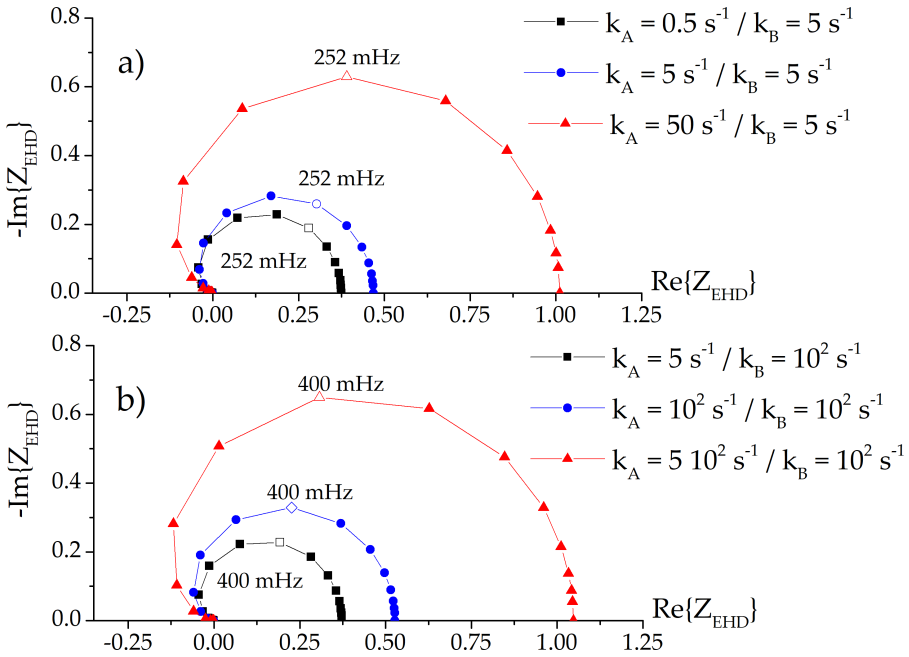

Figure 5.22: Nyquist plot of Z_{EHD} for systems with different equilibrium constants: a) slow kinetics; b) fast kinetics.

5.2.3 Effect of Sc_A and Sc_B

Our simulations show that the impact of varying the Schmidt number depends on whether it corresponds to the electroactive or to the electroinactive species. Differently from the reaction rate constants, the effects of Sc_A and Sc_B can be assessed independently and have very distinct effects, as we see below.

For a constant value of Sc_B, we observe that the diffusion impedance magnitude decreases for increasing values of Sc_A - see figure 5.23. Both impedance loops are affected in the same proportion and the characteristic frequencies remain constant. At higher fre-

quencies, the curves converge to the straight line representing the Warburg impedance limit observed when $\omega \to \infty$.

Why does increasing Sc_A decreases the Z_D magnitude? For a constant kinematic viscosity, higher Sc_A is caused by smaller D_A, *i.e.*, a smaller mobility of A species in solution. Inasmuch as a smaller mobility hinders the transport of A from the solution bulk to the electrode surface, the surface C_A gradient gets steeper and, consequently, $Z_D = -\frac{\Delta C_A(0)}{\left.\frac{d\Delta C_A}{dz}\right|_{z=0}}$ gets smaller.

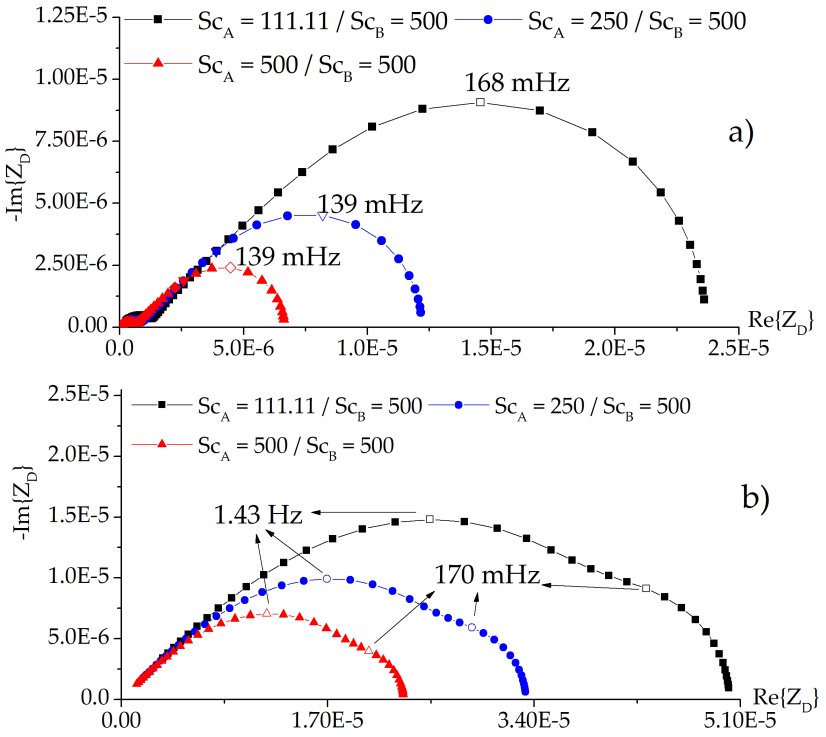

Figure 5.23: Nyquist plot of Z_D for systems with Sc_A values: a) fast kinetics and b) slow kinetics.

The same pattern is observed for the EHD impedance: the magnitude decreases for increasing Sc_A values (see figure 5.24). Nevertheless, the reason for this is not the same presented for the diffusion impedance. Indeed, because $Z_{EHD} = FD_A \frac{\left.\frac{d\Delta C_A}{dz}\right|_{z=0}}{\Delta\Omega}$, we could be lead to think that higher Sc_A should increase the EHD impedance magnitude, since $\left.\frac{d\Delta C_A}{dz}\right|_{z=0}$ gets higher. However, in this situation, we must also consider the *absolute* value of the diffusion coefficient and the calculations show that, even though systems with lower D_A (or higher Sc_A) have higher C_A surface gradients, the actual current is still smaller than that of systems with higher D_A (or lower Sc_A). Also noticeable from the EHD plot is that, for slow kinetics, a reaction impedance loop is observed at higher frequencies, which is in agreement with the diffusion impedance.

The role played by Sc_B is very different, especially because it affects only C_B directly.

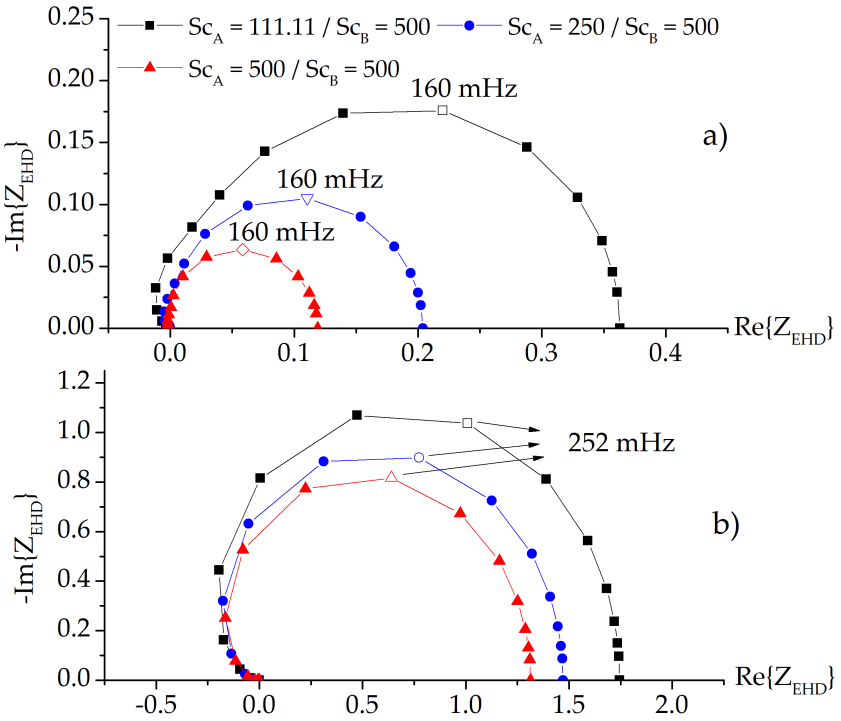

Figure 5.24: Nyquist plot of Z_{EHD} for systems with Sc_A values: a) slow kinetics and b) fast kinetics.

Figure 5.25 shows that increasing Sc_B increases the diffusion impedance, but it only enhances the convection-diffusion loop. This might be due to the fact that B can only replenish A species and, in that case, a very high diffusion coefficient would be necessary to interfere with higher frequency phenomena. A higher mobility of B species, *i.e.*, a lower Sc_B, allows a higher concentration build-up near the electrode surface, thus enhancing the buffering effect. Therefore, we can expect steeper slopes for C_A, which explains the lower Z_D magnitudes.

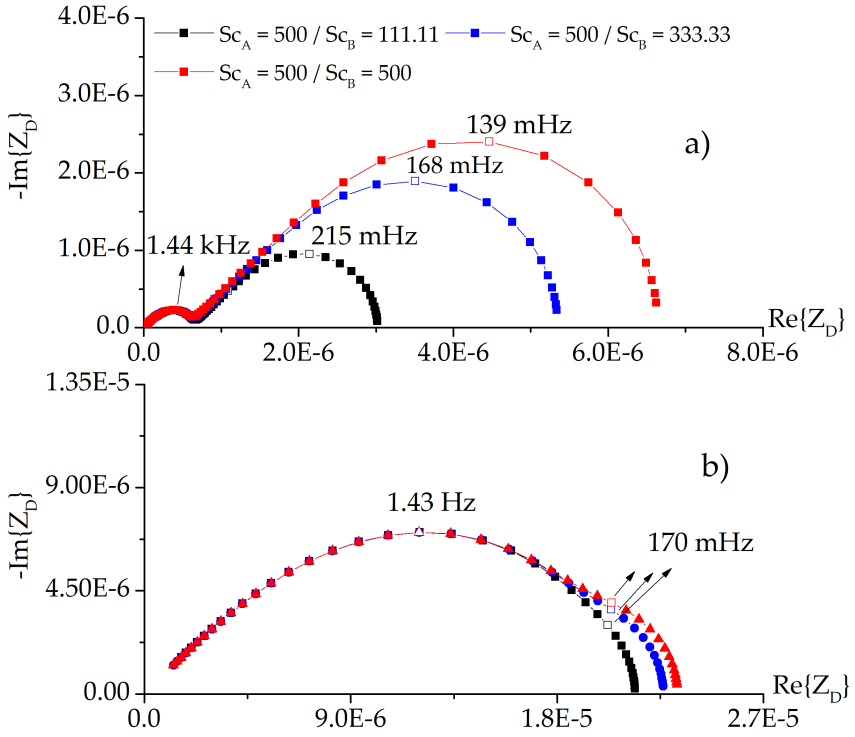

Figure 5.25: Nyquist plot of Z_D for systems with Sc_B values: a) fast kinetics and b) slow kinetics.

The EHD impedance of systems with varying Sc_B values was found to be much more complex. For instance, the effect of increasing Sc_B led to an increase in the Z_{EHD} magnitude for systems with slow kinetics, while the opposite trend was observed for systems with fast kinetics (see figure 5.26). This result shows the considerable level of intricacy of these systems and it cannot be ascribed to a single factor, being more likely due to a combined effect of diffusion, convection and the homogeneous reactions. Figure 5.27 can help us understand this transition. Comparing the ΔC_B profile at $\omega = 0$ for systems with different Sc_B values, we see that, for slow kinetics, $\Delta C_B(0)$ is higher for $Sc_B = 500$ than for $Sc_B = 111.11$. Therefore, the buffer effect will be more pronounced for the former, leading to a higher C_A surface gradient and higher Z_{EHD} magnitude. For fast kinetics, it is the system with $Sc_B = 111.11$ that has the higher $\Delta C_B(0)$, which explains the inverse behaviour in the Z_{EHD} plot.

There is a stark difference between changes in Sc_A and changes in Sc_B. The former is directly linked to the electroactive species and, thus, has a direct effect on the concentration gradient. Increasing Sc_A steepens the concentration profile, because, in this situation, it is the reflex of a decrease in the diffusion coefficient. Consequently, we have higher concentration gradients at the electrode surface, but lower currents. Interpreting the effect of Sc_B is much more complex, since it has no direct effect on the current. Indeed, the availability of B species can only replenish the electroactive species, adding another component to the complete behaviour of the concentration profile. This interplay of transport

modes, involving diffusion, convection and the homogeneous reactions, is responsible for the counterintuitive results obtained.

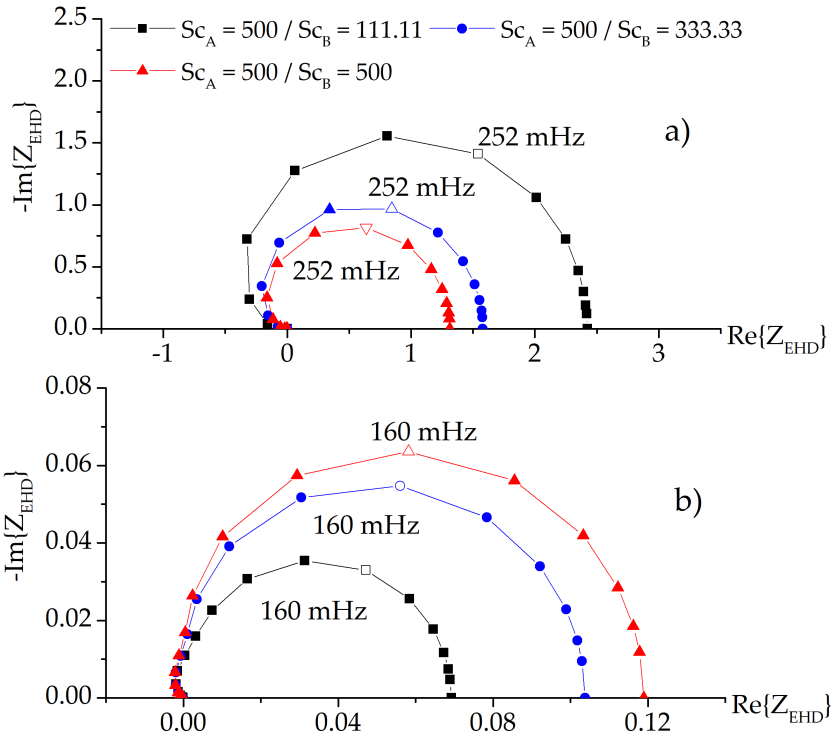

Figure 5.26: Nyquist plot of Z_{EHD} for systems with Sc_B values: a) fast kinetics and b) slow kinetics.

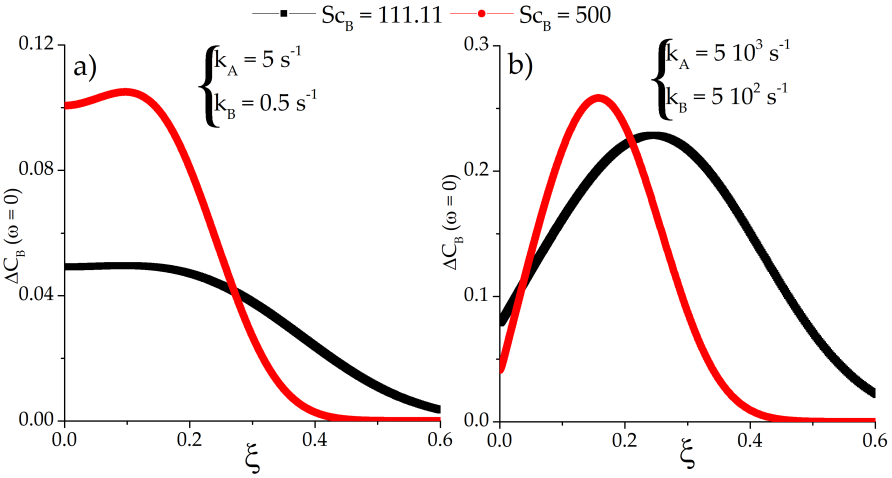

Figure 5.27: Transient concentration profiles of species B at $\omega = 0$ Hz for systems with different Sc_B values: a) slow kinetics and b) fast kinetics.

5.2.4 Comparison with literature data

Diffusion impedance

We have already used the procedure developed by Levart and Schuhmann to validate ours (see section 4.4), so we know that both models are equally capable of calculating the diffusion impedance when the diffusion coefficients are equal.

To our knowledge, the work by Harding *et al.* is the only one presenting simulations for systems with unequal diffusion coefficients [18]. Nevertheless, they employ a two-step chemical reaction while we assume the homogeneous reaction only involves one step. Hence, we cannot make a direct comparison between our calculation and theirs. Still, we can use our procedure to verify one of their statements, namely that the diffusion impedance of CE processes in RDE systems is potential-dependent.

Figure 5.28 compares two Z_D plots obtained at different potentials. It is very clear that the potential has no effect whatsoever on the diffusion impedance. These findings are corroborated by Levart and Schuhmann's method and there is no reason to believe that the equality of diffusion coefficients would have any impact on this behaviour. As mentioned in subsection 3.1.2, none of the hypotheses adopted in the model by Harding *et al.* lead to a potential dependency of Z_D and our results prove that, indeed, such dependency does not exist. Hence, we believe that there must be an error in the numerical procedure developed by these authors.

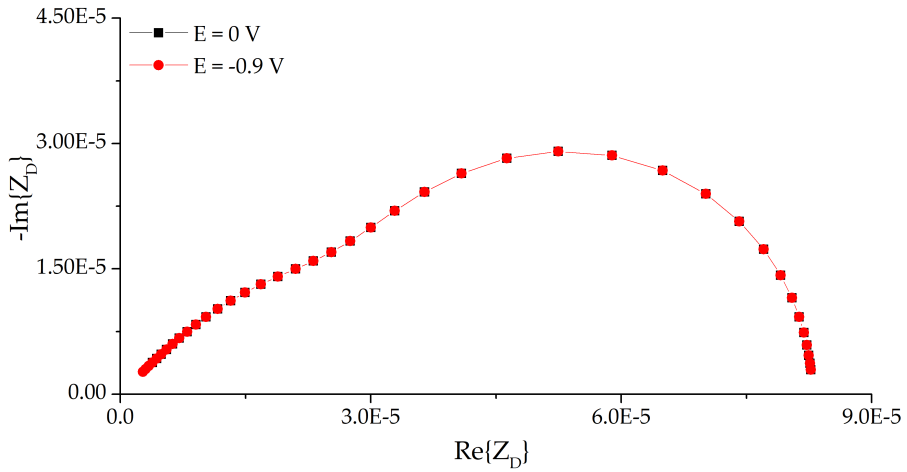

Figure 5.28: Nyquist plot comparing Z_D values for two different potentials. (Sc_A = 111.11, Sc_B = 500, Ω = 10 Hz, k_A = 5 s^{-1}, k_B = 5 s^{-1}, k^0 = 10^{-1} m s^{-1}, b = 15 V^{-1})

Electro-hydrodynamic impedance

The only literature data available for EHD simulations of CE processes in RDE systems is due to Vandeputte *et al.* [17]. However, as explained in subsection 3.1.3, their

analytical model, besides using perturbation methods (which are, themselves approximative), assumes equal diffusion coefficients ($D_A = D_B = D$) and infinite Schmidt numbers. For these reasons, they cannot be taken as *quantitative* references, but as *qualitative ones*.

Figures 5.29 - 5.31 show the comparison between their results and ours for different values of two parameters the authors presented in their article, (a and σ). In our nomenclature, they correspond to:

$$a = \frac{(k_A + k_B)\,\delta_D^2}{D} \tag{5.12}$$

$$\sigma = k_A/k_B = K \tag{5.13}$$

The Bode plots show a very good agreement for lower frequencies and divergence for higher frequencies. This disparity between analytical and numerical values had already been mentioned by the authors in their article. When compared with direct numerical integration, the analytical values for higher frequencies showed considerable deviation. Hence, this disparity with our data should not be seen as a warning sign for possible errors. Instead, what we see is a very good *qualitative* agreement in which the curves generated by both procedures follow the same trends. We take this as evidence that our procedure is both correct and more accurate, since we do take into account the Schmidt corrections the authors have neglected.

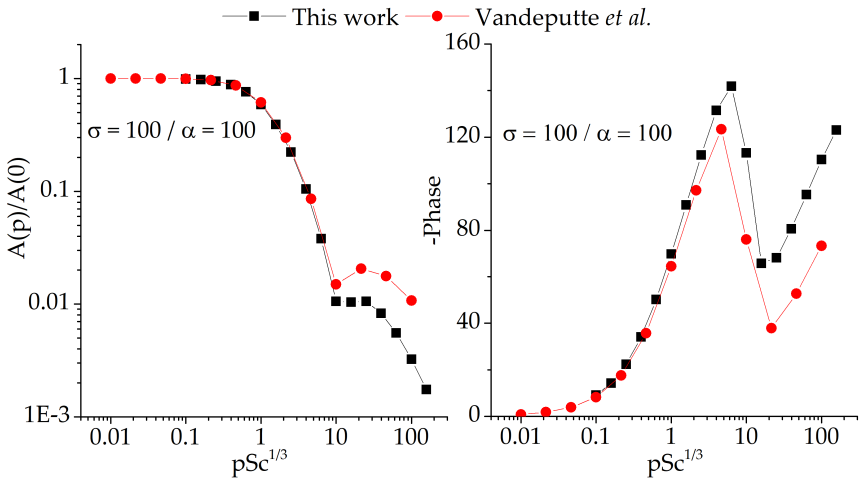

Figure 5.29: Reduced amplitude and negative phase as a function of $pSc^{1/3}$ for systems with $\sigma = 100$ and $a = 100$.

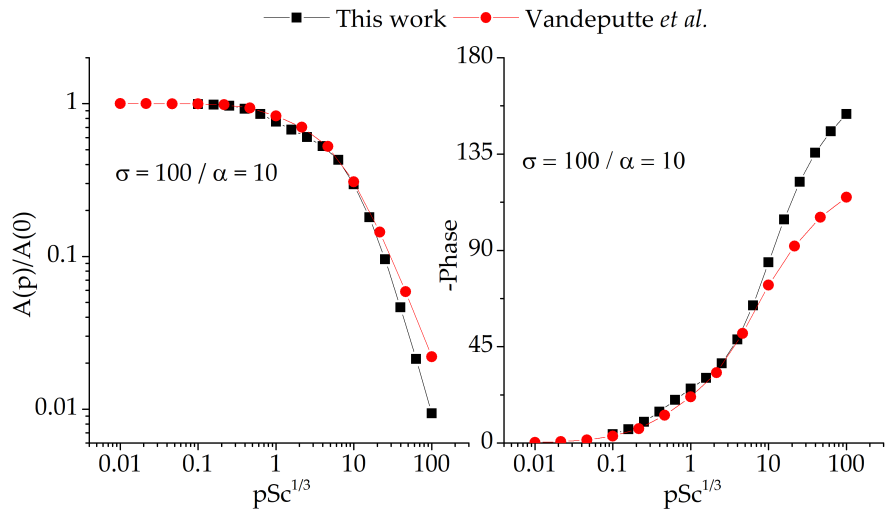

Figure 5.30: Reduced amplitude and negative phase as a function of $pSc^{1/3}$ for systems with $\sigma = 100$ and $a = 10$.

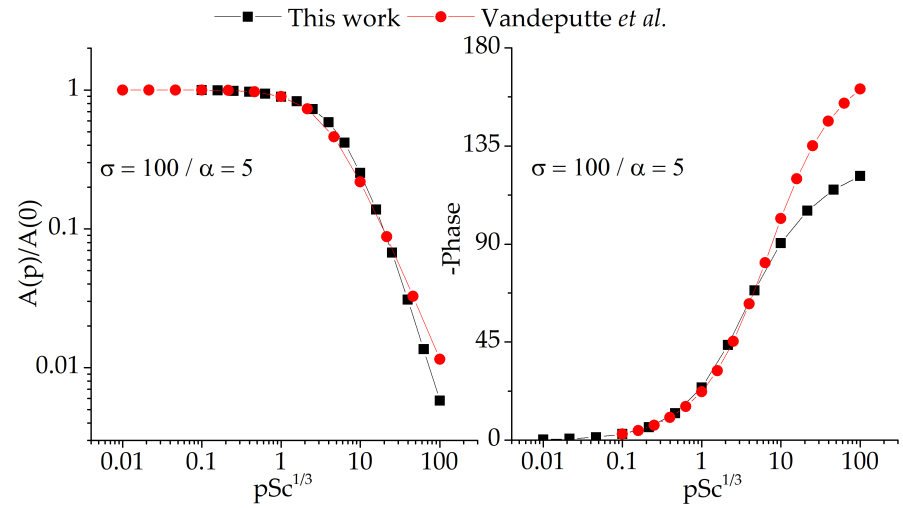

Figure 5.31: Reduced amplitude and negative phase as a function of $pSc^{1/3}$ for systems with $\sigma = 100$ and $a = 5$.

5.3 Here, at last

Finally, we arrive at our destination. The road we built is now behind us: each brick, a piece of knowledge. Almost all of the bricks were lent to us by the researchers who devoted their efforts to the study of electrochemistry. Because of them, we were able to keep walking, using their ideas to develop our own. We have been able to *produce* something new.

In this chapter, we presented the results obtained for new numerical procedures to solve the exact equations for chemical-electrochemical processes in rotating disk electrode systems. Both steady and transient state simulations were validated and confronted

with data from the literature, which we have shown to be less accurate than ours (or even wrong). The influence of different parameters was evaluated and explained in terms of their effects on the concentration profiles that, ultimately, determine the quantities studied in this thesis (i_{lim}, Z_D and Z_{EHD}).

Not all bricks in this road belong to others. At the end of the road, at the very last step, there's an empty space. It must be filled with a different brick, made from our own knowledge. As we fit the last piece in, we look back on the road and think of what we have accomplished.

Chapter 6

Conclusions

During the course of this thesis, we have presented new results concerning the behaviour of chemical-electrochemical reactions when studied with the help of a rotating disk electrode. Our particular intention was to extend the knowledge of these systems by examining conditions which cannot be modelled according to the reaction layer hypothesis. To do so, we employed numerical methods to solve the exact differential equations. This allowed us to investigate both steady state and transient responses; the former by means of the limiting current density and, the latter, by analysing the diffusion and the electro-hydrodynamic impedance.

Regarding steady state phenomena, we showed that the reaction layer hypothesis will always fail to describe systems with arbitrarily large rotating speeds, because it assumes the condition $\delta_R \ll \delta_D$ holds for the whole range of rotation speeds. However, we have proved that, for any system, we can always find a value of Ω past which this will no longer be true. Also, we have shown that every system obeys the equations derived from this hypothesis for sufficiently small rotating speeds. Combining these findings, we suggest that the classification of a kinetic regime as *fast* or *slow* is merely an operational one: any system which can be modelled according to the reaction layer hypothesis throughout the whole rotation speed experimentally employed can be regarded as *fast*. Otherwise, it shall be labelled as *slow*. Finally, our model was shown to be more accurate than the one devised by Compton *et al.*, which also attempts to solve the relevant exact equations, but, contrary to our model, fails to fit the Dogonadze equation under conditions in which the reaction layer hypothesis is still valid.

As for transient phenomena, our investigation was divided in three topics. The first one concerns the effect of the rotation speed. We have found that the impact of Ω is very different for the two components of the diffusion impedance of CE systems; namely, the reaction impedance and the convection-diffusion impedance. As long as the frequency range of these two impedances remain sufficiently apart, only the latter will respond to changes in the rotation speed, both in its magnitude, that will decrease, and its characteristic frequency, which will increase, because it is a function of δ_D^{-2}. However, as the rotation

speed is increased, both loops will start to merge, because convective-diffusive effects will start to dominate the concentration profile, which will also be reflected on the diffusion impedance. This observation is corroborated by our finding that the characteristic frequency of the reaction loop depends on δ_R^{-2}. Hence, for smaller Ω values, $\delta_R \ll \delta_D$ and the loops will not overlap. Because only δ_D depends on Ω, the increase in rotation speed only affects the convection-diffusion impedance. When the frequency range of both loops reach the same order of magnitude, $\delta_D \sim \delta_R$ and convection-diffusion becomes the major mass-transport mechanism. In this respect, electro-hydrodynamic impedance presents a rather distinct picture: for all conditions studied, convection-diffusion dominates the response. Nevertheless, it can still be used to help identify the presence of homogeneous reactions in a qualitative manner. For instance, the limit of the negative phase for higher p values for the CE systems studied always differed from the expected 180° value observed for systems without reactions. Experimentally, this can be used as evidence that additional reaction steps take place in the overall electrochemical process.

The second effect evaluated with transient analysis was that of the reaction rate constants, which relate to that of the equilibrium constant, for k_B was held constant. We observed that increasing k_A (*i.e.*, increasing K) causes the magnitudes of Z_D to decrease and that of Z_{EHD} to increase. Both observations are due to the same phenomenon: a steepening of the concentration profile of the electroactive species at the vicinities of the electrode surface, resulting in higher gradients and current densities. This behaviour is explained by the faster consumption of electroactive species in the chemical step.

The final aspect concerned the effect of the Schmidt numbers (for constant kinematic viscosity) on impedance response. With respect to the electroactive species, we have found that higher Schmidt numbers lead to smaller diffusion and electro-hydrodynamic impedances. The former decreases in magnitude because the increment in Sc_A is caused by lowering D_A. This hinders the replenishment of A species close to the electrode surface, leading to higher concentration gradients and lower Z_D. As for the electro-hydrodynamic impedance, we noticed that, although the concentration gradient increases, the overall current for lower D_A is smaller. Hence, Z_{EHD} magnitudes decrease too. The effect of Sc_B is more complex. When increased, it leads to higher diffusion impedance by increasing the convection-diffusion loop. This can be explained by the lower mobility of B species, which lessens their buffer effect on the concentration of the electroactive species and reduces the concentration gradient. Z_{EHD} response, though, does not follow the same pattern: its magnitude decreases with increasing Sc_B for slow kinetics and follows an inverse trend for fast kinetics. In this case, we were not able to single out a major factor contributing to this behaviour, which is, most likely, due to a combined effect of convection, diffusion and the bulk reactions.

When compared to other transient models available in the literature, our diffusion impedance did not show any dependence on the potential applied, unlike the model by

Harding *et al.*. The fact that other diffusion models, such as the one by Levart and Schuhmann, also do not have a potential dependency corroborates our observations. Insofar as possible, we also compared our Z_{EHD} results with available models and found very good qualitative agreement, which was seen as positive since the other models are only approximate solutions.

6.1 Time to move on

Perhaps we should have warned the reader before we began: this has never really been about the destination, but about the journey. Sure, it feels great to have arrived here after all we've been through, but why stop? Looking in retrospect, we see that, while we have accomplished our goals, new questions and challenges have arisen. Why not pursue them?

So, what's next? Some of the possibilities are:

- Work on a completely nondimensionalized formulation of the problem to find a more elegant and precise boundary to the validity of the reaction layer hypothesis.
- Work on a semi-analytical approach to solve the exact convection-diffusion-reaction equations.
- Extend the model to more complex CE mechanisms, including higher-order reactions and kinetic complications at the electrode surface.
- Extend the model to different mechanisms, such as EC, ECE and EC'.

Everything is packed and we're ready to go. What about you, dear reader? Will you join us?

References

[1] DA COSTA, I. V. L., ROCHEDO, P., IMPÉRIO, M., et al. "Geo.: Gas Production in Offshore Reservoirs in Brazil's Pre-salt Region". In: Grammelis, P. (Ed.), *Energy, Transportation and Global Warming. Green Energy and Technology*, Springer, cap. 45, pp. 617–629, Cham, 2016.

[2] DOS SANTOS NETO, E., DE MORAIS, E., FERREIRA, A., et al. "H2S Risk in Presalt Reservoirs". In: *OTC Brasil*. Offshore Technology Conference, oct 2013.

[3] DE SOUSA, F. V. V., VIANA, P. R. P., TRIBOLLET, B., et al. " Hydrogen Evolution Reaction Evaluation in Aqueous Solutions Containing CO 2 at Different Pressures ", *Journal of The Electrochemical Society*, v. 164, n. 6, pp. C294–C299, 2017.

[4] DAS CHAGAS ALMEIDA, T., BANDEIRA, M. C. E., MOREIRA, R. M., et al. "New insights on the role of CO 2 in the mechanism of carbon steel corrosion", *Corrosion Science*, v. 120, pp. 239–250, may 2017.

[5] REMITA, E., TRIBOLLET, B., SUTTER, E., et al. "Hydrogen evolution in aqueous solutions containing dissolved CO2: Quantitative contribution of the buffering effect", *Corrosion Science*, v. 50, n. 5, pp. 1433–1440, 2008.

[6] KAHYARIAN, A., NESIC, S. "H2S corrosion of mild steel: A quantitative analysis of the mechanism of the cathodic reaction", *Electrochimica Acta*, v. 297, pp. 676–684, feb 2019.

[7] LEVICH, V. G. *Physicochemical hydrodynamics*. 1 ed. Englewood Cliffs, Prentice-Hall, 1962.

[8] OPEKAR, F., BERAN, P. "Rotating disk electrodes", *Journal of Electroanalytical Chemistry and Interfacial Electrochemistry*, v. 69, n. 1, pp. 1–105, apr 1976.

[9] "Rotating disk electrode". `https://www.metrohm.com/easydb/3140_s/450`, . Accessed: 2019-06-19.

[10] "Rotating disk electrode". https://www.origalys.co.uk/Files/120087/Img/20/EM-EDT-Pt-D5-300x249.png, . Accessed: 2019-06-19.

[11] KOUTECKÝ, J., LEVICH, V. G. *Zhurnal Fizicheskoi Khimii*, v. 32, pp. 1965, 1958.

[12] DOGONADZE, R. R. *Zhurnal Fizicheskoi Khimii*, v. 32, pp. 2437, 1958.

[13] COMPTON, R. G., LAING, M. E., MASON, D., et al. "Rotating Disc Electrodes: The Theory of Chronoamperometry and Its Use in Mechanistic Investigations", *Proceedings of the Royal Society A: Mathematical, Physical and Engineering Sciences*, v. 418, n. 1854, pp. 113–154, 1988.

[14] COMPTON, R. G., HARLAND, R. G. "Rotating-disc electrodes and the theory of CE processes. Arbitrary rate constants and diffusion coefficients", *Journal of the Chemical Society, Faraday Transactions 1: Physical Chemistry in Condensed Phases*, v. 85, n. 3, pp. 761, 1989.

[15] LEVART, E., SCHUHMANN, D. "Sur la détermination generale du comportement transitoire d'une electrode a disque tournant soumise a une perturbation electrique de faible amplitude", *Journal of Electroanalytical Chemistry and Interfacial Electrochemistry*, v. 28, n. 1, pp. 45–56, nov 1970.

[16] LEVART, E., SCHUHMANN, D. "Sur la determination générale de l'impedance de concentration (diffusion convective et reaction chimique) pour une electrode a disque tournant", *Electroanalytical Chemistry and Interfacial Electrochemistry*, v. 53, pp. 77–94, 1974.

[17] VANDEPUTTE, S., HUBIN, A., VEREECKEN, J., et al. "AC and Electrohydrodynamic Impedances for a Chemical Preceding Electrochemical Mechanism I. Theory", *Journal of The Electrochemical Society*, v. 147, n. 8, pp. 3054, 2000.

[18] HARDING, M., TRIBOLLET, B., VIVIER, V., et al. "The influence of homogeneous reactions on the impedance response of a rotating disk electrode", *Journal of the Electrochemical Society*, v. 164, n. 11, pp. 3418–3428, 2017.

[19] BARD, A. J., FAULKNER, L. R. *Electrochemical methods: Fundamentals and Applications*. 2 ed. New York, John Wiley & Sons, 2001. ISBN: 0471043729.

[20] PLETCHER, D., GREEF, R., PEAT, R., et al. *Instrumental methods in electrochemistry*. 3 ed. Cambridge, Woodhead Publishing, 2001. ISBN: 9781898563808.

[21] Bard, A. J., Scholz, F., Inzelt, G. (Eds.). *Electrochemical dictionary*. New York, Springer, 2008.

[22] BARCIA, O. E. *Estudo do sulfato e dos halogenetos na dissolução anódica do ferro - Um estudo via impedância eletroquímica e eletro-hidrodinâmica*. Tese de Doutorado, COPPE/UFRJ, Rio de Janeiro, RJ, Brasil, 1989.

[23] BOCKRIS, J. O., REDDY, A. K., GAMBOA-ALDECO, M. E. *Modern Electrochemistry 2A: Fundamentals of Electrodics*. 2 ed. New York, Kluwer Academic/Plenum Publishers, 2000. ISBN: 0-306-47605-3.

[24] MACDONALD, D. D. *Transient Techniques in Electrochemistry*. 1 ed. New York, Plenum Press, 1977. ISBN: 978-1-4613-4147-5.

[25] NEWMAN, J., THOMAS-ALYEA, K. *Electrochemical Systems*. 3 ed. Hoboken, Wiley Interscience, 2004. ISBN: 3175723993.

[26] IBL, N. "Fundamentals of Transport Phenomena in Electrolytic Solutions". In: Yeager, E., Bockris, J. O., Conway, B. E., et al. (Eds.), *Comprehensive Treatise of Electrochemistry*, v. 6, 1 ed., Springer Science+Business Media, cap. 1, pp. 1–64, New York, 1983.

[27] OLDHAM, K. B., ZOSKI, C. G. "Mass Transport to Electrodes". In: Bamford, C. H., Compton, R. G. (Eds.), *Comprehensive Chemical Kinetics*, v. 26, 1 ed., Elsevier, cap. 2, pp. 79–144, Netherlands, 1986.

[28] GIRAULT, H. H. *Analytical and Physical Electrochemistry*. 1 ed. Italy, EPFL Press, 2004.

[29] KORYTA, J., DVORAK, J., KAVAN, L. *Principles of Electrochemistry*. 2 ed. Great Britain, John Wiley & Sons, 1993. ISBN: 0 471 93838 6.

[30] OLDHAM, K. B., MYLAND, J. C., BOND, A. *Electrochemical Science and Technology: Fundamentals and Applications*. 1 ed. Singapore, John Wiley & Sons, 2012.

[31] PONTES, J., MANGIAVACCHI, N. *Fenômenos de Transferência com Aplicações às Ciências Físicas e à Engenharia. Volume 1: Fundamentos*. 1 ed. Rio de Janeiro, SBM, 2016.

[32] MANZANARES, J. A., KONTTURI, K. "Diffusion and Migration". In: Calvo, E. J. (Ed.), *Encyclopedia of Electrochemistry*, v. 2, 1 ed., Wiley-VCH Verlag GmbH & Co. KGaA, pp. 81–121, Weinheim, Germany, dec 2007.

[33] AMATORE, C., SZUNERITS, S., THOUIN, L., et al. "The real meaning of Nernst's steady diffusion layer concept under non-forced hydrodynamic conditions. A simple model based on Levich's seminal view of convection", *Journal of Electroanalytical Chemistry*, v. 500, n. 1-2, pp. 62–70, 2001.

[34] VON KÁRMÁN, T. "Über Laminare und turbulente Reibung", *Zeitschrift für angewandte Mathematik und Mechanik*, p. 232, 1921.

[35] COCHRAN, W. G. "The flow due to a rotating disc", *Mathematical Proceedings of the Cambridge Philosophical Society*, v. 30, n. 03, pp. 365, jul 1934.

[36] ROGERS, M. H., LANCE, G. N. "The rotationally symmetric flow of a viscous fluid in the presence of an infinite rotating disk", *Journal of Fluid Mechanics*, v. 7, n. 04, pp. 617, apr 1960.

[37] SMYRL, W. H., NEWMAN, J. "Limiting Current on a Rotating Disk with Radial Diffusion", *Journal of The Electrochemical Society*, v. 118, n. 7, pp. 1079, 1971.

[38] HOGGE, E. A., KRAICHMAN, M. B. "The Limiting Current on a Rotating Disc Electrode in Potassium Iodide-Potassium Triiodide Solutions", *Journal of the American Chemical Society*, v. 76, n. 5, pp. 1431–1433, 1954.

[39] BEACOM, S. E., ROBERT N. HOLLYER, J. "Rotating Disk Electrode Techniques for the Study of Addition Agents", *Journal of The Electrochemical Society*, v. 109, n. 6, pp. 495–497, 1962.

[40] KASSNER, T. F. "Rate of Solution of Rotating Tantalum Disks in Liquid Tin", *Journal of The Electrochemical Society*, v. 114, n. 7, pp. 689, 1967.

[41] GREGORY, D. P., RIDDIFORD, A. C. "Transport to the surface of a rotating disc", *Journal of the Chemical Society (Resumed)*, v. 6, n. 3756, pp. 3756, 1956.

[42] NEWMAN, J. "Schmidt Number Correction for the Rotating Disk", *The Journal of Physical Chemistry*, v. 70, n. 4, pp. 1327–1328, apr 1966.

[43] NEWMAN, J. "Current Distribution on a Rotating Disk below the Limiting Current", *Journal of The Electrochemical Society*, v. 113, n. 12, pp. 1235, 1966.

[44] MARATHE, V., NEWMAN, J. "Current Distribution on a Rotating Disk Electrode", *Journal of The Electrochemical Society*, v. 116, n. 12, pp. 1704, 1969.

[45] BRUCKENSTEIN, S., MILLER, B. "An Experimental Study of Nonuniform Current Distribution at Rotating Disk Electrodes", *Journal of The Electrochemical Society*, v. 117, n. 8, pp. 1044, 1970.

[46] OGATA, K. *Modern Control Engineering*. Upper Saddle River, Prentice Hall, 2012. ISBN: 9780136156734.

[47] GABRIELLI, C. *Identification of electrochemical processes by frequency response analysis*. Solartron Analytical 004/83, 1998.

[48] MACDONALD, J. R., JOHNSON, W. B. "Fundamentals of Impedance Spectroscopy". In: Macdonald, J. R., Evgenij, B. (Eds.), *Impedance Spectroscopy: Theory, experiment and applications*, 2 ed., cap. 1, New York, USA, John Wiley and Sons, 2005.

[49] *Electrochemical impedance spectroscopy*, v. 48. Hoboken, John Wiley & Sons, 2008. ISBN: 978-0-470-04140-6.

[50] BAI, L., CONWAY, B. E. "AC Impedance of Faradaic Reactions Involving Electrosorbed Intermediates : Examination of Conditions Leading to Impedance Spectroscopy Diagrams", *Journal of the Electrochemical Society*, v. 138, n. 10, pp. 2897–2907, 1991.

[51] PRABHAKARA RAO, G., MISHRA, A. "A.C. techniques to evaluate the kinetics of corrosion reactions", *Journal of Electroanalytical Chemistry and Interfacial Electrochemistry*, v. 77, n. 1, pp. 121–125, 1977.

[52] MACDONALD, D. D., MCKUBRE, M. C. H. "Measurement techniques and data analysis". In: Macdonald, J. R., Barsoukov, E. (Eds.), *Impedance Spectroscopy: Theory, experiment and applications*, 2 ed., cap. 3, New York, USA, John Wiley and Sons, 2005.

[53] WARBURG, E. "Ueber das Verhalten sogenannter unpolarisirbarer Elektroden gegen Wechselstrom", *Annalen der Physik*, v. 303, n. 3, pp. 493–499, 1899.

[54] MARTINHON, P. T., CARREÑO, J., SOUSA, C. R., et al. "Electrochemical impedance spectroscopy of lead(II) ion-selective solid-state membranes", *Electrochimica Acta*, v. 51, n. 15, pp. 3022–3028, abr. 2006.

[55] LASIA, A. *Electrochemical Impedance Spectroscopy and its Applications*. 1 ed. New York, NY, Springer New York, 2014. ISBN: 978-1-4614-8932-0.

[56] COUEIGNOUX, J. M., SCHUHMANN, D. "Sur la validite de l'approximation de Nernst en regime transitoire lineaire pour une electrode a disque tournant", *Journal of Electroanalytical Chemistry and Interfacial Electrochemistry*, v. 17, n. 3-4, pp. 245–252, jun 1968.

[57] DESLOUIS, C., EPELBOIN, I., KEDDAM, M., et al. "Impédance de diffusion d'un disque tournant en régime hydrodynamique laminaire. Étude experimentale et comparaison avec le modele de Nernst", *Journal of Electroanalytical Chemistry and Interfacial Electrochemistry*, v. 28, n. 1, pp. 57–63, nov 1970.

[58] LEVART, E., SCHUHMANN, D. “Analyse du transport transitoire sur un disque tournant en regime hydrodynamique laminaire et permanent”, *International Journal of Heat and Mass Transfer*, v. 17, n. 5, pp. 555–566, may 1974.

[59] HOMSY, R. V., NEWMAN, J. “An Asymptotic Solution for the Warburg Impedance of a Rotating Disk Electrode”, *Journal of The Electrochemical Society*, v. 121, n. 4, pp. 521, 1974.

[60] SCHERSON, D., NEWMAN, J. “The Warburg Impedance in the Presence of Convective Flow”, *Journal of The Electrochemical Society*, v. 127, n. 1, pp. 110–113, 1980.

[61] LEVART, E., SCHUHMANN, D. “Comparison of Some Solutions for the Warburg Impedance of a Rotating Disk Electrode”, *Journal of The Electrochemical Society*, v. 122, n. 8, pp. 1082, 1975.

[62] LEVART, E., SCHUHMANN, D. “Discussion of The Warburg Impedance in the Presence of Convective Flow [Daniel A. Scherson and John Newman (pp. 110113, Vol. 127, No. 1)]”, *Journal of The Electrochemical Society*, v. 127, n. 12, pp. 2649, 1980.

[63] TRIBOLLET, B., NEWMAN, J. “The Modulated Flow at a Rotating Disk Electrode”, *Journal of The Electrochemical Society*, v. 130, n. 10, pp. 2016, 1983.

[64] DESLOUIS, C., GABRIELLI, C., TRIBOLLET, B. “An analytical solution of the nonsteady convective diffusion equation for rotating electrodes”, *Journal of The Electrochemical Society*, v. 10, n. October, pp. 2044–2046, 1983.

[65] GABRIELLI, C., TRIBOLLET, B. “A Transfer Function Approach for a Generalized Electrochemical Impedance Spectroscopy”, *Journal of The Electrochemical Society*, v. 141, n. 5, pp. 1147, 1994.

[66] GABRIELLI, C., KEDDAM, M., LIZEE, J. “Frequency analysis of a temperature perturbation technique in electrochemistry”, *Journal of Electroanalytical Chemistry*, v. 359, n. 1-2, pp. 1–20, nov 1993.

[67] ROTENBERG, Z. “Thermoelectrochemical impedance”, *Electrochimica Acta*, v. 42, n. 5, pp. 793–799, 1997.

[68] CITTI, I., AABOUBI, O., CHOPART, J., et al. “Thermoelectrochemical impedance (TEC) II. Validation for an electrochemical mass transport-controlled system by stationary and dynamic investigations”, *Electrochimica Acta*, v. 41, n. 17, pp. 2731–2736, aug 1996.

[69] GABRIELLI, C., KEDDAM, M., TAKENOUTI, H. "New trends in the investigation of electrochemical systems by impedance techniques: multi-transfer function analysis", *Electrochimica Acta*, v. 35, n. 10, pp. 1553–1557, 1990.

[70] BOURKANE, S., GABRIELLI, C., KEDDAM, M. "Kinetic study of electrode processes by ac quartz electrogravimetry", *Journal of Electroanalytical Chemistry*, v. 256, n. 2, pp. 471–475, 1988.

[71] BOURKANE, S., GABRIELLI, C., KEDDAM, M. "Study of electrochemical phase formation and dissolution by ac quartz electrogravimetry", *Electrochimica Acta*, v. 34, n. 8, pp. 1081–1092, 1989.

[72] MILLER, B., BRUCKENSTEIN, S. "Submicromolar Analysis with Rotating and Hydrodynamically Modulated Disk Electrodes", *Analytical Chemistry*, v. 46, n. 13, pp. 2026–2033, 1974.

[73] MILLER, B., BRUCKENSTEIN, S. "Theoretical and Experimental Study of Hydrodynamically Modulated Current-Potential Curves at Rotating Disk Electrodes under Conditions of Mixed Electron and Mass Transfer Control", *Journal of The Electrochemical Society*, v. 121, n. 12, pp. 1558, 1974.

[74] DESLOUIS, C., EPELBOIN, I., GABRIELLI, C., et al. "Impédance électromécanique obtenue au courant limite de diffusion à partir d'une modulation sinusoidale de la vitesse de rotation d'une électrode à disque", *Journal of Electroanalytical Chemistry and Interfacial Electrochemistry*, v. 82, n. 1-2, pp. 251–269, sep 1977.

[75] CAPRANI, A., DESLOUIS, C., KEDDAM, M., et al. "Study of partially blocked electrodes by means of electromechanical impedance measurements", *Electrochimica Acta*, v. 22, n. 11, pp. 1231–1235, nov 1977.

[76] CAPRANI, A., DESLOUIS, C., ROBIN, S., et al. "Transient mass transfer at partially blocked electrodes: a way to characterize topography", *Journal of Electroanalytical Chemistry*, v. 238, n. 1-2, pp. 67–91, 1987.

[77] DESLOUIS, C., TRIBOLLET, B., DUPRAT, M., et al. "Transient Mass Transfer at a Coated Rotating Disk Electrode", *Journal of The Electrochemical Society*, v. 134, n. 10, pp. 2496, oct 1987.

[78] BARCIA, O. E., MATTOS, O. R., PEBERE, N., et al. "Mass-transport study for the electrodissolution of copper in 1M hydrochloric acid solution by impedance", *Journal of The Electrochemical Society*, v. 140, n. 10, pp. 2825, 1993.

[79] BARCIA, O. E. “Anodic Dissolution of Iron in Acid Sulfate Under Mass Transport Control”, *Journal of The Electrochemical Society*, v. 139, n. 2, pp. 446, 1992.

[80] DESLOUIS, C., TRIBOLLET, B. “Recent developments in the electrohydrodynamic (EHD) impedance technique”, *Journal of Electroanalytical Chemistry*, v. 572, n. 2, pp. 389–398, 2004.

[81] VIELSTICH, W., JAHN, D. “Zur Messung schneller Reaktionen in Lösung mit Hilfe der rotierenden Scheibenelektrode”, *Zeitschrift für Elektrochemie, Berichte der Bunsengesellschaft für physikalische Chemie*, v. 64, n. 1, pp. 43–44, 1960.

[82] BELL, R. P., ALBERY, W. J. “The Kinetics of the Dissociation of Weak Acids measured by a Rotating Platinum Disc Electrode”. In: *Proceedings of the Chemical Society*, n. June, pp. 169–170, 1963.

[83] TOLMACHEV, Y. V., SCHERSON, D. A. “Electrochemical reduction of bisulfite in mildly acidic buffers: Kinetics of sulfur dioxide bisulfite interconversion”, *Journal of Physical Chemistry A*, v. 103, n. 11, pp. 1572–1578, 1999.

[84] HALE, J. “Transients in convective systems I. Theory of galvanostatic and galvanostatic with current reversal transients at a rotating disc electrode”, *Journal of Electroanalytical Chemistry (1959)*, v. 6, n. 3, pp. 187–197, sep 1963.

[85] HALE, J. “Transients in convective systems II. Limiting current and kinetically complicated galvanostatic transients at rotating disc electrodes”, *Journal of Electroanalytical Chemistry (1959)*, v. 8, n. 5, pp. 332–349, jan 1964.

[86] GERISCHER, H., VETTER, K. J. “Konzentrationspolarisation bei vorgelagerter chemischer Reaktion im Elektrolyten und ihr Anteil am stationären Polarisationswiderstand beim Gleichgewichtspotential”, *Zeitschrift für Physikalische Chemie*, v. 197, n. 1, pp. 92–104, jan 1951.

[87] CUMINATO, J. A., JUNIOR, M. M. *Discretização de Equações Diferenciais Parciais: Técnicas de Diferenças Finitas*. 1 ed. Rio de Janeiro, SBM, 2013.

[88] FORNBERG, B. “Generation of finite difference formulas on arbitrarily spaced grids”, *Mathematics of Computation*, v. 51, n. 184, pp. 699–706, 1988.

[89] BRITZ, D., STRUTWOLF, J. *Digital Simulation in Electrochemistry*. Monographs in Electrochemistry. 4 ed. Cham, Springer International Publishing, 2016. ISBN: 978-3-319-30290-4.

Appendix A

Mass conservation

In this section, we present a brief proof of equation 2.4, which describes the mass conservation of species in a fluid [31]:

$$\frac{\partial c_i}{\partial t} = -\nabla \cdot \mathbf{J}_i + R_i \tag{A.1}$$

First, consider a control volume,V, fixed in space and simply connected. A fluid with velocity field $\mathbf{v}$, measured with respect to an arbitrary inertial frame, and with molar concentration of species i c_i flows through this volume. Also, let S be the external surface of V and $\mathbf{n}$ be the unit vector perpendicular to S and oriented outwards. The accumulation rate of species i within the control volume (measured in mol) over a period of time will be given by:

$$\int_V \frac{\partial c_i}{\partial t} \mathrm{d}V = \oint_S (-\mathbf{J}_i \cdot \mathbf{n})\, \mathrm{d}S + \int_V R_i \mathrm{d}V \tag{A.2}$$

What this equation states is that *any* change on the *net* amount of i within V over a period of time is either due to a non-zero *net* concentration flux (represented by $\oint_S (-\mathbf{J}_i \cdot \mathbf{n})\, \mathrm{d}S$) or the generation/consumption of i within the volume (represented by $\int_V R_i \mathrm{d}V$). For the flux to contribute to any change in the value of c_i, it must be oriented outwards S, therefore only the term $\mathbf{J}_i \cdot \mathbf{n}$ is taken into account. Also, since this integration calculates the amount of i *leaving* V, we take the negative value to correctly calculate the amount *added* to V.

We now proceed to apply the Gauss's theorem, which states that:

$$\oint_S (\mathbf{J}_i \cdot \mathbf{n})\, \mathrm{d}S = \int_V (\nabla \cdot \mathbf{J}_i)\, \mathrm{d}V \tag{A.3}$$

Thus, equation A.2 becomes:

$$\int_V \frac{\partial c_i}{\partial t} \mathrm{d}V = -\int_V (\nabla \cdot \mathbf{J}_i)\, \mathrm{d}V + \int_V R_i \mathrm{d}V \tag{A.4}$$

And, after rearrangement:

$$\int_V \left(\frac{\partial c_i}{\partial t} + \nabla \cdot \mathbf{J}_i - R_i \right) \mathrm{d}V = 0 \tag{A.5}$$

Since this result must hold for *any* arbitrary volume V, we get:

$$\begin{aligned} \frac{\partial c_i}{\partial t} + \nabla \cdot \mathbf{J}_i - R_i &= 0 \\ \frac{\partial c_i}{\partial t} &= -\nabla \cdot \mathbf{J}_i + R_i \end{aligned} \tag{A.6}$$

Appendix B

Terminal velocity of ions in solution

In this section, we derive the expression for the terminal velocity of an ion moving under a potential gradient in solution (equation 2.7) [27]:

$$\bar{\mathbf{v}}_i = \frac{z_i F \chi}{\kappa \eta N_A R_i} \tag{B.1}$$

As a first approximation, we consider the ion to behave as a sphere, so that the *drag force* due to the viscosity of the solution can be calculated according to a version of Stoke's law adapted to ionic solutions:

$$f_{drag} = \kappa \eta R_i v(t) \tag{B.2}$$

The other force acting on the ion is, of course, the electrostatic force:

$$f_e = \frac{z_i F \chi}{N_A} \tag{B.3}$$

Applying Newton's second law, we get:

$$f_e - f_{drag} = m_{ion} a_{ion} = \frac{M}{N_A} \frac{\mathrm{d}v(t)}{\mathrm{d}t} \tag{B.4}$$

But we also know that:

$$f_e - f_{drag} = \frac{z_i F \chi}{N_A} - \kappa \eta R_i v(t) \tag{B.5}$$

After substitution and rearrangement, we get a first order ordinary differential equation of $v(t)$:

$$\frac{\mathrm{d}v(t)}{\mathrm{d}t} + \frac{N_A \kappa \eta R_i}{M} v(t) = \frac{z_i F \chi}{M} \tag{B.6}$$

Assuming $v(t = 0) = 0$ and a constant electric field leads to:

$$v(t) = \frac{z_i F \chi}{N_A \kappa \eta R_i} \left[1 - \exp\left(-\frac{N_A \kappa \eta R_i}{M} t \right) \right] \tag{B.7}$$

Using typical values found M, η, R_i and z_i, Oldham *et al.* showed that the time needed for $v(t)$ is of the order of 10^{-14} s, *i.e.*, practically nil [27]. Consequently, one can safely assume the value of $v(t)$ to be time-independent. Hence:

$$v = \frac{z_i F \chi}{N_A \kappa \eta R_i} \tag{B.8}$$